Dissertation

submitted to the
Combined Faculty of Mathematics, Engineering and Natural Sciences
of Heidelberg University, Germany
for the degree of

Doctor of Natural Sciences

HIGH-PRECISION PENNING-TRAP DETERMINATION OF THE
ELECTRON CAPTURE Q-VALUE IN ^{163}HO FOR THE
DETERMINATION OF THE ELECTRON NEUTRINO MASS

put forward by

CHRISTOPH SCHWEIGER

born in Oberkirch.

Oral examination: April 22nd, 2024

Max-Planck-Institute for Nuclear Physics
Combined Faculty of Mathematics, Engineering and Natural Sciences
Heidelberg University

February 2024

ABSTRACT

The ECHo and Holmes experiments investigate the effective electron neutrino mass following the least model-dependent approach by studying the kinematic of the electron capture in ^{163}Ho using cryogenic microcalorimeters. Possible systematic shifts in the calorimetric measurements can originate from the decay of ^{163}Ho within the solid gold absorber material of the calorimeter. In order to assess if such a systematic shift is present on the current sensitivity level of those experiments, the Q-value of this decay from microcalorimetry is compared to an independently measured one. This cumulative thesis is based on the experimental developments towards and the independent measurement of the Q-value of ^{163}Ho electron capture using Penning-trap mass spectrometry. In the first part of this thesis, an injection system for an electron beam ion trap capable of operating with rare isotopes, specifically the artificially produced ^{163}Ho, was developed for the creation of highly charged ions. For the Penning-trap measurement, a single highly charged ion in the correct charge state is required and has to be selected from the different charge states produced within in the electron beam ion trap. A Bradbury-Nielsen gate and a very fast high-voltage push-pull switch based on silicon carbide MOSFETs was developed within this thesis to separate the different charge states according to their time-of-flight in the beamline following the electron beam ion trap. These technical developments allowed a measurement of the Q-value of ^{163}Ho with the Penning-trap mass spectrometer Pentatrap as the main result of this thesis.

ZUSAMMENFASSUNG

Die Experimente ECHo und Holmes untersuchen die effektive Elektron-Neutrino-Masse indem sie die Kinematik des Elektroneneinfangs in ^{163}Ho mit kryogenen Mikrokalorimetern untersuchen, was den am wenigsten modellabhängigen Ansatz darstellt. Mögliche systematische Abweichungen in den kalorimetrischen Messungen können durch den Zerfall von ^{163}Ho innerhalb des Goldabsorbermaterials des Kalorimeters entstehen. Um zu beurteilen, ob eine solche systematische Abweichung auf dem derzeitigen Empfindlichkeitsniveau dieser Experimente vorhanden ist, wird der Q-Wert dieses Zerfalls aus der Mikrokalorimetrie mit einem unabhängig gemessenen Q-Wert verglichen. Diese kumulative Arbeit basiert auf den experimentellen Entwicklungen und der unabhängigen Messung des

Q-Wertes des ^{163}Ho-Elektroneneinfangs mit Hilfe der Penning-Fallen-Massenspektrometrie. Im ersten Teil dieser Arbeit wurde ein Injektionssystem für eine Elektronenstrahlionenfalle zur Erzeugung hochgeladener Ionen entwickelt, um mit seltenen Isotopen, insbesondere dem künstlich hergestellten ^{163}Ho, arbeiten zu können. Für die Messung mit der Penningfalle wird nur ein einzelnes hochgeladenes Ion im richtigen Ladungszustand benötigt, das aus den verschiedenen in der Elektronenstrahlionenfalle erzeugten Ladungszuständen separiert werden muss. Ein Bradbury-Nielsen-Gate und ein sehr schneller Hochspannungs-Schalter auf der Basis von Siliziumkarbid-MOSFETs wurden im Rahmen dieser Arbeit entwickelt, um die verschiedenen Ladungszustände entsprechend ihrer Flugzeit in der der Elektronenstrahl-Ionenfalle folgenden Beamline zu trennen. Diese technischen Entwicklungen ermöglichten eine Messung des Q-Wertes von ^{163}Ho mit dem Penningfallen-Massenspektrometer PENTATRAP als Hauptergebnis dieser Arbeit.

CONTENTS

LIST OF FIGURES

LIST OF TABLES

ACRONYMS

AME   Atomic Mass Evaluation

BNG   Bradbury-Nielsen-Gate

BSM   Beyond Standard Model

CRES   Cyclotron Radiation Emission Spectroscopy

ECHo   Electron Capture in Holmium

EBIT   Electron Beam Ion Trap

EDM   Electric Dipole Moment

FWHM Full Width at Half Maximum

HC-EBIT Heidelberg Compact Electron Beam Ion Trap

HCI   Highly Charged Ion

GERDA Germanium Detector Array

KATRIN Karlsruhe Tritium Neutrino Experiment

MAC-E Magnetic Adiabatic Collimation with an Electrostatic filter

MMC   Metallic Magnetic Calorimeter

MR-ToF Multi-Reflection Time-of-Flight

PLA   Polylactic Acid

PMNS Pontecorvo–Maki–Nakagawa–Sakata

PNP   Pulse and Phase

PT   Penning Trap

PTMS Penning-Trap Mass Spectrometry

QED   Quantum Electrodynamics

SNR   Signal to Noise Ratio

SM   Standard Model

SQUID Superconducting Quantum Interference Device

TES   Transition Edge Sensor

ToF   Time of Flight

INTRODUCTION

In 1913, when J.J. Thomson discovered two different isotopes of neon, separating them using electric and magnetic fields, "mass spectrometry", a new field in physics, established a first important result in nuclear physics: Elements have different isotopes [119]. Nowadays, a standard technique in various fields including medicine, chemistry and biology, Thomson also suggested the use of mass spectrometry as a method for chemical analysis already at this early stage. F.W. Aston, a student of Thomson, continued this work and studied the isotopic composition of several elements, finding that all masses fall on whole numbers [12, 38]. For these studies, mass resolving powers of a few parts in 10^3 were reported by Aston. Years later with continuous improvements to his mass spectrometer, he as well as J.-L. Costa discovered that the masses deviate from the "whole number rule", giving rise to the "mass defect" [13, 36]. The mass defect ("mass excess") is a direct result from the strong, weak and electromagnetic interactions within the atomic nucleus giving rise to the slightly smaller atomic mass compared to the atomic mass number. This is the value that is typically published, e.g. in the Atomic Mass Evaluation (AME).

Even these early results showed that the mass of an atom at rest is one of the most fundamental and unique properties that gives insight into various fields of fundamental physics. Albert Einsteins' famous formula $E = mc^2$ [44] connects this mass to an energy by including the speed of light c as a proportionality constant. Thereby, it connects the atomic mass to electronic and nuclear binding energies and excitations, in this way being a sensitive probe for the interactions between constituents of the atom.

With today's achievable precision on the atomic mass, scientists are able to gain insight into the fundamental interactions within an atom and its nucleus which can be measured with an extremely high precision and compared to theory. In addition, many experiments in the broad field of fundamental physics require high-precision mass data for the determination of other quantities. Even matter and anti-matter are compared in high-precision mass spectrometers testing the charge–parity–time symmetry [20]. Among others (see Section 1.1), high-precision mass spectrometry can contribute in the field of neutrino physics by measuring the Q-values of specific nuclear decays.

In this introductory part, I would like to first start with an overview of the fundamental physics applications of Penning-Trap Mass Spectrometry (PTMS) before the next section 1.2 will be dedicated to the Standard Model (SM) of particle physics and the implications of a

finite neutrino mass. Section 1.3 introduces the most important experiments currently investigating the electron (anti-)neutrino mass by a kinematic study of nuclear decays with a focus on the Electron Capture in Holmium (ECHo) experiment.

Following the introductory Chapter, in Chapter 2, I will introduce the experimental methods used in the scope of this thesis resulting in the three publications presented in Chapter 3. This thesis closes with a discussion and outlook in Chapter 4 and a summary of the results in Chapter 5.

1.1   HIGH-PRECISION MASS SPECTROMETRY WITH PENNING TRAPS

Mass measurements with highest precision using singly and highly charged ions are performed with Penning traps. Mass measurements in Penning traps rely on the precise determination of the free-space cyclotron frequency $\nu_c = \frac{1}{2\pi}\frac{qB}{m}$ of the ion of interest of mass m in the charge state q in a strong magnetic field B. Since the analyzing fields define the measured quantities, for Penning traps, the motional frequencies, it is of crucial importance that the analyzing fields are sufficiently stable during the time the frequency measurement take place. With the most advanced Penning Trap (PT) setups today, it is possible to achieve fractional uncertainties up to the order of a few parts in 10^{12} for stable and long-lived species [54, 66, 90, 103–105, 115]. These experimental setups are usually designed for the purpose of a specific measurement or measurements in a specific mass region where trap designs are tailored to reduce systematic uncertainties in order to achieve ultimate precisions. A comprehensive overview of mass spectroscopic techniques and PTMS is given in [17, 41] while a review of the cases that require very high precision can be found in [90].

The performance of a mass spectrometer in terms of precision is characterized by the fractional uncertainty δ_{frac} that is achieved in a measurement. The fractional uncertainty is defined as the total uncertainty divided by the quantity itself, e.g. for cyclotron frequency ratio R measurements:

$$\delta_{\mathrm{frac}} = \frac{\delta R}{R}. \tag{1.1}$$

For mass measurements the span of interest ranges from $\delta_{\mathrm{frac}} \sim 10^{-5}$ for applications in chemistry to $\delta_{\mathrm{frac}} \sim 10^{-6} - 10^{-10}$ for nuclear structure physics [93], nuclear astrophysics and weak interaction studies [14, 71, 125] using PTs at online facilities [50, 85, 89]. Even smaller fractional uncertainties are reached with cryogenic Penning traps for tests of fundamental symmetries [20] and mass measurements for fundamental physics [80]. While the precision characterizes the resolution and reproducibility, the accuracy of the result is a second important measure characterizing how close the measurement is to the true value.

Through a careful systematic analysis Penning traps are considered to be very accurate since systematic shifts can be avoided by design and construction (e.g. minimizing the imperfections of the electromagnetic trapping fields) or the systematic effects can be measured, calculated or simulated very precisely (relativistic and image charge shifts), see also Section 2.2.2).

A selection of applications in fundamental physics where fractional uncertainties of $\leq 10^{-11}$ are required is given in the following.

DIRECT TEST OF $E = mc^2$ The theory of special relativity can be directly tested e.g. in the neutron capture reaction: $^{35}\text{Cl} + {}^{1}\text{n} \rightarrow {}^{36}\text{Cl} + \gamma$ [69]. The photons emitted in the de-excitation process following the neutron capture are measured using a crystal Bragg-diffraction spectrometer while the mass difference is obtained from PTMS:

$$\left[m\left({}^{35}\text{Cl}\right) - m\left({}^{36}\text{Cl}\right) + m(n)\right] \cdot c^2 = \sum_i E\left(\gamma_i\right). \tag{1.2}$$

DETERMINATION OF THE FINE STRUCTURE CONSTANT α The fine structure constant can be determined by a measurement of the recoil frequency in a matter-wave interferometer. In recent experiments, the recoil frequency of ^{87}Rb [88] and ^{133}Cs [95] is measured. For next-generation experiments the uncertainties of many effects will be significantly reduced which would leave the masses of ^{87}Rb and ^{133}Cs as the dominant uncertainty. A refined measurement using PTMS is required.

TESTS OF QUANTUM ELECTRODYNAMICS IN THE STRONG FIELD REGIME   Measurements of the bound-state electron g-factors and their comparison to the predictions of Quantum Electrodynamics (QED) have become the most stringent tests of QED in strong electric fields [67, 117, 118]. For the determination of the g-factor, the atomic mass of the investigated Highly Charged Ion (HCI) is required. In addition, high-precision PTMS can perform this type of QED test with a pure mass measurement by measuring the binding energy of an electron in a HCI.

Q-VALUES OF NUCLEAR DECAYS FOR NEUTRINO PHYSICS   Precise and independently measured Q-values are required for the experimental determination of the neutrino mass in order to exclude possible systematic uncertainties (see Section 1.3) but also in the search for keV-scale sterile neutrinos, neutrino oscillation experiments or the onging search for neutrinoless double-β-decay [47].

1.2   THE STANDARD MODEL OF PARTICLE PHYSICS AND THE AB-SOLUTE SCALE OF THE NEUTRINO MASS

The SM of particle physics is in many aspects considered to be one of the most precisely experimentally verified theories in fundamental physics. This success manifested itself already in the early stages with the prediction of fundamental particles such as the W- and Z-bosons [62, 109, 123] or the Higgs-boson [49, 68], which, years after their prediction, were experimentally validated in high-energy particle collision experiments at CERN, leading to several Nobel Prizes in the years 1979, 1984 and 2013. While describing the interactions between fundamental particles to a great precision there are experimentally observed aspects that the SM does not address or that are even contradicting the SM, such as e.g.

- the existence of dark matter and dark energy [99],

- the Baryon asymmetry [29, 42] or

- neutrino flavor oscillations [5, 58].

Theories that try to address these aspects are generally termed Beyond Standard Model (BSM) theories.

Not only large scale high-energy particle physics experiments are searching for BSM physics but also smaller scale "table-top" experiments are exploring the limits of the current understanding of the SM [52] and place limits on BSM theories in a complementary way. These experiments focus on low-energy precision measurements such as measurements of the Electric Dipole Moment (EDM) of fundamental (electron) [10, 28, 107] and composite particles (neutron) [1] or the magnetic moment of the electron [51, 95] and muon [4] and aim to compare those to the SM predictions. Some BSM theories predict larger values, e.g. for the EDM of the electron, than the SM. If an EDM larger than the SM prediction is found it would be a signature for BSM physics while on the other hand BSM theories can be excluded when the found limit is smaller.

Since the existence of an absolute neutrino mass was established with the discovery of neutrino flavor oscillations [5, 58], the neutrino mass scale is one of the most sought-after quantities for fundamental physics to constrain BSM theories addressing neutrino mass generation mechanisms [63, 74, 96] but also in astrophysics and cosmology [82]. As the SM describes neutrinos as massless, neutral, fermionic particles, the discovery of neutrino flavor oscillations is a key signature of BSM physics. Since neutrinos do not carry an electric charge they interact exclusively by the weak interaction with other SM particles. This significantly complicates the direct experimental investigation since large detector volumina [33] or measurements where the neutrino is not directly detected are required.

Initially the neutrino was postulated by Wolfgang Pauli in 1930 in order to explain the continuous β-decay spectrum. The existence of neutrinos was validated only in 1956 using the inverse β-decay to detect neutrinos originating from a nuclear reactor [37]. Since then, different neutrino sources (the sun, the atmosphere, nuclear reactors and accelerators) in a multitude of experiments were used to study these fundamental particles.

There are three known neutrino flavors $f \in \{e, \mu, \tau\}$ originating from weak charged-current reactions ($W^{\pm}$-decay) where a neutrino is emitted together with the respective lepton, either an electron (e), a muon (μ) or a tau (τ). A flavor eigenstate $|\nu_f\rangle$ is a superposition of the three mass eigenstates $|\nu_i\rangle$, with $i \in \{1, 2, 3\}$:

$$|\nu_f\rangle = \sum_{i=1}^{3} U_{fi} |\nu_i\rangle, \tag{1.3}$$

where U_{fi} represents the Pontecorvo–Maki–Nakagawa–Sakata (PMNS) matrix which is commonly parametrized with three mixing angles and a phase related to CP-violation [127]. Experiments investigating the neutrino mass typically extract the parameter

$$m_{\nu_f}^2 = \sum_{i=1}^{3} |U_{fi}|^2 m_i^2 \tag{1.4}$$

which is the *effective neutrino rest mass*, i.e. the mass of a neutrino in a specific flavor eigenstate is an admixture of the three mass eigenstates with the weights for each mass eigenstate given by the PMNS matrix. More specifically, the experiments search for the *effective electron neutrino mass*:

$$m_{\nu_e} = m_{\beta} = \sqrt{\sum_{i=1}^{3} |U_{ei}|^2 m_i^2}. \tag{1.5}$$

The currently best upper limit on the effective electron neutrino rest mass from a laboratory experiment is $m_{\nu_e} < 0.8 \, \text{eV}/c^2$ [6], c.f. Section 1.3.

The oscillation experiments that proved the existence of an absolute mass of neutrinos are not sensitive to the absolute mass scale but allow to extract the differences of the squared masses:

$$\Delta m_{\nu_{ij}}^2 = m_{\nu_i}^2 - m_{\nu_j}^2, \tag{1.6}$$

which are given in the normal ordering by [127]:

$$\Delta m_{\nu_{21}}^2 = (7.53 \pm 0.18) \cdot 10^{-5} \, \text{eV}^2/c^4$$
$$|\Delta m_{\nu_{31}}^2| = (2.453 \pm 0.033) \cdot 10^{-3} \, \text{eV}^2/c^4.$$

From these results it is known that at least two neutrinos have a mass while the lightest neutrino in principle could have a vanishing rest

mass. From the interaction of solar neutrinos with matter it is also known that $m_2 > m_1$ [94] resulting in two possible mass orderings: The normal ($\Delta m^2_{\nu_{31}} > 0$) and inverted ($\Delta m^2_{\nu_{31}} < 0$) hierarchy depicted in Figure 1.1.
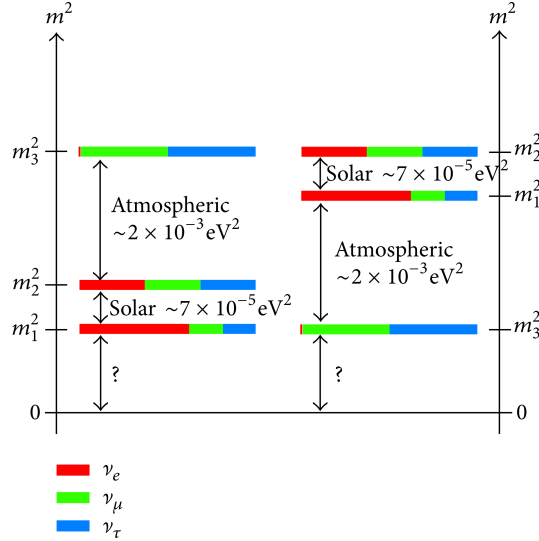

Figure 1.1: Normal and inverted hierarchy of the neutrino mass eigenstates. From oscillation experiments with solar and atmospheric neutrinos the mass splittings are known and from matter effects $m_2 > m_1$ [94]. With this information the normal hierarchy and the inverted hierarchy are possible mass orderings of the neutrino mass eigenstates. In both hierarchies the mass of the lightest mass eigenstate can in principle be zero. Figure taken from [94].

The most stringent limit on the sum of the neutrino masses is extracted from cosmological observations and results in a range of $< 120 - 540\,\text{meV}/c^2$ depending on the underlying cosmological model [100]. Cosmological observations are based on data of the cosmic microwave background and on galaxy survey data where massive neutrinos leave an imprint on some observables (large-scale structure of the universe, red-shift) [82, 83]. Experiments with improved sensitivity are planned for the future.

From experiments investigating if the neutrino is a Dirac fermion or a Majorana fermion (Majorana neutrinos are their own antiparticles) constraints of the effective neutrino rest mass can be extracted as well. These experiments investigate nuclei that decay via double-β-decay (often written as $2\nu\beta\beta$-decay) where two electrons (positrons) and two anti-neutrinos (neutrinos) are emitted assuming neutrinos are Dirac fermions. In the case that neutrinos are Majorana fermions, the neutrinos can annihilate and two electrons of the same energy would be detected instead of the continuous decay spectrum - hence these experiments search for neutrinoless double-β-decay ($0\nu\beta\beta$-decay). Although up to now no events have been recorded that would support the Majorana nature of neutrinos, e.g. in the Germanium Detector

Array (GERDA) experiment [3] it was still possible to set a constraint on the effective neutrino rest mass of $< 79 - 180 \, \text{eV}/c^2$ (assuming neutrinos are Majorana fermions) [2]. Future experiments with a larger detector mass and hence improved sensitivity are planned [30].

1.3 KINEMATIC STUDIES OF THE EFFECTIVE ELECTRON NEUTRINO MASS

In this section, I would like to present an overview of the leading experiments and methods studying the effective electron-neutrino mass (in the following referred to as "neutrino mass") by kinematic investigations of suitable nuclear decays. Kinematic studies are considered the least model-dependent method (sometimes also termed "direct methods") for the determination of the neutrino mass in contrast to the neutrino mass limits extracted from astrophysical observations which depend on cosmological models. Suitable nuclear decays have the smallest possible Q-value which helps to improve the statistics in the endpoint region. Even with a relatively low Q-value of about 18.6 keV in the tritium β-decay, there are only about $2 \cdot 10^{-13}$ events in the last 1 eV below the endpoint [31]. In addition, there are further practical limits like the lifetime of the nuclide or its availability and handling. This reduces the number of possible nuclides to only a few and searches for other suitable candidates are still ongoing at radioactive ion beam facilities [55, 72]. Currently, the ^{3}H (tritium) β-decay and the ^{163}Ho electron capture decay are investigated.

KATRIN   The Karlsruhe Tritium Neutrino Experiment (KATRIN) has determined the currently most sensitive upper limit of any of the laboratory experiments studying the kinematics of the tritium β-decay:

$$^3\text{H} \rightarrow {}^3\text{He}^+ + \bar{\nu}_e + e^- \tag{1.7}$$

with an upper limit on the neutrino mass of $m_{\nu_e} < 0.8 \, \text{eV}/c^2$ for $m_{\bar{\nu}_e}$ [6]. Experimentally, KATRIN uses a Magnetic Adiabatic Collimation with an Electrostatic filter (MAC-E) [84, 97] for the measurement of the kinetic energy of the decay electron which combines a high luminosity and excellent energy resolution with a low background level. Two superconducting solenoids create a magnetic guiding field for the decay electrons with a geometry such that the magnetic field in the center of the spectrometer is by several orders of magnitude smaller than at the position of the solenoids. As the electrons travel along the magnetic field lines, the energy in their cyclotron motion (transversal motion) is mostly transformed into their longitudinal motion. Electrodes in the analyzing plane of the energy filter can be used to block and reflect electrons with lower energy as only the most energetic electrons can pass the potential barrier. The electrons that can pass this electrostatic

barrier are guided onto a detector and the integral of the spectrum above the potential barrier is measured. The differential spectrum in the endpoint region is constructed by scanning the retarding potential. The endpoint region is the most crucial part of the spectrum since close to the endpoint, where the electrons have the highest possible energy, the anti electron neutrino will be emitted (almost) at rest having only its rest mass. A range of $-40\,\text{eV}$ to $+130\,\text{eV}$ around the endpoint is used in the analysis where a theoretical prediction of the spectral shape is fitted from which the neutrino mass is extracted. Ultimately, projected for 2025, KATRIN aims at a sensitivity of $0.2\,\text{eV}/c^2$ on the neutrino mass [7].

PROJECT 8   Like KATRIN, the Project 8 experiment also investigates the tritium beta decay (cf. Equation 1.7) but using the Cyclotron Radiation Emission Spectroscopy (CRES) technique [11, 26, 87]. The CRES technique relies on the measurement of the cyclotron radiation frequency in a magnetic field which allows the determination of the decay electron energy. For this a gaseous tritium source is located in a magnetic field of about $1\,\text{T}$. Following a decay, the released electron moves on a cyclotron orbit radiating cyclotron radiation which is picked up by cryogenic antennas. Compared to MAC-E filters this has the advantage that the entire differential spectrum at the endpoint is measured simultaneously without scanning. The signals from lower energy decay electrons can be efficiently filtered using a low-pass. As for KATRIN, the source with molecular tritium leads to a line broadening limiting the resolution. In the future an atomic tritium source will be used and a larger volume for tritium in order to have a high number of decays. In 2023, Project 8 published the first neutrino mass limit using the CRES technique at $m_{\nu_e} < 155\,\text{eV}/c^2$ [32]. Ultimately, Project 8 aims at a sensitivity of $40\,\text{meV}/c^2$ [31].

CALORIMETRY BASED MEASUREMENTS ON ^{163}Ho: ECHO AND HOLMES Both ECHo [61, 121] and HOLMES [21] are complementary experiments to KATRIN and Project 8 and investigate the electron capture in ^{163}Ho which has an even smaller Q-value than ^{3}H and is therefore ideal for neutrino mass measurements. In an electron capture decay an electron neutrino instead of an anti-electron neutrino for β-decay is emitted. Furthermore, the decay spectrum features several resonances originating from the capture from different atomic shells. One of the resonances is close to the endpoint region which enhances the count rate in this crucial part of the spectrum.

The two experiments employ cryogenic microcalorimeters where ECHo uses a Metallic Magnetic Calorimeter (MMC) while HOLMES uses Transition Edge Sensor (TES) calorimeters. A schematic of an MMC calorimeter is given in Figure 1.2.
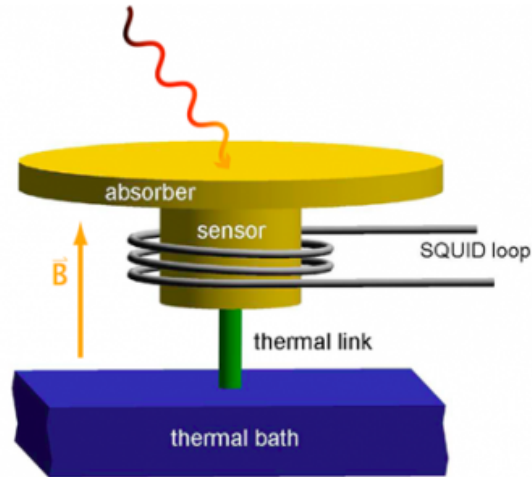
Figure 1.2: Schematic of an MMC calorimeter to illustrate the principle. The ^{163}Ho atoms are implanted directly into the absorber material of the detector ensuring that the emitted radiation is fully absorbed. Following the absorption of decay radiation the temperature of the absorber increases. This temperature increase is measured using a paramagnetic temperature sensor that is located in a weak magnetic field. The change in magnetization is finally read-out using a Superconducting Quantum Interference Device (SQUID) magnetometer [56]. Figure taken from [57].

By implanting the ^{163}Ho directly in the gold absorber material both experiments ensure that all emitted radiation in a decay is absorbed in the calorimeter resulting in an integral measurement of the decay spectrum. Following the absorption, the temperature change of the absorber is measured with a paramagnetic temperature sensor that changes the magnetization which is read-out using a SQUID magnetometer [56]. Using MMCs, it was demonstrated that a very good energy resolution of about 1.6 eV (Full Width at Half Maximum (FWHM)) at a particle energy of 5.9 keV can be achieved [61].

The first neutrino mass determination from the ECHo collaboration using these detectors yielded a limit of $m_{\nu_e} < 150\,\text{eV}/c^2$ (95% C.L.) [121]. The decay spectrum from this measurement is shown in Figure 1.3 alongside with the fits of a theoretically calculated spectral shape to the data. From the fit, the neutrino mass as well as the Q-value of the decay can be extracted. The Q-value from the calorimetric measurement is $Q = 2838(14)\,\text{eV}/c^2$ and in very good agreement with the Q-value measured in the independent measurement at the Penning-trap mass spectrometer SHIPTRAP of $Q = 2833(34)\,\text{eV}/c^2$ [46]. From this agreement, systematic uncertainties due to the decay happening within the solid of the gold absorber material can be excluded on the current sensitivity level.

For the next phase of the ECHo experiment where a higher activity is used, the higher statistics and therefore higher sensitivity to the neutrino mass requires a refined independent measurement of this
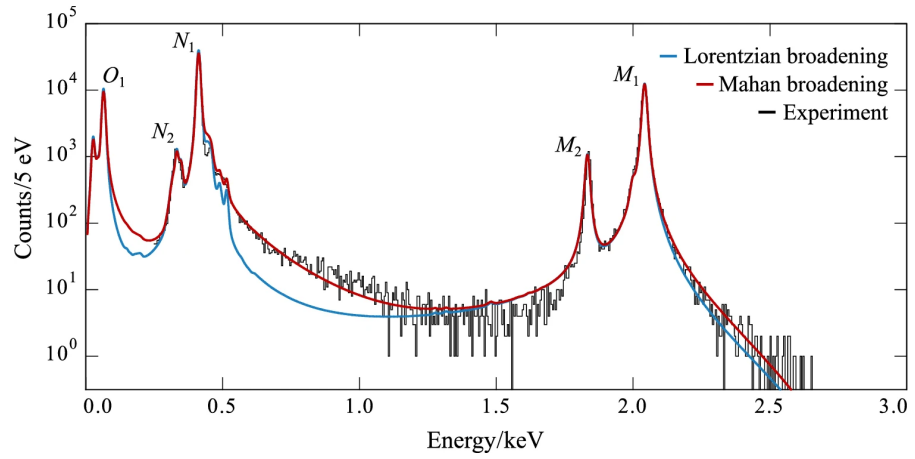
Figure 1.3: Measured decay spectrum of ^{163}Ho from the ECHo experiment showing the data along with fits of theoretically calculated spectral shapes. Figure taken from [121].

Q-value with an uncertainty of less than 10 eV [61] which is the main motivation for this dissertation.

EXPERIMENTAL METHODS

For the measurement of the Q-value of the electron capture in ^{163}Ho, several experimental developments have been made in the scope of this thesis. This Chapter will provide an overview of the Pentatrap experiment, summarize the contributions to the Pentatrap experimental setup within this thesis and introduce the experimental methods used. Additionally, the three publications on which this cumulative thesis is based (see Chapter 3) are put in context with the complete experiment.

The first Section 2.1, covers the production of highly charged ions (HCIs) of ^{163}Ho for this particular measurement and introduces one method for the separation of individual charge states. In the following Section 2.2 the principles of PTMS are summarized. Finally, Section 2.2.1 provides a description of the ion detection technique used at Pentatrap and the frequency measurement techniques that are used within this work. Section 2.2.2 concludes this with a short summary of the data analysis and the final Q_{EC}-value calculation.

Pentatrap is a high-precision multi-Penning-trap (PT) mass spectrometer designed for mass measurements on HCIs. An overview of the Pentatrap experimental setup is given in Figure 2.1. HCIs are produced in and extracted from the TIP-EBIT at a beam energy of about 4 keV. Subsequently, the HCIs are guided through the connecting beamline and directed, using an electrostatic bender [77], towards the five PTs inside the 7 T superconducting magnet. In the scope of this thesis the complete horizontal section was developed and constructed. This includes the development and commissioning of an injection technique for rare species for the TIP-EBIT and the development and construction of the connecting beamline, including the development of a Bradbury-Nielsen beamgate (Bradbury-Nielsen-Gate (BNG)) and a sufficiently fast electronic switching circuit for the BNG.

2.1 CREATION OF HIGHLY CHARGED IONS IN ELECTRON BEAM ION TRAPS

HCIs can be efficiently created by electron impact ionization of atoms using highly energetic electrons. This principle is used in an Electron Beam Ion Trap (EBIT) where a high-current (in this case tens of mA), high-energy electron beam (few keV) is impinged on a gaseous atomic sample, typically injected into the residual gas of the vacuum system. The electron beam is additionally compressed using a strong inhomogeneous magnetic field to further increase the current density in
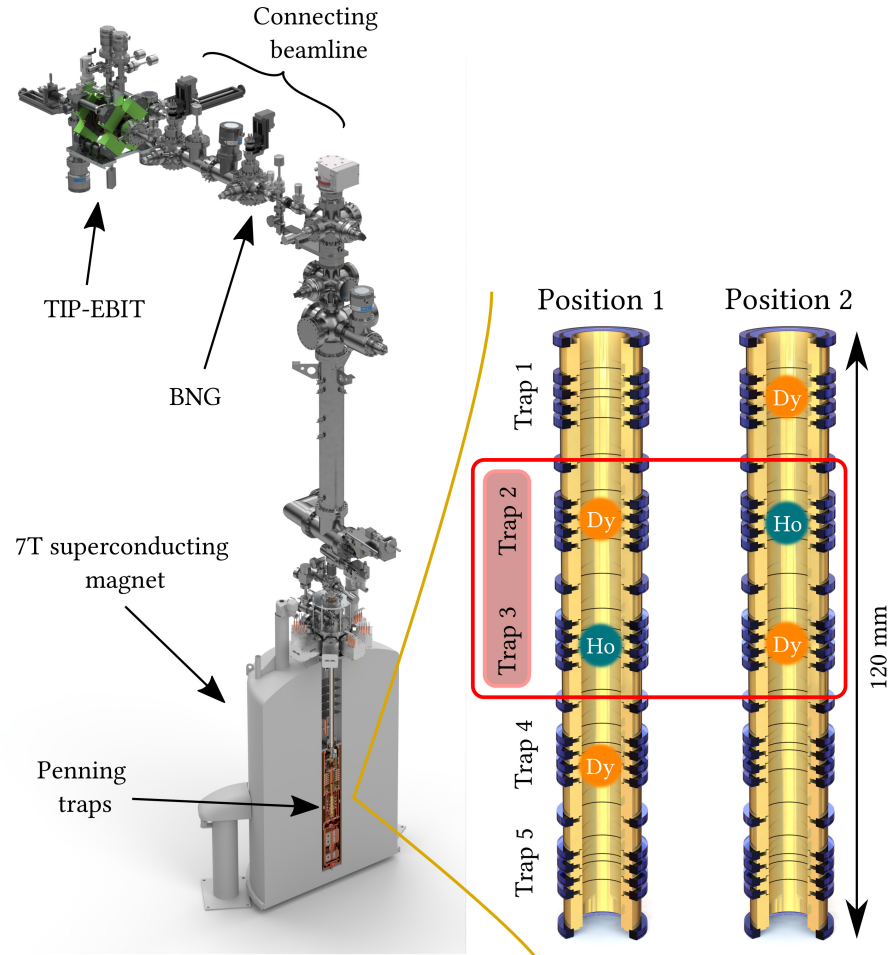
Figure 2.1: Rendered overview of the PENTATRAP experimental setup. The HCIs are extracted from the "TIP-EBIT" and guided through the connecting beamline. An individual charge state is selected using a BNG before the HCIs are directed towards the superconducting magnet. The five PTs of the PENTATRAP experiment are located in the cold bore of the 7 T superconducting magnet in a dedicated room in the basement of the building. Two of the five Penning traps (Trap 2 and 3) are fitted with a detection system and are used for the measurements (red box). For details see main text. The magnified Penning traps on the right side are reproduced from [79].

the target region to yield a higher ionization rate. Ions created by electron impact ionization are trapped radially by the space charge of the electron beam (assisted by the magnetic field) and axially using a set of electrodes with suitable applied voltages. The electrode on the collector side of the EBIT (see Figure 2.2) can be switched in order to extract and accelerate the HCIs from the trapping region of the EBIT for use in other experiments. Since the created ions are trapped within the high density and high energy electron beam, subsequent ionizing collisions sequentially ionize the ions into high charge states. In principle, ionization is possible until the ionization energy for the next higher charge state is greater than the electron beam energy. Realistically, several processes limit the highest achievable charge state and the overall evolution of the charge states can be described with a rate equation model. Mainly limiting the highest achievable charge state are charge exchange, radiative recombination and dielectronic recombination [110]. The time during which the series of subsequent ionizing collisions takes place is called the "charge breeding time". This time is defined as the duration between two ion extraction events and starts with a just emptied trap and ends with the ejection. Experimentally, a steady-state charge state distribution can be extracted reproducibly by choosing a charge breeding time longer than the necessary time to reach an equilibrium between ionization and recombination processes. When choosing a shorter charge breeding time it is possible to also vary the extracted charge states by extracting earlier or later. Following the extraction, the HCIs are guided through the electrostatic beamline towards the Penning traps (c.f. 2.1).

2.1.1 *Injection techniques*

In EBITs, the species of interest is usually injected into the residual gas close to the trapping volume where the electron beam drives the ionization process. This method is extensively used for species that are either available in gaseous form or in form of volatile organic compounds [75]. When using this method relatively large quantities of the sample material are required. For the physics case of interest, ^{163}Ho, this is a challenging task since it is a synthetic radioisotope with a half life of 4570 ± 25 years [70]. It therefore has to be artificially produced and only limited quantities, about 10^{16} atoms (corresponding to 2.7 μg), are available for the mass measurement. First experiments with the Heidelberg Compact Electron Beam Ion Trap (HC-EBIT) [86] constructed and commissioned in [110] have been attempted using the so called "wire-probe"-method [48] which were not successful. A very efficient injection method was therefore developed in the scope of this thesis which allows the injection of tiny samples into the trapping volume of an EBIT by means of laser desorption [111].
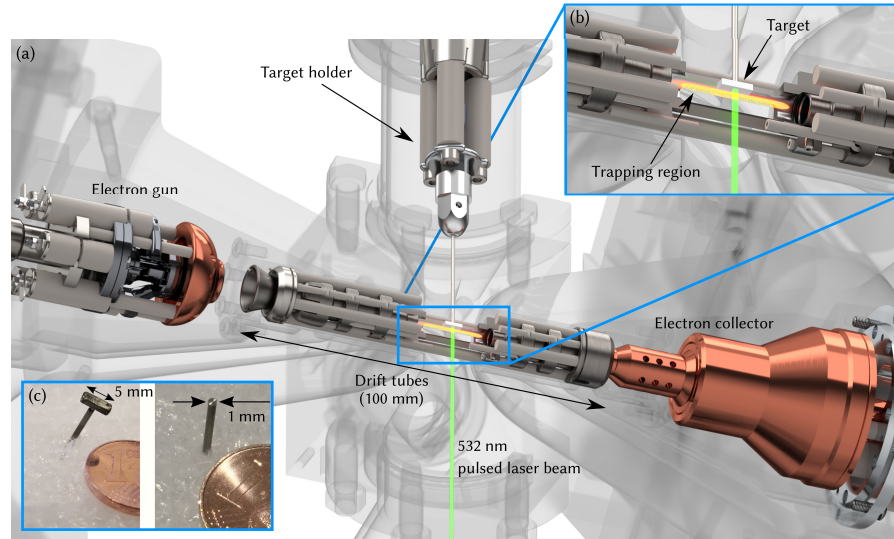
Figure 2.2: Concept of laser-induced desorption close to the trapping volume in a HC-EBIT. (a) General overview showing a rendering of the HC-EBIT with the electron gun on the left, the stack of drift tubes in the center and the electron collector on the right hand side. From the top, a target holder with the species of interest on the tip is moved into trapping region of the HC-EBIT. Part (b) shows a cut through the central drift tube where the HCIs can be seen as an orange cloud in the trapping volume. The target is shown in a position close to the trapping region with the 532 nm laser beam impinging on the target surface. (c) presents two of the used target geometries. The left one is about 5 times 2 mm in size for larger samples, e.g. metal foils which can be spot-welded onto the surface, while the 1 mm diameter target on the right consists just of a turned flat titanium wire with the species of interest on the front surface. The first target geometry can also be used when several species are required which can be prepared on the surface. Figure taken from [111].

This method uses laser-induced desorption very close to the trapping volume within an EBIT. The general idea of this method is shown in Figure 2.2. Using a sample holder that is connected to a three-dimensional manipulator the sample can be precisely and accurately positioned very close to the trapping volume in the EBIT. With a single triggered pulse from a 532 nm pulsed Nd:YAG laser (about 1 mJ), some atoms and ions are desorbed from the target surface directly into the trapping volume of the EBIT, where they are rapidly ionized by the electron beam. Owing to the type of injection - having the sample material on a "tip" that is moved close to the trapping region, this HC-EBIT is named the "TIP-EBIT". Several different target geometries have been tested, two of which are shown in Figure 2.2 (c). Larger targets such as metal foils, can be attached or spot welded to the front of the left target holder which has a surface area of 5 times 2 mm. In particular, this target geometry can also hold multiple species at the same time as was done for the Q_{EC}-value measurement. Switching between the species is then accomplished by moving the laser spot with a piezo controlled mirror and observing the laser spot on the target using a camera. The right target holder is mainly used for very exotic targets where only the smallest quantities are available (down to about 10^{12} atoms).

Different target preparation techniques were developed and used based on the amount of available material and its physical and chemical properties. Some of the species tested and the preparation techniques used are summarized in Table 2.1.

For very rare species where about 10^{16} down to 10^{12} atoms are available, the "drop-on-demand" printing technique is used [65]. Here, small, nanoliter sized droplets of a solution of the species of interest are dried on the target surface. This technique was used for ^{163}Ho, cf. 2.1 and was first tested with the stable ^{165}Ho isotope on targets as shown in Figure 2.2 (c), right side.

Species that are available in microgram to milligram amounts can be prepared in conically shaped deepenings on the surface of the target holder. For these cases, the so called "PLA targets" have been developed, where the species of interest (here enriched ^{163}Dy in oxide form was used) is bound within the polymer Polylactic Acid (PLA). For the preparation lactic acid is warmed up in a test tube until just below the boiling point where it starts polymerizing into PLA. Every few minutes the lactic acid is cooled down by putting the test tube in cold water and the viscosity is checked. Ideally the partially polymerized lactic acid should be a little bit more viscous than honey for the target preparation. A very small drop of the partially polymerized PLA is then mixed with the sample material, e.g. the ^{163}Dy and applied into the deepenings on the target holder. The partial polymerization is crucial, otherwise it can happen that when the prepared sample is applied on the target holder, the species of interest sinks to the bottom

Species	Amount	Chemical form	Preparation technique
^{163}Ho	10^{15} atoms	$Ho\,(NO_3)_3$	Solution is dried on the surface [65]
^{163}Dy	μg, enriched	Dy_2O_3	Enriched dysprosium oxide powder bound in PLA.
^{208}Pb/^{209}Bi	bulk material	atomic	mechanically fixed into drilled hole
^{238}U	mg	UO_2	oxide powder bound in PLA
$^{168-176}$Yb	mg	Yb_2O_3	oxide powder bound in PLA

Table 2.1: Summary of the tested sample preparation techniques and target geometries. For details see text.

of the liquid PLA and is not equally distributed following the final curing. Following the application of the sample, the target is cured in a small oven at about 120 degree celsius for six to eight hours to fully polymerize the PLA and fix the species within the polymer and on the target. This preparation technique did not show issues regarding possible outgassing of the polymer within the EBIT vacuum.

For species, that are available in large quantities (e.g. solid "bulk material"), the preparation simplifies to fixing it onto the target holder. This technique can be used for metal foils which can be often spot-welded onto the target holder or attached with something electrically conducting (e.g. by mixing small aluminum particles into the epoxide) and vacuum compatible epoxide glue. Materials that are easy to deform can be pressed into small holes in the target, as used e.g. for ^{208}Pb and ^{209}Bi, cf. 2.1.

Additionally, the EBIT was constructed with a two-stage, differentially pumped gas injection system that was constructed in order to inject gaseous species in form of an atomic beam directed towards the trapping volume of the EBIT without influencing the main vacuum.

With this technique, PENTATRAP has the possibility to use species in almost any available sample size and can choose from a variety of preparation techniques matched to each sample size.

The targets used for the measurement of the Q_{EC}-value with PENTA-TRAP were prepared using the first two methods shown in Table 2.1. The PLA preparation technique was specifically developed for enriched
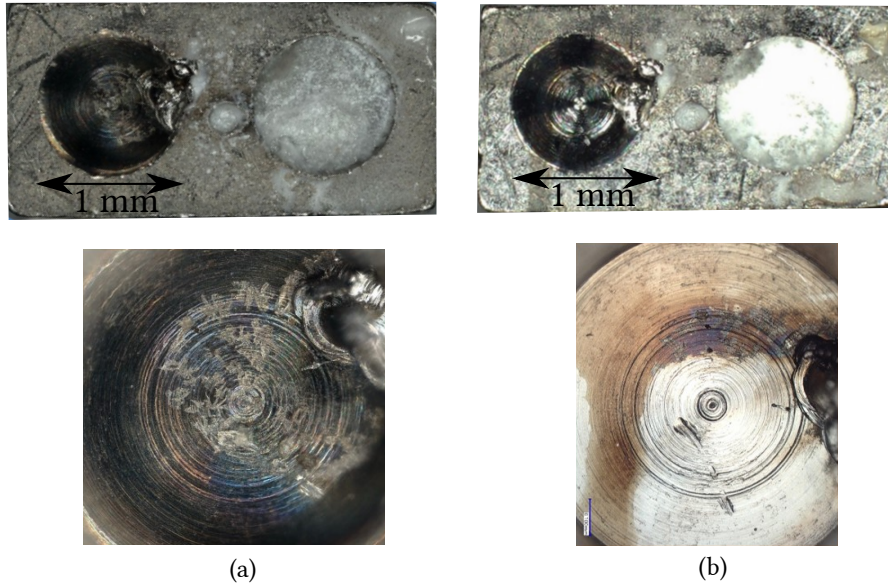
(a)   (b)

Figure 2.3: The first target with both species ^{163}Ho and ^{163}Dy prepared on the surface which was used in the measurement campaign. (a) shows the prepared target where ^{163}Ho is deposited in the small deepening on the left side while the ^{163}Dy is prepared in oxide form within polymerized PLA. In this first target there is also some of the PLA distributed around the deepening. Below the full target a closer view on the area where ^{163}Ho is deposited is shown. The ^{163}Ho was deposited in nanoliter sized droplets of a holmium nitrate solution on the surface [65]. When the water evaporated from the solution holmium nitrate crystals form on the surface which are visible with a microscope. Here, about 10^{14} atoms of ^{163}Ho are prepared on the surface. (b) illustrates the same target after use. There is still plenty of the ^{163}Dy in the deepening while the crystals of holmium nitrate are no longer visible following the laser desorption.

^{163}Dy in oxide form within this thesis. One of these targets is shown in Figure 2.3 where the left side (a) shows the freshly prepared target and the right side (b) the target surface following depletion of the target. Comparing the new target (a) with the used target in (b) illustrates the vast amount of ^{163}Dy that is available (μg) compared to the 10^{14} atoms of ^{163}Ho. The developed injection technique was published in *Review of Scientific Instruments* and is attached in Section 3.1.

2.1.2 *Charge state separation*

For PENTATRAP only a single HCI with the correct charge state is stored in the PT, i.e. a HCI with the correct mass-to-charge ratio. For this measurement, isotopically enriched ^{163}Ho and ^{163}Dy samples were used. The selection of the correct charge state thus requires only moderate resolving powers on the order of $\Delta R / R \simeq 40$ for which

PEEK insulators
first set of wires

Silvered multistrand
connecting wire

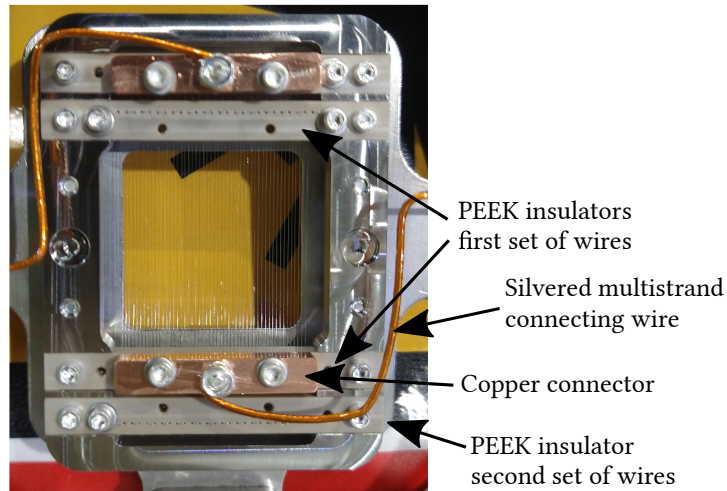Copper connector

PEEK insulator
second set of wires

Figure 2.4: Picture of the developed BNG for charge state separation. The flight direction of the HCIs is into or out of the paper plane. The two sets of wires are visible, one is wound through the inner set of PEEK insulators, the other through the outer set. Visible are as well the two copper blocks that connect all wires of each set at the same time which helps in fast switching of the potential on the wires. For this picture a screening plate was removed which blocks HCIs that would collide with the PEEK insulators. Figure taken from [112].

the Time of Flight (ToF) separation aquired while passing through the horizontal part of the beamline is sufficient. With a length of about 2.25 m, individual charge states are separated by about 70 ns which is sufficient to select charge states using a Bradbury-Nielsen gate (BNG). With a BNG the unwanted species can be deflected while it allows the correct charge state to pass [22, 25, 126].

A picture of the BNG is shown in Figure 2.4. It consists of two sets of parallel wires aranged alternately and placed perpendicular to the ion beam direction. As long as both sets of wires are at ground potential the ion beam can pass the BNG with a high transmission. However, as soon as potentials with opposite polarity are applied to the two sets of wires, the ion beam is deflected. The plane with the wires having alternating polarity in a BNG has several advantages compared to switching an electrode:

- The electric field is only present very close to the wires and influences the flight path of the ions of interest only weakly.

- A set of wires has a small capacity allowing for a very fast change of the potential applied to the wires.

A specific charge state is separated by always applying a potential to the wires except for the short period of time when the charge state of interest comes close and passes through the set of wires. For this period of time the wires are switched to ground potential with a fast

switching electronic circuit. The BNG as well as the fast switching electronic circuit were developed within the scope of this thesis. The fast switching electronic circuit was published in *Reviews of Scintific Instruments*, see Section 3.2.

2.2 PENNING TRAP MASS SPECTROMETRY

The highest precisions in mass spectrometry are reached using Penning trap (PT) mass spectrometers which are often engineered for specific mass ranges [66], long-lived and stable [15, 90, 98, 101, 104] or short-lived [40, 50, 89] isotopes, and use sophisticated ion detection and frequency measurement techniques [45, 53, 64, 91, 101, 124]. Stable and long-lived species of interest can be stored for days and weeks in a PT which allows for long observation times and exceptional control of the ion motion. A comprehensive overview of PTMS and the techniques used is given in [17].

The Penning trap mass spectrometer PENTATRAP is designed to achieve fractional uncertainties on the order of a few $\frac{\delta R}{R} \simeq 10^{-12}$ and is designed to use HCIs of the species of interest [104, 108, 114]. This can be advantageous compared to the use of singly charged ions:

- The free cyclotron frequency $\omega_c = qB/m$ scales with the charge state q of the ion. Therefore, the ion's frequency increases when a higher charge state is used, reducing the fractional uncertainty $\delta\nu = \Delta\nu/\nu$ of the frequency measurement when the uncertainty $\Delta\nu$ of the frequency measurement stays constant. [15]

- The HCI is confined to a smaller volume, thereby the systematic uncertainties due to field imperfections are reduced.

- A higher charge state results in a larger image current being induced in the PT electrodes and therefore improves the Signal to Noise Ratio (SNR) ratio [17] and allows smaller excitations during the measurement.

- The cooling of the ion's motions is faster reducing the measurement cycle time.

THE IDEAL PENNING TRAP   Mass measurements in a PT rely on the precise determination of the free-space cyclotron frequency ν_c of an ion of mass m and charge q in a static homogenous magnetic field $\vec{B} = B \cdot \vec{e}_z$:

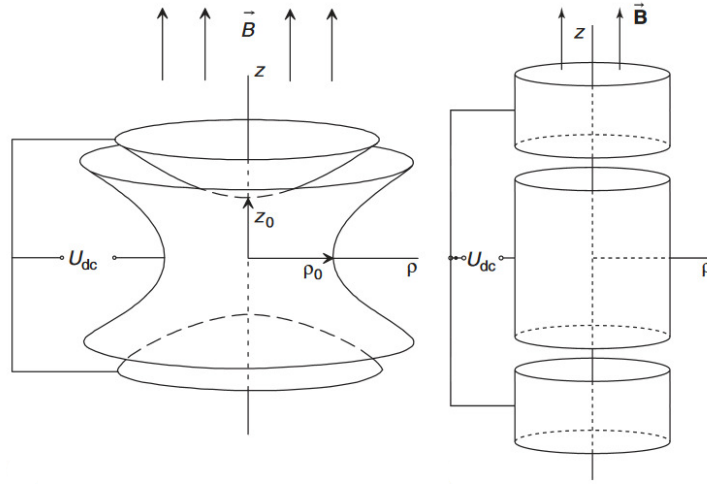$$\nu_c = \frac{1}{2\pi}\frac{q}{m}B. \tag{2.1}$$

Figure 2.5: Schematic of two possible electrode configurations for a PT. The left electrode configuration is a "hyperbolic trap" where the electrode shape resembles the equipotential lines of the electrostatic potential. The right electrode configuration shows a "cylindrical trap" which can also produce a quadrupolar field geometry close to the center of the trap with a carefully chosen trap geometry and the use of additional correction electrodes [59]. For both configurations, the upper and lower electrodes are called "endcap" electrodes while the central one is named the "ring electrode". The cylindrical trap geometry is more commonly used today and is also employed in the PENTATRAP experiment where it simplifies the transport from one trap to another. The inner radius of a trap at PENTATRAP is $\rho = 5\,\mathrm{mm}$ [108]. Figure taken from [17].

The magnetic field is typically not known with sufficient precision and the free-space cyclotron frequency of the ion of interest ($\nu_{c,\mathrm{IOI}}$) is compared to a reference ion ($\nu_{c,\mathrm{RI}}$) in (ideally) the same magnetic field

$$\frac{m_{\mathrm{IOI}}}{m_{\mathrm{RI}}} = \frac{\nu_{c,\mathrm{RI}}}{\nu_{c,\mathrm{IOI}}} \frac{q_{\mathrm{IOI}}}{q_{\mathrm{RI}}} = R, \tag{2.2}$$

yielding the mass ratio of the two ions. If both ions are in the same charge state, the cyclotron frequency ratio R is the inverse of the mass ratio.

The magnetic field forces the ion on a circular orbit and provides the radial confinement but still allows the ion to escape along the magnetic field lines. Long observation times require a confinement also along the magnetic field lines which is possible by a superposition of an additional quadrupolar electrostatic field. The field is generated by either of the two electrode configurations shown in Figure 2.5 and voltage U_{dc} applied between the electrodes.

The superposition of both confining fields results in three independent harmonic eigenmotions of the ion: the modified cyclotron

motion (with respective frequency ν_+), the axial motion (ν_z) and the magnetron motion (ν_-) [17]:

$$\nu_\pm = \frac{\nu_c}{2} \pm \sqrt{\frac{\nu_c^2}{4} - \frac{\nu_z^2}{2}} \tag{2.3}$$

$$\nu_z = \frac{1}{2\pi} \sqrt{\frac{qU_{\mathrm{dc}}}{m} 2c_2}. \tag{2.4}$$

Here, U_{dc} is the potential applied between the ring and endcap electrodes, defining the depth of the axial trapping potential and thereby the axial frequency. c_2 is a parameter that reflects the strength of the hyperbolic potential in the center of a cylindrical PT with respect to the applied voltage.

There is a distinct order of the three eigenfrequencies with the modified cyclotron frequency being the fastest motion (26.4 MHz at PENTATRAP for ^{163}Ho) followed by the axial motion (740.3 kHz) and the slowest being the magnetron motion (10.4 kHz).

Using the invariance theorem [23]

$$\nu_c^2 = \nu_+^2 + \nu_z^2 + \nu_-^2, \tag{2.5}$$

the free-space cyclotron frequency of the HCI in the trap can be reconstructed from a measurement of the three eigenfrequencies. The invariance theorem is furthermore insensitive to a tilt between the magnetic field and quadrupolar electrostatic field and to an elliptic deformation of the electrostatic field to first order.

THE REAL PENNING TRAP   In the ideal PT described above, all three eigenmotions are harmonic, i.e. the motional frequencies do not change with the amplitude of the ion motion. In a real PT, field imperfections of both, the electrostatic quadrupolar field and of the homogenous magnetic field distort the ideal potential shape resulting in amplitude dependent shifts of the eigenfrequencies which can be a limiting systematic effect of a mass measurement. These frequency shifts can be quantified by an expansion of the electrostatic potential in Legendre polynomials (and similarly for the magnetic field) [73]. For small motional amplitudes and similar mass-to-charge ratios of the HCIs this effect cancels in the ratio of the free-space cyclotron frequencies [54, 90].

Moreover, the trapping voltage U_{dc} or the magnetic field $\vec{B}$ can change over time e.g. due to the influence of environmental parameters such as the temperature. Since the quantity that is measured, the motional frequencies of the ion in a superposition of confining fields, it is of vital importance for high precision mass spectrometry to keep these fields as constant as possible during the measurement time. At PENTATRAP several measures are taken in order to ensure that the trapping fields are as stable as possible:

- An ultra-stable voltage source "STAREP" is used for the generation of the voltages applied to the PT electrodes [19, 27].

- The laboratory housing the superconducting magnet with the PTs and the STAREP is temperature stabilized [78].

- Within the laboratory the superconducting magnet is resting on an as much as possible vibration-free floor.

- A stabilization system for the liquid helium level around the Penning trap vacuum chamber and for the gaseous helium pressure above it was implemented [15, 19, 78, 106]. This system suppresses the magnetic field changes related to the temperature dependent susceptibility of the materials directly surrounding the PTs. This effect was first reported in [43] and led to the development of a stabilization system for the PT mass spectrometer SMILETRAP [15] which used HCIs as well.

- Measurements are typically run during night time or over a weekend which reduces external magnetic field fluctuations resulting e.g. from the elevator in the building and other external sources.

When these environmental influences are stabilized the variation of the magnetic field is reduced to a linear decay which is taken into account in the data analysis (see Section 2.2.2). This decay of the magnetic field originates from the flux creep effect [8, 9] and can be approximated linearly for reasonable measurement times [17].

2.2.1   *Ion detection and frequency measurement techniques*

At PENTATRAP, the trapped ion's axial motion is detected via the image currents that it induces in the PT electrodes while oscillating in the trap. The induced image current of the axial motion is picked up with a tuned resonance circuit with a high quality factor [24, 53, 91, 124] and subsequently amplified using a cryogenic amplifier [104]. When the ion's axial motion is in resonance with the circuit, the ion dissipates motional energy into the circuit until it is in thermal equilibrium [24, 124]. Also the amplitudes of the radial modes can be reduced by resonant coupling of a radial to the axial mode [35]. A low temperature is favorable since the trapped ion is less exposed to electric and magnetic field imperfections. Following the amplification, the signal is Fourier transformed and the ion can be observed as a "dip" in the noise spectrum of the resonant circuit ("dip technique"). The position of this "dip" in the frequency spectrum corresponds directly to the axial frequency of the ion. When the sideband coupling is applied also the radial frequencies can be measured using this method ("double dip").

Due to the distinct frequency hierarchy, when the invariance theorem is used, the uncertainty of the modified cyclotron frequency has the highest contribution to the final uncertainty and needs to be measured with the highest precision. The modified cyclotron frequency is therefore measured using the phase sensitive Pulse and Phase (PNP) technique [34] while the axial frequency is measured during the phase evolution time using the dip technique. Being the smallest of the three frequencies, the magnetron frequency has the least contribution to the total uncertainty on the free-space cyclotron frequency and is therefore measured only once per day using the double dip technique.

For the Q-value measurement, HCIs of ^{163}Ho and ^{163}Dy are loaded into the PTs in the sequence shown in Figure 2.1. Four of the five PTs are used in this measurement where Trap 1 and Trap 4 serve as storage traps while Traps 2 and 3 are fitted with a detection system. Starting in Position 1 the motional frequencies are measured in both traps simultaneously, then the ions are shuttled into Position 2 and the measurement is repeated. The shuttling effectively swaps the ions in Traps 2 and 3 and when repeating this sequence alternating measurements of the two species are performed in each of the two traps. The measurement in two traps effectively doubles the statistics while it also allows comparing the cyclotron frequency ratios obtained in both traps in order to assess systematic shifts.

2.2.2 *From frequency measurement to the Q_{EC}-value*

The Q-value of the electron capture in ^{163}Ho is finally determined by the following relation:

$$Q = m_{\mathrm{Dy}}^{q+} (R - 1) + \Delta E_B. \tag{2.6}$$

Here, m_{Dy}^{q+} is the (reference) mass of the HCI of dysprosium, $R = \nu_c(^{163}\mathrm{Dy})/\nu_c(^{163}\mathrm{Ho})$ the cyclotron frequency ratio and ΔE_B the difference in the sum of binding energies of the n missing electrons in the HCIs of both species. m_{Dy}^{q+} is calculated starting from the mass of the neutral dysprosium atom [122] and subtracting the mass of the n missing electrons [116, 120] as well as their respective binding energies [76].

The cyclotron frequency ratio R is determined from the alternating datapoints in the frequency measurement by linear interpolation as shown in Figure 2.6. From the linearly interpolated datapoint between the first two ^{163}Dy datapoints and the first ^{163}Ho datapoint the cyclotron frequency ratio is determined. This technique is used throughout the dataset yielding a set of ratios from which the weighted mean is determined. The uncertainty is determined by calculating the inner and outer errors [16, 92] and using the larger one as final uncertainty for the datset. This technique was compared to the also well
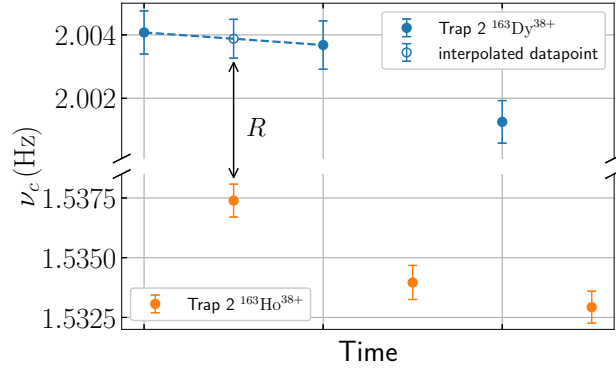
Figure 2.6: Detailed plot of the first few datapoints of a measurement. From the frequency values an offset of 25081589 Hz is subtracted. Between the first two ^{163}Dy datapoints the frequency is linearly interpolated to the time at which ^{163}Ho was measured. From the interpolated datapoint the ratio is then determined. Figure taken from [113].

established analysis technique using polynomial fits [39] and agrees very well [54].

SYSTEMATIC UNCERTAINTIES ^{163}Ho and ^{163}Dy form a perfect "mass doublet", i.e. the difference in charge-to-mass ratio is very small, in this case on the order of only a few 10^{-8}. This small difference allows the same trapping potentials to be used for both species on the PT electrodes and also the excitation frequencies are sufficiently similar and thus it can be assumed that also the excitation radii are the same. Therefore, when the cyclotron frequency ratio is calculated, the systematic effects cancel out which is a great advantage when a mass doublet is measured. A table with the considered systematic uncertainties is given in the publication in Section 3.3.

In addition to the systematic uncertainties in the determination of the cyclotron frequency ratio R, the independent simultaneous measurement in two PTs allows the comparison of the determined cyclotron frequency ratios R from two measurements. For instance, systematic shifts of the motional frequencies due to a contaminant HCI in one trap can be detected when the determined cyclotron frequency ratios R of both traps do not agree. This allows to exclude systematic effects due to ion-ion interactions to a large extent. Similarly, a systematic disagreement of the cyclotron frequency ratio in the two traps in different measurement runs can also point to a HCI being in an electronically excited metastable state. Finally, in the measurement of the ^{163}Ho and ^{163}Dy Q-value the charge states $q = \{38, 39, 40\} \cdot e$ were measured. For the three charge states the final Q-values agree within the errorbar. Therefore systematic shifts of R and the theoretically calculated binding energy difference ΔE_B^{q+} can be ruled out since it is

very unlikely that the theoretical calculation compensates a possible systematic shift in R for all three charge states.

PUBLICATIONS

<div style="text-align: right">3</div>

In this section the three publications are listed on which is cumulative dissertation is based. The first two publications in Sections 3.1 and 3.2 summarize the developments on the production of HCIs of rare isotopes and the selection of individual charge states. The main result of this thesis is presented in the publication in Section 3.3 which reports on the measurement of the ^{163}Ho Q-value with the Penning trap mass spectrometer PENTATRAP.

3.1 PUBLICATION 1: PRODUCTION OF HIGHLY CHARGED IONS OF RARE SPECIES BY LASER-INDUCED DESORPTION INSIDE AN ELECTRON BEAM ION TRAP

In this article an injection technique for electron beam ion traps for using rare species is described. The article was published in *Review of Scientific Instruments*.

AUTHORS **Ch. Schweiger**, C.M. König, J.R. Crespo López-Urrutia, M. Door, H. Dorrer, Ch.E. Düllmann, S. Eliseev, P. Filianin, W. Huang, K. Kromer, P. Micke, M. Müller, D. Renisch, A. Rischka, R.X. Schüssler, K. Blaum

AUTHOR'S CONTRIBUTIONS **CS** and CMK conducted the experiment and took the data. **CS** analyzed the data and wrote the manuscript. All authors took part in the critical review of the manuscript before and after submission.

ABSTRACT This paper reports on the development and testing of a novel, highly efficient technique for the injection of very rare species into electron beam ion traps (EBITs) for the production of highly charged ions (HCI). It relies on in-trap laser-induced desorption of atoms from a sample brought very close to the electron beam resulting in a very high capture efficiency in the EBIT. We have demonstrated a steady production of HCI of the stable isotope ^{165}Ho from samples of only 10^{12} atoms ($\sim$ 300 pg) in charge states up to 45+. HCI of these

species can be subsequently extracted for use in other experiments or stored in the trapping volume of the EBIT for spectroscopic measurements. The high efficiency of this technique expands the range of rare isotope HCIs available for high-precision nuclear mass and spectroscopic measurements. A first application of this technique is the production of HCI of the synthetic radioisotope ^{163}Ho for a high-precision measurement of the Q_{EC}-value of the electron capture in ^{163}Ho within the "**E**lectron **C**apture in **Ho**lmium" experiment [60, 61] (ECHo collaboration) ultimately leading to a measurement of the electron neutrino mass with an uncertainty on the sub-eV level.

Production of highly charged ions of rare species by laser-induced desorption inside an electron beam ion trap SCI F
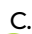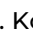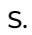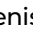
Ch. Schweiger,[1,a] iD C. M. König,[1,2] J. R. Crespo López-Urrutia,[1] iD M. Door,[1] iD H. Dorrer,[3] iD
Ch. E. Düllmann,[3,4,5] iD S. Eliseev,[1] P. Filianin,[1] iD W. Huang,[1] iD K. Kromer,[1,2] iD P. Micke,[1,6] iD
M. Müller,[1,2] iD D. Renisch,[3,4] iD A. Rischka,[1] iD R. X. Schüssler,[1] iD and K. Blaum[1] iD

AFFILIATIONS

[1] Max-Planck-Institut für Kernphysik, Saupfercheckweg 1, 69117 Heidelberg, Germany
[2] Fakultät für Physik und Astronomie, Universität Heidelberg, Im Neuenheimer Feld 226, 69120 Heidelberg, Germany
[3] Institut für Kernchemie, Johannes Gutenberg-Universität Mainz, Fritz-Strassmann-Weg 2, 55128 Mainz, Germany
[4] Helmholtz-Institut Mainz, Staudingerweg 18, 55128 Mainz, Germany
[5] GSI Helmholtzzentrum für Schwerionenforschung GmbH, Planckstraße 1, 64291 Darmstadt, Germany
[6] Physikalisch-Technische Bundesanstalt, Bundesallee 100, 38116 Braunschweig, Germany

[a] christoph.schweiger@mpi-hd.mpg.de

ABSTRACT

This paper reports on the development and testing of a novel, highly efficient technique for the injection of very rare species into electron beam ion traps (EBITs) for the production of highly charged ions (HCI). It relies on in-trap laser-induced desorption of atoms from a sample brought very close to the electron beam resulting in a very high capture efficiency in the EBIT. We have demonstrated a steady production of HCI of the stable isotope ^{165}Ho from samples of only 10^{12} atoms (~300 pg) in charge states up to 45+. HCI of these species can be subsequently extracted for use in other experiments or stored in the trapping volume of the EBIT for spectroscopic measurements. The high efficiency of this technique extends the range of rare isotope HCIs available for high-precision atomic mass and spectroscopic measurements. A first application of this technique is the production of HCI of the synthetic radioisotope ^{163}Ho for a high-precision measurement of the Q_{EC}-value of the electron capture in ^{163}Ho within the "**E**lectron **C**apture in **Ho**lmium" experiment [L. Gastaldo *et al.*, J. Low Temp. Phys. **176**, 876–884 (2014); L. Gastaldo *et al.*, Eur. Phys. J.: Spec. Top. **226**, 1623–1694 (2017)] (ECHo collaboration) ultimately leading to a measurement of the electron neutrino mass with an uncertainty on the sub electronvolt level.

Published under license by AIP Publishing. https://doi.org/10.1063/1.5128331

I. INTRODUCTION

Many experiments require access to highly charged ions (HCI) of species that cannot be found in nature and hence have to be synthesized in nuclear reactions at rare-ion-beam facilities[3,4] and research reactors.[5] These species can be produced only in very small quantities (rare species), often only in the subnanogram region. Applications requiring the production of HCI of these species include a direct test of the theory of special relativity,[6,7] involving a precise measurement of the neutron binding energy in ^{36}Cl by measuring the mass ratio of ^{35}Cl and ^{36}Cl, as well as high-precision mass

measurements of transuranium elements to establish new anchor points in α decay chains, thereby reducing the uncertainty in the masses of superheavy nuclides allowing the identification of nuclear shell closures.[8] High-precision mass measurements of HCI can furthermore support g-factor measurements[9] and searches for dark matter in high-resolution isotope shift measurements[10–12] using, e.g., enriched samples of rare Ca isotopes.

One of these experiments is the "**E**lectron **C**apture in **Ho**lmium" experiment[1,2] (ECHo collaboration) aiming at a measurement of the neutrino mass with an uncertainty on the sub electronvolt level. Since the discovery of neutrino oscillations,[13,14] establishing that

neutrinos have a finite mass, the measurement of the absolute scale of the neutrino mass remains a challenging task due to the exclusively weak interaction with other standard model particles and the small absolute mass scale. For an improvement towards the sub-electronvolt level, the ECHo collaboration calorimetrically measures a high statistics spectrum of the electron capture in ^{163}Ho. In the analysis of this spectrum, the precise knowledge of the energy available for the decay, Q_{EC}, from an independent source is required to investigate systematic effects in the calorimetric measurement. As the Q_{EC} value corresponds to the mass difference between mother and daughter nuclides, it can be directly accessed using a mass spectrometer. The required uncertainty of 1 eV, corresponding to a relative uncertainty of $\frac{\delta Q_{EC}}{m} \sim 6 \times 10^{-12}$, can currently only be reached using high-precision Penning-trap mass spectrometry.[15,16] The high-precision Penning-trap mass spectrometer PENTATRAP[17] has recently shown its capability to reach the required uncertainty using HCI of xenon, rhenium, and osmium.[18,19] ^{163}Ho is a synthetic radioisotope with a half-life of 4570(25) years of which only small amounts can be produced by the neutron irradiation of an enriched ^{162}Er target in a research reactor and subsequent chemical isolation.[5,20,21] In order to measure a high-statistics decay spectrum, as many of the produced ^{163}Ho atoms as possible are required for the calorimetric measurement and only a minor fraction of that amount (max. 10^{16} atoms corresponding to ~2.7 μg) is available for the direct Q_{EC}-value measurement.

HCI can be produced and studied in electron beam ion traps (EBITs),[22,23] which allow the production of a large variety of different species and charge states up to even the highest charge states of heavy elements.[24] EBITs are built for and operated at a broad range of electron beam energies starting from a few hundred electronvolts to a few hundred kiloelectronvolts. The EBITs operated at higher electron beam energies typically employ a superconducting magnet which generates a magnetic field with a maximum strength of several Tesla for the compression of the electron beam. In the last decades, EBITs operated at room-temperature have also been developed.[25–27] The magnetic field in these EBITs is created by means of permanent magnets, and therefore, less maintenance is required. The disadvantage is that the achievable vacuum pressures are higher than in cryogenic, superconducting EBITs resulting in a larger charge exchange rate and lower charge states. For stable isotopes that are available in gaseous form or as volatile, organic compounds, the injection into an EBIT is typically achieved using a differentially pumped injection system or by the introduction of a tiny leak into the vacuum system through which the species of interest are injected into the background gas. However, since the background gas in the vacuum system is flooded with the injected gas, a large quantity of the species introduced in the background gas is again pumped out of the system without being ionized and trapped by the electron beam. When HCI of very rare and radioactive species are required, a more efficient injection method has to be used in order to reduce the loss of the sample material. The PENTATRAP experiment requires, among others, HCI of the long-lived, synthetic radioisotope ^{163}Ho. Therefore, a dedicated Heidelberg compact EBIT[27] was constructed and an in-trap laser desorption source developed. This paper reports on the development of an in-trap laser desorption technique that allows the production of HCI from very rare isotopes available in sample sizes down to 10^{12} atoms.

II. METHODS

For the work presented in this paper, a Heidelberg compact electron beam ion trap[27] (HC-EBIT) was built for HCI production. The inhomogeneous magnetic field needed for electron-beam compression is generated by 24 stacks of 3 permanent magnets each and is guided and focused by soft-iron elements resulting in a magnetic field of around 850 mT in the 2 cm long trapping region. With a maximum of 10 keV electron beam energy and 80 mA electron beam current, a broad range of HCI in the medium to heavy mass region as well as bare nuclei of lighter elements are accessible. The background vacuum pressure in this room-temperature EBIT is typically in the lower 10^{-9} mbar region.

Using laser ablation, it is possible to ablate small amounts of atoms and singly charged ions from a surface with about 10^{16} atoms of ^{163}Ho.[8,28] To utilize the possibility of using very small samples, the laser ablation technique is implemented in the HC-EBIT to produce HCI of ^{163}Ho. In order to maximize the efficiency, the desorption process takes place at submillimeter distances from the electron beam in the trapping region using laser pulse energies below the ablation threshold. This results in a much higher yield than the use of an external, dedicated laser ablation ion source and the subsequent transfer and the capture of singly charged ions in the EBIT,[29] since laser ablation in those sources removes mostly neutral atoms from the surface and the small fraction of ions that is produced experiences losses in the aforementioned transfer and capture process in the EBIT. Our method brings a substantial fraction of the ablated atoms to the electron beam while needing less laser pulse energy than the laser ion sources, thereby reducing the amount of the material ablated per laser shot. Due to the lower power density on the target surface, it is likely that the process in which atoms are removed from the surface is no longer an ablation process and will be named desorption process in the following.

A rendered model of the basic setup is shown in Fig. 1. The outer, transparent parts are the vacuum chamber, and surrounding it are the permanent magnets and soft-iron elements guiding the magnetic field and shaping it around the trapping region. Inside the vacuum chamber, the electron gun is shown on the left, the electron collector on the right side, and the stack of drift tubes between them. HCIs stored in the EBIT are ejected by pulsing down the trapping potential applied to the drift tube on the collector side. Optical access to the trapping region is provided by four slotted apertures in the central drift tube (cut open in Fig. 1). From above, the target holder with the sample on the surface is lowered into the central drift tube very near to the trapping region (orange). Its position is adjusted using a three-axis, step-motor controlled manipulator. For desorption, we use a pulsed, frequency-doubled Nd:YAG laser with a few mJ pulse energy and 7 ns pulse duration at 532 nm pointed through a vacuum viewport at the target using a piezoelectric-driven mirror outside the vacuum. The spot diameter on the target is approximately 300–400 μm and was estimated by inspecting the target surface with a scanning electron microscope after it was used. Attached to the two remaining access ports to the trapping region (not visible in Fig. 1) are an x-ray detector (Ketek AXAS-D Vitus H50) and a gas injection setup.

For the identification of the produced ions and charge states a diagnostic setup consisting of a quadrupole lens, a dipole magnet and two detectors [microchannel plate (MCP) detector in Chevron
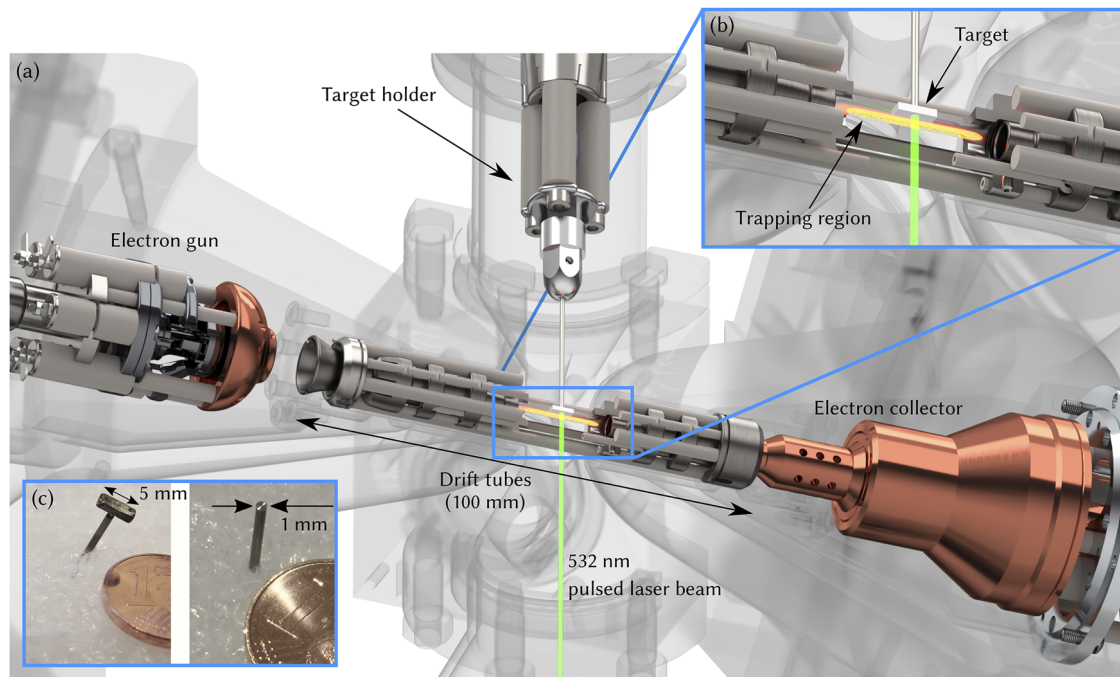
FIG. 1. (a) Model of the HC-EBIT with the in-trap laser desorption setup. The most relevant parts of the EBIT are the electron gun on the left, the stack of drift tubes in the center, and the electron collector on the right side. In order to show the arrangement for in-trap laser desorption, the central drift tube is cut open. Through a slit in the central drift tube, the electrically insulated target holder is moved from above into the central drift tube near to the trapping region (the position of the ion cloud is shown in orange) using a three-axis, step-motor controlled manipulator. The 532 nm pulsed laser beam (green) propagates along the vertical axis through the trapping region onto the target. This particular arrangement of the trapping region, laser target, and laser beam is shown in (b). (c) Pictures of the laser targets used for the commissioning of the in-trap laser desorption technique. The left one shows the "massive" target with a thin foil of stable holmium spot-welded onto the target holder surface (2×5 mm). The right side shows a laser target with 10^{12} atoms of ^{165}Ho prepared on the surface of a 1 mm thick titanium wire using the "Drop-on-Demand" ink-jet printing technique[30] as it was used for the presented measurements. The dried drop of the diluted solution is not visible by eye. A 1 cent coin is shown for size comparison.

configuration with a phosphor screen and a camera as well as a Faraday cup (FC)] is attached to the HC-EBIT as shown in Fig. 2. By detecting the ion signal on the MCP as a function of the field of the dipole magnet while scanning this parameter, an isotopically resolved charge-state spectrum of the produced species is obtained. The gain setting of the MCP was reduced in order to only detect HCI and suppress the background from ions in lower charge states. Initially, a reference species has to be measured in order to calibrate the dipole magnet, where in our case, xenon gas (natural isotopic composition) is injected into the background gas of the HC-EBIT using a gas dosing valve. In the obtained spectrum of natural xenon, the overlap of xenon isotopes from adjacent charge states allows the identification of the charge states and the calibration of the magnetic field to a charge-to-mass ratio.

Different targets [cf. Fig. 1(c)] containing the stable isotope ^{165}Ho were used for commissioning (natural holmium is monoisotopic). The target holder is manufactured from titanium and consists of a wire (1 mm diameter) and a 2×5 mm^2 titanium plate welded to its end. Initial tests were performed with a thin holmium foil which was spot-welded to the target holder giving a sample size that is almost infinite for our purposes. These tests showed that the operation of the HC-EBIT remains stable while a laser pulse is fired onto the target very close to the trapping region in the EBIT and

that desorbed atoms or ions are subsequently trapped and ionized to high charge states and remain trapped. The produced HCI of stable holmium were extracted and the charge states identified using the test setup (cf. Fig. 2) as described above.
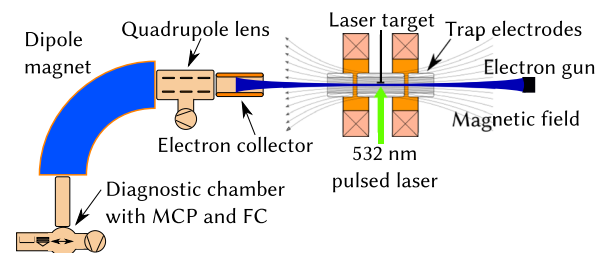
FIG. 2. Overview of the test setup for the commissioning of the in-trap laser desorption technique. The right side of the figure schematically shows the main parts of the HC-EBIT as described in Fig. 1 including the laser beam (green arrow) and the target (black). Ions ejected from the HC-EBIT pass through the electron collector and a quadrupole lens which is used for beam steering and focusing. The dipole magnet separates the ion bunches according to their charge-to-mass ratio, and the selected ion species is subsequently detected in the detector chamber fitted with a microchannel plate (MCP) detector and a Faraday cup (FC).

In the following, we used targets with a specific total number of holmium atoms deposited on the surface. For sample preparation, the "Drop-on-Demand" ink-jet printing technique[30] is used where a diluted standard solution of stable holmium is printed into one spot of the target. Note that the printed drop has a volume of just 8 nl and is visually not recognizable on the target surface [cf. Fig. 1(c)]. A total uncertainty of 3% of the number of atoms in the sample results from uncertainties of 2% in the drop volume, 2% in the solution concentration, and 1% due to aging of the solution, respectively. Since a smaller target surface significantly facilitates the adjustment of the laser spot onto the invisible sample, only the 1 mm diameter titanium wire (flattened on one side using a lathe) was used for the smallest samples. Titanium was chosen as the target holder material since it is a comparably light element and titanium HCI reach only lower charge states than the much heavier holmium HCI. This leads to selective evaporative cooling of titanium HCI and favors the accumulation of holmium HCI.[31]

For an efficient injection of atoms from the sample into the EBIT's trapping volume, the position of the target and the applied bias voltage are crucial. Fine positioning of the target into its final position is performed with the HC-EBIT in operation in order to monitor any changes in its performance caused by the target as it approaches the trapping region and the electron beam. At about 20 mm from the trapping region, the potential of the target is set to the same potential as the central drift tube to avoid a deflection of the electron beam and discharges when moving through the slot in the central drift tube. From here on, the target position in relation to the drift tubes is observed with a camera into the propagation direction of the laser. With the target inside the central drift tube, steps of about 100 μm are used to move it toward the electron beam. Following each step, the count rate on the x-ray detector and its spectrum are monitored to avoid moving the target into the electron beam which causes a considerable amount of bremsstrahlung. As soon as the count rate increases, the target is moved back by 100 μm and the bias voltage applied to the target is adjusted for the maximum extracted ion signal on the MCP. This ensures that the HCI-trapping potential is not perturbed by the presence of the target holder while reaching a minimum distance between the laser target and the electron beam.

For the extraction of ion bunches, the HC-EBIT is operated in cycles where the inventory of trapped HCI is extracted at regular intervals. In each cycle, the loading with a single laser pulse and HCI breeding are followed by a pulsed lowering of the potential of the trap electrode closest to the collector. The time interval when the trap is closed is referred to as the charge breeding time t_{br} and the short time during which the drift tube is pulsed to a lower potential as the ejection time t_{ejec}. For the measurements presented in Sec. III, the HC-EBIT was operated with a cycle time of 1.001 s of which the last $t_{ejec} = 5$ μs were reserved for the ion extraction. The laser pulse was triggered 1 ms after the cycle starts, leaving about $t_{br} = 1$ s for charge breeding of the injected atomic species.

For a new target, the lowest possible laser pulse energy setting should be used for positioning the laser spot onto the region where the species of interest is presumed to be on the target. This pulse energy setting can be found by monitoring the x-ray spectrum while the laser pulse energy is increased until a characteristic x-ray line of the injected species (shifted to higher energy since the species is quickly ionized to high charge states) is observed. The laser

positioning procedure is monitored again using the camera and thereby ensuring that the laser spot stays on the target surface while adjusting its position. Once the laser spot is positioned, the dipole magnet is tuned to a current setting which should guide HCI of the injected species to the MCP. Typically, the first atoms are removed from the target surface and injected into the trap when the laser pulse energy reaches 1 mJ. Within a few trap cycles after the laser is switched off, the injected species completely vanishes from both, the x-ray spectrum and the MCP, resulting in an accurately controllable injection leaving no contamination in the background gas.

III. RESULTS

The setup presented in Fig. 2 was used to test the reliability of the HC-EBIT with in-trap laser desorption and to identify the HCI species in the extracted ion bunches by recording isotopically resolved charge-state spectra when scanning the magnetic field of the dipole magnet. For each current setting, only HCI with a specific charge-to-mass ratio can pass through the dipole magnet and are detected by one of the detectors in the diagnostic chamber located after the magnet. For each scan, a few thousand extracted ion bunches were needed to obtain a full spectrum of the produced charge states.

For the first test, a massive target made of solid natural holmium foil (mainly ^{165}Ho) was used. A measured spectrum of ^{165}Ho charge states obtained with this target is shown in Fig. 3. The blue curve was measured with laser desorption, while the orange curve shows a background measurement without laser desorption but with the target still positioned in the trapping region. As long as holmium was injected into the EBIT, the spectrum was essentially free of any background since the relatively heavy holmium ions experience a deeper trapping potential than the lighter, lower
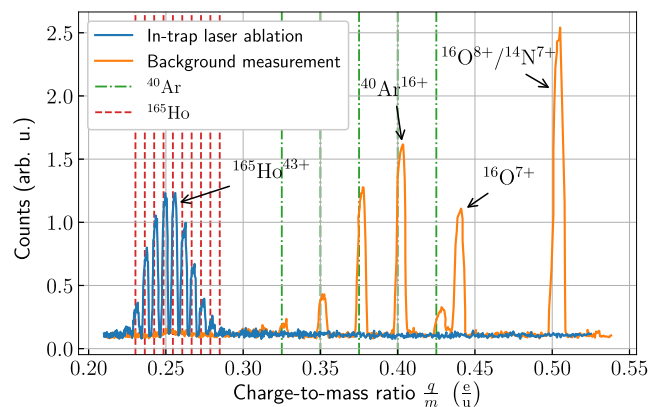
FIG. 3. Measured distribution of holmium charge states (blue) using a foil of ^{165}Ho as laser target and background measurement (orange) without laser desorption. Dashed lines indicate the expected positions of holmium (red) and dashed-dotted lines argon charge states (green). The blue spectrum exclusively shows peaks which coincide with the expected positions of holmium charge states centered around ^{165}Ho$^{42+/43+}$. Otherwise, no background was observed and holmium seems to be the sole species in the trap. In the measurement without laser desorption, we observed mainly argon in high charge states as well as light, fully ionized rest gas atoms such as oxygen and nitrogen at a charge-to-mass ratio around 0.5.

charged ions from the residual gas. These evaporate more easily from the trap and thereby cool the holmium HCI. This measurement demonstrates the successful implementation of the in-trap laser desorption technique and also that the desorption process does not perturb the HCI production or their trapping.

In order to find the practical limit in the sample size of this injection technique, samples with a decreasing amount of stable holmium (^{165}Ho) were tested. For each new sample, a spectrum of charge states was measured to verify the presence of holmium and exclude possible contaminants that are easily possible for these sample sizes. The smallest sample size that could be reliably used so far contained 10^{12} stable holmium atoms, corresponding to a quantity of 300 pg. For each spectrum, we needed about 3500–5000 laser shots, mainly depending on the time needed to optimize ion ejection (about 500–1500 laser shots) and the current range over which the dipole magnet was scanned. A typical result for this sample size is shown in Fig. 4. The spectrum was measured at a charge breeding time of $t_{br} = 1$ s, an electron beam energy of 5.9 keV, and 45 mA electron beam current with laser pulses of up to 4 mJ. In comparison to a continuously injected species, only a narrow distribution of charge states was observed since the pulsed injection once per trap cycle lets all ions experience the same charge breeding time, and therefore, no ions in lower charge states were present. Moreover, with $t_{br} = 1$ s, the presented charge state distribution had already reached its equilibrium, and a longer t_{br} would not have changed the distribution. With an improved pumping system, recombination by charge-exchange would be better suppressed narrowing the charge state distribution even further.

With one sample, it was possible to measure the charge-state distribution several times without observing a reduction in the intensity of the ion spot on the MCP. In order to characterize the "durability" of the targets, a measurement of the target lifetime was performed using again the smallest reliably tested sample size of 10^{12} stable holmium atoms, although conceivably lower limits could be achieved if needed for Q_{EC}-measurements.

Experimentally, we measured the target lifetime by tuning the dipole magnet to the current setting for the most abundant charge state ^{165}Ho^{42+} (cf. Fig. 4). Before the lifetime measurement was started, the number of ions per laser shot was measured using the FC and a charge amplifier (Femto HQA-15M10T, Gain: 10 V/pC). Then, we continued with firing laser pulses onto the target until the holmium HCI in this charge state were not visible anymore, indicating the depletion of the target at the laser spot location. Finally, the number of ions was again measured using the FC, and the lifetime measurement with the MCP was cross calibrated against the two FC measurements at the beginning and at the end of the lifetime measurement. An exemplary dataset of such a measurement is shown in Fig. 5 that was acquired following two measurements of the charge-state distribution. It was obtained using 4 mJ laser pulses focused on a single spot on the target surface. Increasing the pulse energy as well as moving the laser spot can increase the ion yield again if the laser spot is smaller than the sample area. Including the two measurements of charge state spectra such as the one shown in Fig. 4 (8000 laser pulses) and the lifetime measurement (15 000 laser pulses) for a total of 23 000 laser shots HCI of holmium in the charge state 42+ could be extracted from a target with 10^{12} atoms of ^{165}Ho. By integration of the curve in Fig. 5, the total number of extracted HCI in this charge state was estimated to be around 5×10^6 with about 10% uncertainty resulting from the analysis of the MCP data. This number takes only the ion number during the lifetime measurement into account and not the extracted ions during the measurements of the charge state spectra.

The given numbers depend strongly on the EBIT settings, electron beam current, target position, laser spot position on the target, and the beamline settings and are therefore not exactly reproducible, i.e., the laser spot position might have to be reoptimized during ion extraction. In addition, the exact location of the sample on the target is not visible; therefore, it was not possible to verify that the laser spot exactly coincided with the sample material on the target. Hence, the given numbers are estimates for only one laser spot position and can vary for different settings and positions. When the laser spot position is changed, the number of ions that are detected can increase
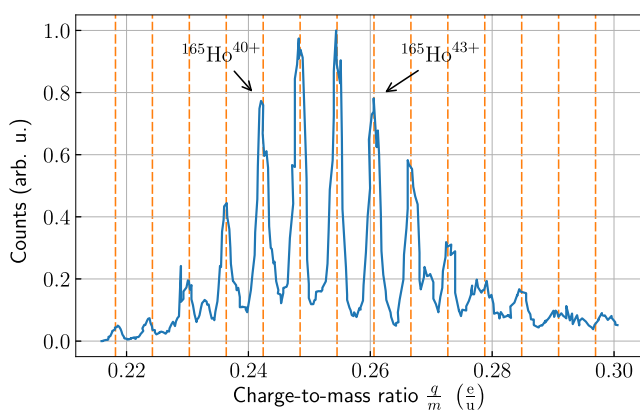
FIG. 4. Charge state distribution of holmium HCI extracted from the HC-EBIT following injection by in-trap laser desorption from a target with 10^{12} atoms. About 8 charge states centered around ^{165}Ho^{42+} were observed. The dashed lines mark the charge-to-mass ratios where the holmium HCI were expected to appear after the calibration of the dipole magnet.
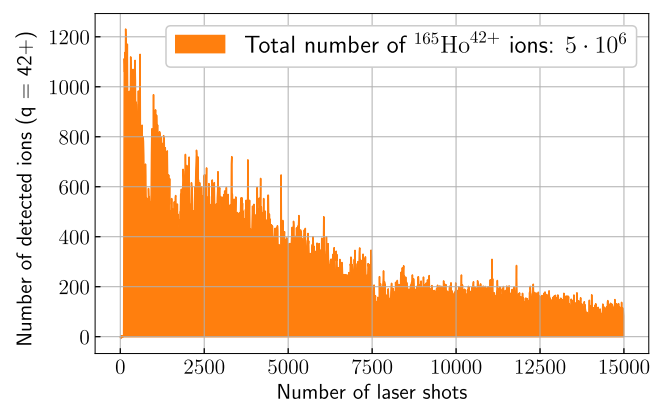
FIG. 5. Measurement of the lifetime of a sample with 10^{12} atoms of ^{165}Ho using an MCP detecting only HCI in the charge state 42+ following a charge-to-mass separation with the dipole magnet. The total number of extracted HCI was about 5×10^6 with 10% uncertainty.

again. However, extracted ions are always observed once the laser spot is on the sample and the spot position can be subsequently optimized.

IV. DISCUSSION AND CONCLUSION

The presented experiments demonstrate injection, charge breeding, and extraction of rare species HCI with a HC-EBIT by means of in-trap laser desorption using extremely small samples containing on the order of 10^{12} atoms. Compared to the previously used dedicated laser ion source producing singly charged ions which are then injected into the EBIT for charge breeding,[29] our method improves the efficiency by several orders of magnitude since desorbed neutral atoms are also captured in the EBIT and ion-transport losses between laser-ion source and EBIT are eliminated altogether. The results were reliably obtained with holmium samples of 10^{12} atoms which lasted for a reasonable number of laser shots as required for high-precision mass-ratio measurements at the PENTATRAP experiment. Our technique can be further used to produce HCI of any other species, especially also of sufficiently long-lived, medium heavy synthetic radionuclides and transuranium elements[8] produced in nuclear reactors and only available in small quantities. The thereby produced HCI can be extracted as in our case, but it is also possible to perform spectroscopic measurements on the HCI in the EBIT using either electron impact excitation or external radiation sources, e.g., synchrotrons or x-ray lasers for electronic excitation.[27]

In comparison with the wire probe method,[32] the use of a laser pulse triggering the trap loading allows a much better experimental control and is better adapted to experiments requiring regular ion extraction. To compare the performance of the two methods, one has to consider that the spectroscopic measurements on uranium isotopes with the wire probe method did not require the ejection of HCI but ions accumulated for several minutes and have been stored for several hours which reduces the consumption of sample material. The smallest used sample of uranium consisted of about 10^{14} atoms of ^{233}U. For spectroscopic measurements of this type, just one single laser pulse is required to load the trap and the ions can then be stored in the EBIT for a similarly long measurement time using samples with two orders of magnitude fewer atoms. In principle, if the intended experiments can be tuned and optimized using a more abundant HCI of the same charge-to-mass ratio, then even smaller sample sizes toward the 10^{10} atoms region are conceivable.

With the present technique, the range of rare isotopes that can be made available for high-precision nuclear mass measurements and spectroscopic experiments has been substantially expanded, and the use of samples of picogram size has become a real possibility with interesting consequences for nuclear as well as atomic physics and other fundamental studies.

ACKNOWLEDGMENTS

REFERENCES

[1] L. Gastaldo, K. Blaum, A. Doerr, Ch. E. Düllmann, K. Eberhardt, S. Eliseev, C. Enss, A. Faessler, A. Fleischmann, S. Kempf, M. Krivoruchenko, S. Lahiri, M. Maiti, Y. N. Novikov, P. C.-O. Ranitzsch, F. Simkovic, Z. Szusc, and M. Wegner, "The electron capture ^{163}Ho experiment ECHo," J. Low Temp. Phys. **176**, 876–884 (2014).

[2] L. Gastaldo, K. Blaum, K. Chrysalidis, T. Day Goodacre, A. Domula, M. Door, H. Dorrer, Ch. E. Düllmann, K. Eberhardt, S. Eliseev, C. Enss, A. Faessler, P. Filianin, A. Fleischmann, D. Fonnesu, L. Gamer, R. Haas, C. Hassel, D. Hengstler, J. Jochum, K. Johnston, U. Kebschull, S. Kempf, T. Kieck, U. Köster, S. Lahiri, M. Maiti, F. Mantegazzini, B. Marsh, P. Neroutsos, Y. N. Novikov, P. C. O. Ranitzsch, S. Rothe, A. Rischka, A. Saenz, O. Sander, F. Schneider, S. Scholl, R. X. Schüssler, Ch. Schweiger, F. Simkovic, T. Stora, Z. Szücs, A. Türler, M. Veinhard, M. Weber, M. Wegner, K. Wendt, and K. Zuber, "The electron capture in ^{163}Ho experiment—ECHo," Eur. Phys. J.: Spec. Top. **226**, 1623–1694 (2017).

[3] E. Kugler, "The isolde facility," Hyperfine Interact. **129**, 23–42 (2000).

[4] L. Gastaldo, P.-O. Ranitzsch, F. von Seggern, J.-P. Porst, S. Schäfer, C. Pies, S. Kempf, T. Wolf, A. Fleischmann, C. Enss, A. Herlert, and K. Johnston, "Characterization of low temperature metallic magnetic calorimeters having gold absorbers with implanted ^{163}Ho ions," Nucl. Instrum. Methods Phys. Res., Sect. A **711**, 150–159 (2013).

[5] H. Dorrer, K. Chrysalidis, T. D. Goodacre, Ch. E. Düllmann, K. Eberhardt, C. Enss, L. Gastaldo, R. Haas, J. Harding, C. Hassel, K. Johnston, T. Kieck, U. Köster, B. Marsh, C. Mokry, S. Rothe, J. Runke, F. Schneider, T. Stora, A. Türler, and K. Wendt, "Production, isolation and characterization of radio-chemically pure ^{163}Ho samples for the ECHo-project," Radiochim. Acta **106**, 535–547 (2018).

[6] S. Rainville, J. K. Thompson, E. G. Myers, J. M. Brown, M. S. Dewey, E. G. Kessler, R. D. Deslattes, H. G. Börner, M. Jentschel, P. Mutti, and D. E. Pritchard, "A direct test of $E = mc^2$," Nature **438**, 1096–1097 (2005).

[7] M. Jentschel and K. Blaum, "Balancing energy and mass with neutrons," Nat. Phys. **14**, 524 (2018).

[8] M. Eibach, T. Beyer, K. Blaum, M. Block, Ch. E. Düllmann, K. Eberhardt, J. Grund, S. Nagy, H. Nitsche, W. Nörtershäuser, D. Renisch, K. P. Rykaczewski, F. Schneider, C. Smorra, J. Vieten, M. Wang, and K. Wendt, "Direct high-precision mass measurements on ^{241,243}Am, ^{244}Pu, and ^{249}Cf," Phys. Rev. C **89**, 064318 (2014).

[9] F. Köhler, K. Blaum, M. Block, S. Chenmarev, S. Eliseev, D. A. Glazov, M. Goncharov, J. Hou, A. Kracke, D. A. Nesterenko, Y. N. Novikov, W. Quint, E. M. Ramirez, V. M. Shabaev, S. Sturm, A. V. Volotka, and G. Werth, "Isotope dependence of the Zeeman effect in lithium-like calcium," Nat. Commun. **7**, 10246 (2016).

[10] V. V. Flambaum, A. J. Geddes, and A. V. Viatkina, "Isotope shift, nonlinearity of king plots, and the search for new particles," Phys. Rev. A **97**, 032510 (2018).

[11] D. Anyupas, O. Tretiak, A. Garcon, R. Ozeri, G. Perez, and D. Budker, "Scalar dark matter in the radio-frequency band: Atomic-spectroscopy search results," Phys. Rev. Lett. **123**, 141102 (2019).

[12] T. Manovitz, R. Shaniv, Y. Shapira, R. Ozeri, and N. Akerman, "Precision measurement of atomic isotope shifts using a two-isotope entangled state," Phys. Rev. Lett. **123**, 203001 (2019).

[13] Y. Fukuda, T. Hayakawa, E. Ichihara, K. Inoue, K. Ishihara, H. Ishino, Y. Itow, T. Kajita, J. Kameda, S. Kasuga, K. Kobayashi, Y. Kobayashi, Y. Koshio, M. Miura, M. Nakahata, S. Nakayama, A. Okada, K. Okumura, N. Sakurai, M. Shiozawa, Y. Suzuki, Y. Takeuchi, Y. Totsuka, S. Yamada, M. Earl, A. Habig, E. Kearns, M. D. Messier, K. Scholberg, J. L. Stone, L. R. Sulak, C. W. Walter, M. Goldhaber, T. Barszczxak, D. Casper, W. Gajewski, P. G. Halverson, J. Hsu, W. R. Kropp, L. R. Price, F. Reines, M. Smy, H. W. Sobel, M. R. Vagins, K. S. Ganezer, W. E. Keig, R. W. Ellsworth, S. Tasaka, J. W. Flanagan, A. Kibayashi, J. G. Learned, S. Matsuno, V. J. Stenger, D. Takemori, T. Ishii, J. Kanzaki, T. Kobayashi, S. Mine, K. Nakamura, K. Nishikawa, Y. Oyama, A. Sakai, M. Sakuda, O. Sasaki, S. Echigo, M. Kohama, A. T. Suzuki, T. J. Haines, E. Blaufuss, B. K. Kim, R. Sanford,

R. Svoboda, M. L. Chen, Z. Conner, J. A. Goodman, G. W. Sullivan, J. Hill, C. K. Jung, K. Martens, C. Mauger, C. McGrew, E. Sharkey, B. Viren, C. Yanagisawa, W. Doki, K. Miyano, H. Okazawa, C. Saji, M. Takahata, Y. Nagashima, M. Takita, T. Yamaguchi, M. Yoshida, S. B. Kim, M. Etoh, K. Fujita, A. Hasegawa, T. Hasegawa, S. Hatakeyama, T. Iwamoto, M. Koga, T. Maruyama, H. Ogawa, J. Shirai, A. Suzuki, F. Tsushima, M. Koshiba, M. Nemoto, K. Nishijima, T. Futagami, Y. Hayato, Y. Kanaya, K. Kaneyuki, Y. Watanabe, D. Kielczewska, R. A. Doyle, J. S. George, A. L. Stachyra, L. L. Wai, R. J. Wilkes, K. K. Young, and Super-Kamiokande Collaboration, "Evidence for oscillation of atmospheric neutrinos," Phys. Rev. Lett. **81**, 1562–1567 (1998).

[14]Q. R. Ahmad, R. C. Allen, T. C. Andersen, J. D. Anglin, J. C. Barton, E. W. Beier, M. Bercovitch, J. Bigu, S. D. Biller, R. A. Black, I. Blevis, R. J. Boardman, J. Boger, E. Bonvin, M. G. Boulay, M. G. Bowler, T. J. Bowles, S. J. Brice, M. C. Browne, T. V. Bullard, G. Bühler, J. Cameron, Y. D. Chan, H. H. Chen, M. Chen, X. Chen, B. T. Cleveland, E. T. H. Clifford, J. H. M. Cowan, D. F. Cowen, G. A. Cox, X. Dai, F. Dalnoki-Veress, W. F. Davidson, P. J. Doe, G. Doucas, M. R. Dragowsky, C. A. Duba, F. A. Duncan, M. Dunford, J. A. Dunmore, E. D. Earle, S. R. Elliott, H. C. Evans, G. T. Ewan, J. Farine, H. Fergani, A. P. Ferraris, R. J. Ford, J. A. Formaggio, M. M. Fowler, K. Frame, E. D. Frank, W. Frati, N. Gagnon, J. V. Germani, S. Gil, K. Graham, D. R. Grant, R. L. Hahn, A. L. Hallin, E. D. Hallman, A. S. Hamer, A. A. Hamian, W. B. Handler, R. U. Haq, C. K. Hargrove, P. J. Harvey, R. Hazama, K. M. Heeger, W. J. Heintzelman, J. Heise, R. L. Helmer, J. D. Hepburn, H. Heron, J. Hewett, A. Hime, H. Howe, J. G. Hykawy, M. C. P. Isaac, P. Jagam, N. A. Jelley, C. Jillings, G. Jonkmans, K. Kazkaz, P. T. Keener, J. R. Klein, A. B. Knox, R. J. Komar, R. Kouzes, T. Kutter, C. C. M. Kyba, J. Law, I. T. Lawson, M. Lay, H. W. Lee, K. T. Lesko, J. R. Leslie, I. Levine, W. Locke, S. Luoma, J. Lyon, S. Majerus, H. B. Mak, J. Maneira, J. Manor, A. D. Marino, N. McCauley, A. B. McDonald, D. S. McDonald, K. McFarlane, G. McGregor, R. Meijer Drees, C. Mifflin, G. G. Miller, G. Milton, B. A. Moffat, M. Moorhead, C. W. Nally, M. S. Neubauer, F. M. Newcomer, H. S. Ng, A. J. Noble, E. B. Norman, V. M. Novikov, M. O'Neill, C. E. Okada, R. W. Ollerhead, M. Omori, J. L. Orrell, S. M. Oser, A. W. P. Poon, T. J. Radcliffe, A. Roberge, B. C. Robertson, R. G. H. Robertson, S. S. E. Rosendahl, J. K. Rowley, V. L. Rusu, E. Saettler, K. K. Schaffer, M. H. Schwendener, A. Schülke, H. Seifert, M. Shatkay, J. J. Simpson, C. J. Sims, D. Sinclair, P. Skensved, A. R. Smith, M. W. E. Smith, T. Spreitzer, N. Starinsky, T. D. Steiger, R. G. Stokstad, L. C. Stonehill, R. S. Storey, B. Sur, R. Tafirout, N. Tagg, N. W. Tanner, R. K. Taplin, M. Thorman, P. M. Thornewell, P. T. Trent, Y. I. Tserkovnyak, R. Van Berg, R. G. Van de Water, C. J. Virtue, C. E. Waltham, J.-X. Wang, D. L. Wark, N. West, J. B. Wilhelmy, J. F. Wilkerson, J. R. Wilson, P. Wittich, J. M. Wouters, M. Yeh, and SNO Collaboration, "Direct evidence for neutrino flavor transformation from neutral-current interactions in the sudbury neutrino observatory," Phys. Rev. Lett. **89**, 011301 (2002).

[15]K. Blaum, "High-accuracy mass spectrometry with stored ions," Phys. Rep. **425**, 1–78 (2006).

[16]J. Dilling, K. Blaum, M. Brodeur, and S. Eliseev, "Penning-trap mass measurements in atomic and nuclear physics," Annu. Rev. Nucl. Part. Sci. **68**, 45–74 (2018).

[17]J. Repp, C. Böhm, J. R. Crespo López-Urrutia, A. Dörr, S. Eliseev, S. George, M. Goncharov, Y. N. Novikov, C. Roux, S. Sturm, S. Ulmer, and K. Blaum, "PENTATRAP: A novel cryogenic multi-Penning-trap experiment for high-precision mass measurements on highly charged ions," Appl. Phys. B **107**, 983–996 (2012).

[18]A. Rischka, H. Cakir, M. Door, P. Filianin, Z. Harman, W. Huang, P. Indelicato, C. H. Keitel, C. M. König, K. Kromer, M. Müller, Yu. N. Novikov, R. X. Schüssler, Ch. Schweiger, S. Eliseev, and K. Blaum, "Mass-difference measurements on heavy nuclides with an eV/c^2 accuracy with PENTATRAP," Phys. Rev. Lett. (submitted).

[19]R. X. Schüssler, H. Bekker, M. Brass, H. Cakir, J. R. C. Lòpez-Urrutia, M. Door, P. Filianin, P. Indelicato, Z. Harman, M. Haverkort, W. Huang, C. Keitel, C. M. König, K. Kromer, Yu. N. Novikov, A. Rischka, Ch. Schweiger, S. Sturm, S. Ulmer, S. Eliseev, and K. Blaum, "Discovery of metastable electronic states by Penning-trap mass spectrometry" (unpublished).

[20]V. Mocko, W. A. Taylor, F. M. Nortier, J. W. Engle, T. E. Barnhart, R. J. Nickles, A. D. Pollington, G. J. Kunde, M. W. Rabin, and E. R. Birnbaum, "Isolation of [163]Ho from dysprosium target material by HPLC for neutrino mass measurements," Radiochim. Acta **103**, 577–585 (2015).

[21]S. Heinitz, N. Kivel, D. Schumann, U. Köster, M. Balata, M. Biasotti, V. Ceriale, M. D. Gerone, M. Faverzani, E. Ferri, G. Gallucci, F. Gatti, A. Giachero, N. Nisi, A. Nucciotti, A. Orlando, G. Pessina, A. Puiu, and S. Ragazzi, "Production and separation of [163]Ho for nuclear physics experiments," PLoS One **13**, e0200910 (2018).

[22]M. A. Levine, R. E. Marrs, J. R. Henderson, D. A. Knapp, and M. B. Schneider, "The electron beam ion trap: A new instrument for atomic physics measurements," Phys. Scr. **T22**, 157 (1988).

[23]M. Levine, R. Marrs, J. Bardsley, P. Beiersdorfer, C. Bennett, M. Chen, T. Cowan, D. Dietrich, J. Henderson, D. Knapp, A. Osterheld, B. Penetrante, M. Schneider, and J. Scofield, "The use of an electron beam ion trap in the study of highly charged ions," Nucl. Instrum. Methods Phys. Res., Sect. B **43**, 431–440 (1989).

[24]R. E. Marrs, S. R. Elliott, and D. A. Knapp, "Production and trapping of hydrogenlike and bare uranium ions in an electron beam ion trap," Phys. Rev. Lett. **72**, 4082–4085 (1994).

[25]H. Khodja and J. P. Briand, "A warm electron beam ion trap: The micro-EBIT," Phys. Scr. **T71**, 113 (1997).

[26]V. Ovsyannikov, G. Zschornack, F. Großmann, O. Koulthachev, S. Landgraf, F. Ullmann, and T. Werner, "A novel room temperature electron beam ion trap for atomic physics and materials research," Nucl. Instrum. Methods Phys. Res., Sect. B **161-163**, 1123–1127 (2000).

[27]P. Micke, S. Kühn, L. Buchauer, J. R. Harries, T. M. Bücking, K. Blaum, A. Cieluch, A. Egl, D. Hollain, S. Kraemer, T. Pfeifer, P. O. Schmidt, R. X. Schüssler, Ch. Schweiger, T. Stöhlker, S. Sturm, R. N. Wolf, S. Bernitt, and J. R. C. López-Urrutia, "The Heidelberg compact electron beam ion traps," Rev. Sci. Instrum. **89**, 063109 (2018).

[28]S. Eliseev, K. Blaum, M. Block, S. Chenmarev, H. Dorrer, Ch. E. Düllmann, C. Enss, P. E. Filianin, L. Gastaldo, M. Goncharov, U. Köster, F. Lautenschläger, Y. N. Novikov, A. Rischka, R. X. Schüssler, L. Schweikhard, and A. Türler, "Direct measurement of the mass difference of [163]Ho and [163]Dy solves the q-value puzzle for the neutrino mass determination," Phys. Rev. Lett. **115**, 062501 (2015).

[29]V. Mironov, M. Trinczek, A. Werdich, A. G. Martinez, P. Guo, X. Zhang, J. Braun, J. R. Crespo López-Urrutia, and J. Ullrich, "Tests of a laser ion source at the Heidelberg electron beam ion trap," in *11th International Conference on the Physics of Highly Charged Ions* [Nucl. Instrum. Methods Phys. Res., Sect. B **205**, 183–186 (2003)].

[30]R. Haas, S. Lohse, Ch. E. Düllmann, K. Eberhardt, C. Mokry, and J. Runke, "Development and characterization of a drop-on-demand inkjet printing system for nuclear target fabrication," Nucl. Instrum. Methods Phys. Res., Sect. A **874**, 43–49 (2017).

[31]M. B. Schneider, M. A. Levine, C. L. Bennett, J. R. Henderson, D. A. Knapp, and R. E. Marrs, "Evaporative cooling of highly charged ions in EBIT: An experimental realization," AIP Conf. Proc. **188**, 158–165 (1989).

[32]S. Elliott and R. Marrs, "A wire probe as an ion source for an electron beam ion trap," Nucl. Instrum. Methods Phys. Res., Sect. B **100**, 529–535 (1995).

3.2   PUBLICATION 2: FAST SILICON CARBIDE MOSFET BASED HIGH-VOLTAGE PUSH-PULL SWITCH FOR CHARGE STATE SEPARATION OF HIGHLY CHARGED IONS WITH A BRADBURY-NIELSEN GATE

In this article a fast high-voltage push-pull switch based on silicon carbide MOSFETS that was developed in the scope of this thesis is described. The article was published in *Review of Scientific Instruments*.

AUTHORS   **Ch. Schweiger**, M. Door, P. Filianin, J. Herkenhoff, K. Kromer, D. Lange, D. Marschall, A. Rischka, T. Wagner, S. Eliseev, K. Blaum

AUTHOR'S CONTRIBUTIONS   **CS**, DM and TW designed the electronic circuit. **CS** and DM conducted the experiment and took the data. **CS** analyzed the data and and wrote the manuscript. All authors took part in the critical review of the manuscript before and after submission.

ABSTRACT   In this paper we report on the development of a fast high-voltage switch, which is based on two enhancement mode N-channel Silicon Carbide Metal Oxide Semiconductor Field-Effect Transistors in push-pull configuration. The switch is capable of switching high voltages up to 600 V on capacitive loads with rise and fall times on the order of 10 ns and pulse widths $\geq$20 ns. Using this switch it was demonstrated that from the charge state distribution of bunches of highly charged ions ejected from an electron beam ion trap with a specific kinetic energy, single charge states can be separated by fast switching of the high voltage applied to a Bradbury-Nielsen Gate with a resolving power of about 100.

Fast silicon carbide MOSFET based high-voltage push–pull switch for charge state separation of highly charged ions with a Bradbury–Nielsen gate

View Online   Export Citation   CrossMark

Christoph Schweiger,[a] iD Menno Door, iD Pavel Filianin, iD Jost Herkenhoff, iD Kathrin Kromer, iD
Daniel Lange, iD Domenik Marschall, Alexander Rischka, iD Thomas Wagner, Sergey Eliseev, iD
and Klaus Blaum iD

AFFILIATIONS

Max-Planck-Institut für Kernphysik, Saupfercheckweg 1, 69117 Heidelberg, Germany

[a] Author to whom correspondence should be addressed: christoph.schweiger@mpi-hd.mpg.de

ABSTRACT

In this paper, we report on the development of a fast high-voltage switch, which is based on two enhancement mode N-channel silicon carbide metal–oxide–semiconductor field-effect transistors in push–pull configuration. The switch is capable of switching high voltages up to 600 V on capacitive loads with rise and fall times on the order of 10 ns and pulse widths ≥20 ns. Using this switch, it was demonstrated that, from the charge state distribution of bunches of highly charged ions ejected from an electron beam ion trap with a specific kinetic energy, single charge states can be separated by fast switching of the high voltage applied to a Bradbury–Nielsen Gate with a resolving power of about 100.

I. INTRODUCTION

Many experiments addressing fundamental physics require highly charged ions (HCI) (see Refs.[1–4], which are produced in ion sources employing different ionization mechanisms, e.g., electron impact ionization, such as in electron beam ion traps (EBITs).[5] In EBITs, the distribution of charge states is produced of which often only a single charge state is experimentally required. In order to separate the charge state of interest and remove the background of unwanted species, different charge-to-mass ratio selective techniques can be employed, such as Wien-type velocity filters, sector magnets, or Time-of-Flight (ToF) separation.[6] Here, resolving powers of 20–200 are achievable using a Wien-type velocity filter[7] (depending on the aperture) and around 150 for the sector magnet.[8] For the single-pass ToF separation reported here, a resolving power of around 100 is possible.

In our specific setup, a compact, room-temperature EBIT[9,10] is used for the production of HCI, which are extracted and transported to a Penning-trap setup for high-precision mass spectrometry.[11] In the Penning trap, only a single HCI is stored, requiring background

reduction and the selection of a single charge state. Upon extraction from the EBIT, a bunch of ions is accelerated by an electrostatic potential. This results in slightly different velocities of the ions depending on their charge state $v \sim \sqrt{q}$ (assuming the same mass). The ions in higher charge states propagate slightly faster through the beamline than the ones in lower charge states and, therefore, arrive earlier at the detector plane. Individual charge states can now be selected by deflecting all other species, e.g., by applying a voltage to some electrode and switching it to the ground only for the short time window when the charge state of interest passes the electrode. This concept is experimentally realized using a Bradbury–Nielsen Gate (BNG)[6,12–14] combined with a fast switching electronic circuit in order to resolve individual charge states.

Fast and efficient switching of high voltages is commonly used in power electronics nowadays, e.g., in power supplies and driving electronics for electrically powered vehicles. Due to the increasing number of required devices, different types of power Metal Oxide Semiconductor Field-Effect Transistors (MOSFETs) with very fast rise and fall times as well as low drain to source resistances are developed and commercially available at the present time for these

applications. In the context of this paper, two power MOSFETs are used in order to build a fast switching electronic circuit controlled using a 5 V TTL-logic signal. The application requires that the duration of the high-voltage pulse can be as short as 20 ns and that the time it takes to switch from one voltage to the other is on a timescale of around 10 ns for voltages of up to 500 V. Similar solid-state switches suitable for even significantly higher voltages are commercially available today and are summarized in Table I. Except for the two electrical modules for the switch from Berkeley Nucleonics, these solid state switches do not fulfill all our requirements for switching, e.g., the minimum pulse width. Furthermore, when switching high-voltage, the load (e.g., a capacitive load) and the signal path from the switching device to the electrodes have to be considered. For commercial devices, the connections are typically done using either BNC or SHV (secure high-voltage) connector and the respective cables. Depending on the size of the device, these have to be installed in a dedicated place, sometimes even with a dedicated power supply, which further increases the cable length and can potentially lead to performance reduction due to the increased capacitance. The switching circuit presented in this paper, specifically the printed circuit board that hosts the switching circuit, can be easily adapted to the experimental requirements by the builder and, in this way, generally reduces cable lengths and allows better control of the signal paths' impedance. Ultimately, it can be even designed to be placed within the vacuum directly attached to the relevant electrode.

In addition to the commercial devices listed above, there are a number of publications of high-voltage solid-state switches with similar performances but different designs optimized for the specific application and not necessarily using the push–pull principle.[18–23] This can be favorable, e.g., for use as Pockels cell drivers in Q-switched lasers, where a very fast rise-time is relevant but the pulse duration and the fall-time are not similarly important.[24]

In the following sections, the fast switching electronic circuit is described (Sec. II) and measurements of the switching performance are shown (Sec. III). Finally, the separation of individual charge states is experimentally demonstrated, showing a resolving power of the order of 100 (Sec. IV).

II. ELECTRONIC CIRCUIT

A schematic overview of the electronic circuit of the push–pull switch is given in Fig. 1, showing the main electrical components. The complete and detailed circuit can be found in the supplementary material. The timing and pulse duration of the high-voltage pulse

are controlled with a 5 V TTL trigger input. The trigger logic is designed such that as long as the trigger signal is high (low), the higher (lower) voltage is active on the output. In this way, the pulse length of the high-voltage output pulse is controlled by the width of the trigger pulse Δt_{TRIG}. The trigger section consists of the logic gates, a delay timing element, and the input side of the optocouplers (dashed box in Fig. 1), which are all supplied from a single DC/DC converter with the ground connected to the main ground. Each of the two trigger signals then passes through an optocoupler (Broadcom HCPL-0723[25]), which insulates the trigger logic part from the gate drivers and the MOSFETs. In order to be able to switch voltages up to ±500 V with rise and fall times in the few tens of nanosecond range, Silicon Carbide based MOSFETs (SiC-MOSFETs) have shown the best performance in our tests. More specifically, we used two N-channel enhancement mode SiC-MOSFETs (Wolfspeed CREE C2M0280120D[26]), which were chosen specifically for their fast rise and fall times of around 10 ns and the approximately symmetric time constants. This type of MOSFET has shown the best performance for our purposes compared to other MOSFETs from different manufacturers, which were tested based on silicon, SiC, and gallium nitride (GaN). These MOSFETs were found by searching specifically for high-voltage and fast rise and fall times, which have roughly the same time constant. Each of the MOSFETs had to be tested individually since the specifications listed in the datasheets are usually measured in specific conditions that do not necessarily reflect the ones that are used for the switch operation, e.g., the load on the output as well as the used gate driver are mostly different. Among the tested models were MOSFETs from ST Microelectronics N.V., e.g., STP45N40DM2AG,[27] Texas Instruments Inc., e.g., LMG3410R150,[28] and GaN Systems Inc., e.g., GS-065-004-1-L.[29] Several more products from manufacturers, such as Infineon Technologies AG, Microchip Technology Inc. (SiC-type), and Navitas Semiconductor (GaN-type), were also considered. As newer MOSFET types with possibly faster characteristics become available, the electronic circuit can be easily adapted to use these together with an appropriate gate driver. The two MOSFETs used in the circuit are each controlled by an individual gate driver (Onsemi NCP81074A[30]), which charges and discharges the MOSFET gate with rise and fall times as well of the order of 10 ns.

The measured pulses from the gate drivers are shown in Fig. 2. The switching sequence from one voltage to the other is visible here: First, the MOSFET that is initially conducting (blue curve) is switched off before the other one (orange curve) is switched to the conducting mode. When switching back to the original voltage, the reverse order is followed. Due to the high voltage that is switched,

TABLE I. Comparison of commercially available solid-state high-voltage switches.

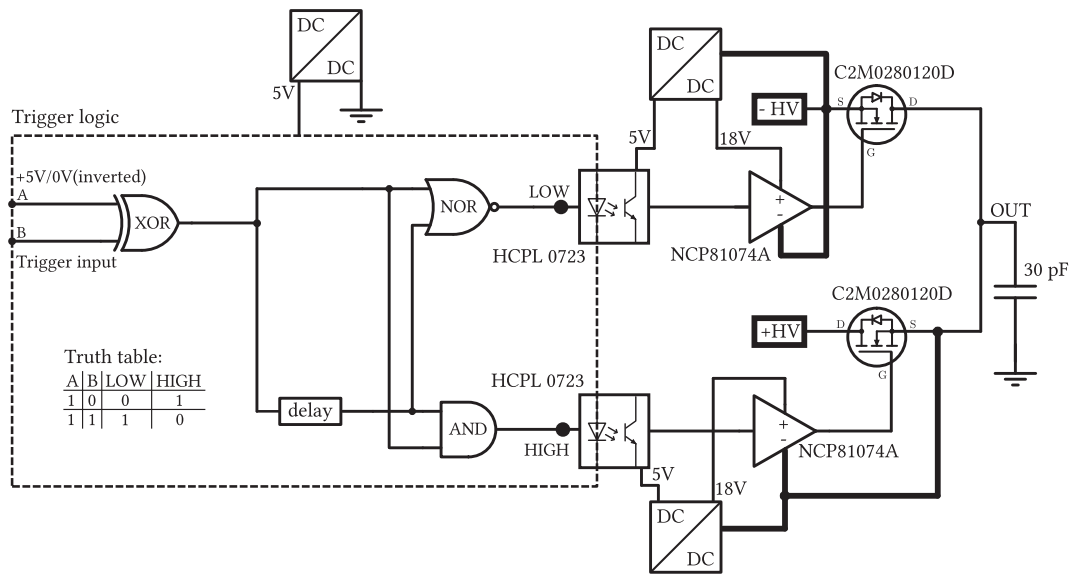| Company	Switch type	Rise/fall times (ns)	Pulse width (ns)	Voltage rating (V)
Behlke power electronics GmbH	HTS61-05[15]	5	50	6000
CGC Instruments	NIM-AMX500-3[16]	20	150	500
Berkeley Nucleonics Corp.	Model 6040-310H[17]	15	25	800
Berkeley Nucleonics Corp.	Model 6040-202H[17]	5	12	300

FIG. 1. Schematic overview of the electronic circuit. The dashed box surrounds the logic gates that form the two trigger pulses for the gate drivers from a single input trigger pulse. For the two logic gate combinations, a combined truth table is shown for the non-inverted case, i.e., when A is "high," such that the output depends only on the trigger input B. The input A can also be set to 0 V, which inverts the output of the trigger logic. The results given in the truth table correspond to the points "LOW" and "HIGH." Following the trigger logic, an optical insulator separates the floating grounds of the gate drivers from the trigger ground. In the final stage, the optically insulated trigger signal reaches the gate drivers, which produce an 18 V signal in order to quickly charge the gate capacitance of the MOSFET. A 30 pF capacitive load is shown on the output, which was used for laboratory testing of the switch and is comparable to the capacitive load of the BNG.

the voltage on the source pin of the MOSFET will quickly become larger than the voltage on the gate in which case the MOSFET is no longer conducting. In order to avoid that the MOSFET switches off, the gate and the corresponding driver have to be floating together with the source voltages of the MOSFETs, as indicated in Fig. 1 with the wider connection lines. This is implemented by having a floating ground and an insulated DC/DC-converter for each of the gate drivers and the corresponding MOSFETs, which is insulated toward the trigger logic part with the optocouplers and connected to the

source on the MOSFET. For the connected high voltages, it is important that the +HV is always more positive than the −HV. In turn, this means that −HV does not necessarily have to be negative. In the printed circuit board layout of the switch, the ground planes were clearly separated to avoid any coupling from the floating grounds to the main ground at high voltages. Furthermore, in order to achieve fast rise and fall times, the connections between the MOSFETs and the capacitive load should be designed with a surface as large as possible in order to maximize the conduction on the surface (skin effect) and reduce parasitic inductance.
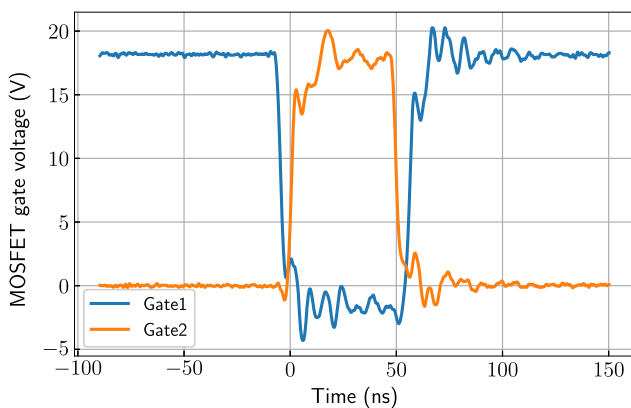
III. PUSH–PULL SWITCHING PERFORMANCE

Initial testing of the electrical circuit was done in a bench setup using a similar capacitance as the BNG, which is of the order of 30 pF. The capacitor is connected between the output of the switch and the main ground as shown in Fig. 1. This setup is not fully realistic since the BNG is not connected to the main ground with one side but to a second switch. In order to measure the rise and fall times (t_r and t_f, respectively) as well as the pulse width Δt of the high-voltage pulse on the capacitive load, a fast high-voltage probe[31] was used together with an oscilloscope[32] for data acquisition and measurement.

The output voltage of the switch obtained with the described test setup is shown in Fig. 3. Rise and fall times (10% to 90%) and the pulse width [full width at half maximum (FWHM)] measured with the built-in measurement function of the oscilloscope for ten averages are listed in Table II. The types of switch operations are illustrated for which the switch is typically used in our laboratory,
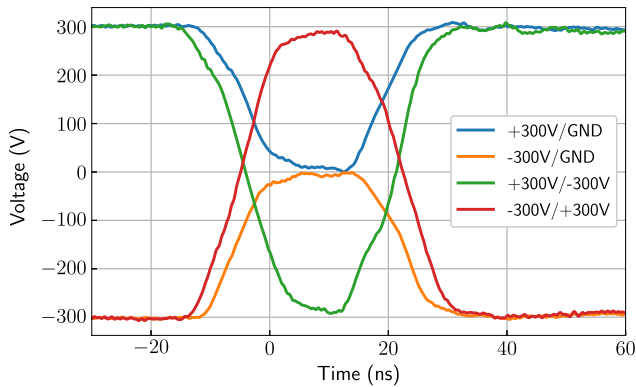

FIG. 2. MOSFET gate pulses for $\Delta t = 50$ ns pulse width. For details, see text.

FIG. 3. Measured output voltage using the bench test setup with 30 pF capacitance connected to the output. The rise and fall times as well as the measured pulse widths are listed in Table II. Typical in our experiment[4] is the operation of switching a positive or a negative voltage to the ground (blue and orange curves); see Sec. IV. Furthermore, switching a positive to a negative voltage or vice versa (green and red curves) is interesting. For all curves the trigger point is at $t = 0$ ns.

TABLE II. Measured rise and fall times for different switch operations in ns for the switching curves shown in Fig. 3. The measured pulse width Δt_{FWHM} is slightly larger than the pulse width of the trigger pulse used for controlling the switch Δt_{TRIG}.

Switched voltage (V)	t_r	t_f	Δt_{FWHM}	Δt_{TRIG}
$+300 \rightarrow 0$	9.4	11.2	23.2	20
$-300 \rightarrow 0$	9.2	11.0	28.6	20
$+300 \rightarrow -300$	12.4	13.8	26.4	20
$-300 \rightarrow +300$	11.6	14.0	28.0	20

that is switching a positive or negative voltage to ground potential (blue and orange curves) or switching from a positive to a negative voltage (green and red curves). Furthermore, it is possible to switch from one voltage to another voltage of the same polarity, which is not illustrated. Figure 3 shows the switch curves for the shortest possible pulse width of 20 ns. For longer pulse widths, the switching curves become significantly more "rectangular"-shaped. Compared to the commercial devices (see Table I), the rise and fall times as well as the pulse widths are on a similar level if only the numbers are compared. Especially, for the very fast models from Berkeley Nucleonics Corp., a thorough comparison with a similar load and in identical conditions would be interesting, since, as we have noted before, the connections and cables that are used can also change the performance.

IV. CHARGE-STATE SEPARATION OF HIGHLY CHARGED IONS USING A BRADBURY–NIELSEN GATE

In our experimental setup,[4] bunches of highly charged ions are produced in an electron beam ion trap (EBIT)[9,10] and are extracted in bunches containing a distribution of charge states. The developed switch is designed to supply the voltages for a BNG[12] for the separation of individual charge states. Upon extraction from the EBIT, the ion bunch is accelerated by a voltage $U = 4000$ V and propagates through several ion optical elements before passing through

the BNG and finally impinging on a microchannel plate detector (MCP) in Chevron configuration. The final velocity of the ions, following an acceleration by a voltage U, differs slightly depending on the charge state $q_{ion} = n \cdot e$ of the ions. Here, n is the number of missing electrons and e is the elementary charge. Thus, after propagating a finite distance s, the ions arrive at the MCP detector at slightly different times depending on their charge state

$$t(q_{ion}) = \sqrt{\frac{s^2 m}{2eU q_{ion}}}. \tag{1}$$

This assumes that only one ion species with mass m is present in the EBIT. A ToF spectrum of the ejected ion bunch arriving on the MCP detector is shown in Fig. 4(b) (solid curve), where a clear signal appears for each arriving charge state (from $q = 37+$ to $42+$) separated by about 70 ns from each other. In order to separate the individual charge states, a BNG can be used in a similar way as in multi-reflection ToF mass spectrometry.[6,14] A BNG consists of two sets of wires that are alternately arranged in parallel, as shown in Fig. 4(c). The wires, made from 60 μm stainless steel wire, are individually wound through the PEEK insulator material and have a spacing of 0.5 mm. One set of wires is attached to the inner two PEEK insulators, the second set to the outer ones, such that the wires are alternately arranged in parallel without electrical contact. In operation, one set of wires is set to a positive voltage while the other is set to a negative voltage, which leads to a deflection of charged particles passing through the plane of the wires ["BNG closed" in Fig. 4(a)]. If there is no voltage applied, the ions can pass the BNG without being deflected ("BNG open"). The general idea is to switch between these two states and thereby only allow the charge state of interest to pass the BNG, controlled by the precisely controlled timing of the switching process. In order to change the applied voltages very fast, the switch presented in Sec. II is used. Each set of wires is supplied from a separate switch, one switching from a positive voltage to ground, the other one from a negative voltage. The connection is done via a 4 mm copper rod vacuum feedthrough and silvered multistrand wires on the vacuum side in order to maximize the conducting surface. From the multistrand wire to the BNG wire, a solid block of copper is used, which connects to all of the wires [see Fig. 4(c)].

The lower part of Fig. 4(b) shows the ToF spectra for two different time delay settings t_{delay} of the trigger pulse (50 ns pulse width) controlling the switching circuit. This time delay is adjusted such that the BNG wires are switched from ±500 V to ground potential when the selected charge state arrives at the position of the BNG wires, 1.5 m from the ejection point (around 3.5 μs following the ejection). The ions finally arrive at the MCP detector plates following another 75 cm of flight path after a total ToF of ~5.4 μs. With this, the capability of separating individual charge states following each other in close succession in the ToF spectrum is demonstrated. The two separated charge states arrive slightly delayed compared to the reference ToF spectrum. Unlike the ideal model of a BNG, the real BNG can have residual voltages on the wires and the fast switching of the voltages on the BNG wires can cause accelerating or decelerating electric fields when the ions are still close to the plane of the wires. This additional deceleration causes the ions to arrive delayed on the MCP detector and can be minimized by tuning the pulse length of
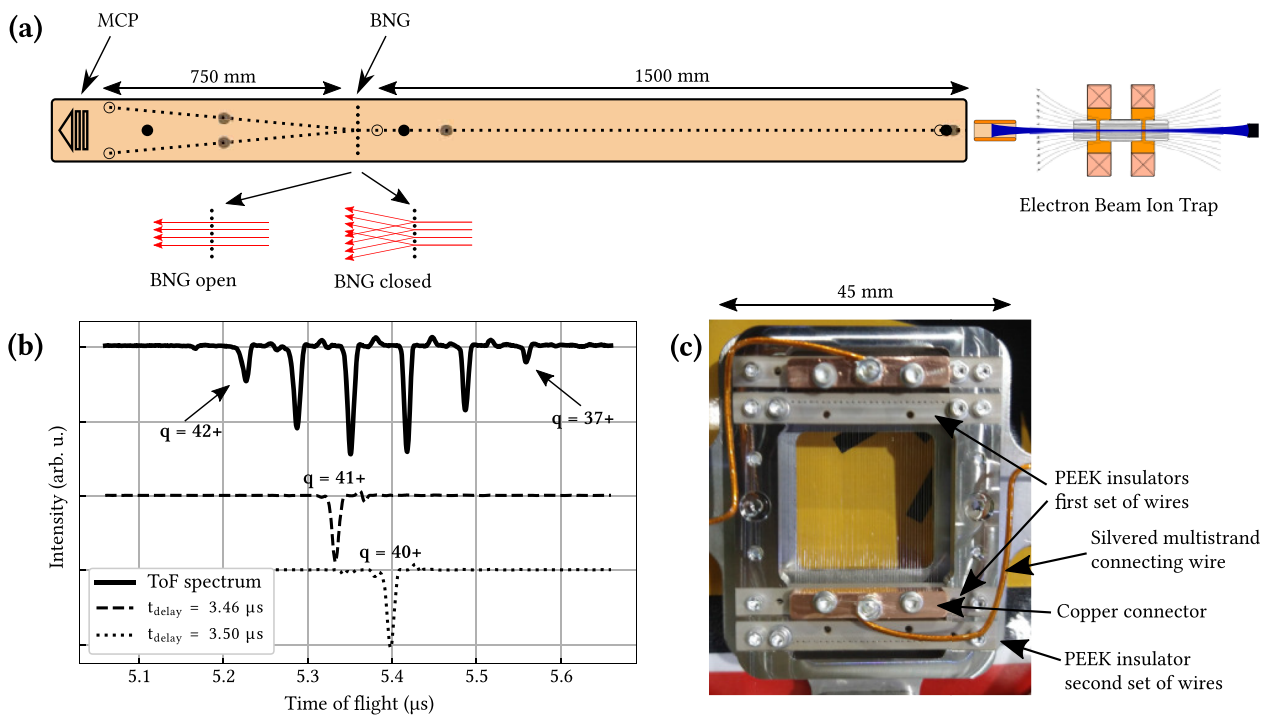
FIG. 4. An overview of the experimental setup is shown in the upper part of (a). Following the ejection of HCI from an EBIT, the HCI with a kinetic energy of 4 keV/q propagate through the beamline and eventually pass the BNG before reaching an MCP detector at the end of the beamline. The black, gray, and unfilled circles represent ions with different charge states. In this illustration, the BNG is only open during the passage time of the ion charge state marked as black circles, leading to a deflection of the ion charge states in gray and unfilled circles. In (b), a measured ToF spectrum of ions is shown where individual charge states of highly charged ^{163}Dy ions are detected on the MCP detector at different times following the ejection from the EBIT and can be observed as dips in the signal extracted from the anode behind the MCP detector plates. The two lower curves in (b) show the ToF spectrum of two individual charge states for which the voltage of the BNG wires was set to ±500 V and only switched to ground potential for a short period of 50 ns with two different time delay settings t_{delay} of the BNG trigger pulse. (c) A photograph of the BNG setup built in the experiment. The square-shaped aperture with the wires is 25 × 25 mm^2 in size. For details, see the text.

the high-voltage pulse on the BNG wires and the time delay of the trigger pulse.

With the pulse width of Δt_{FWHM} = 50 ns and the ToF of about t_{ToF} = 5 μs, we can estimate a resolving power of $R = \frac{t_{ToF}}{\Delta t_{FWHM}} \simeq 100$. This is in the range where other charge-to-mass ratio selective devices also operate, as mentioned in Sec. I. A sufficient separation is already achieved at voltages around ±200 V applied to the wires. In an upgraded version of our experimental setup, a set of slits is used in order to cut away the deflected ions that still reach the MCP surface at lower voltages. In our experimental setup, this fast switching circuit in combination with the BNG allowed the clear separation of individual charge states of HCI within a relatively short beamline of just a few meters using only moderate deflection voltages.

V. CONCLUSION

In this paper, a fast high-voltage push–pull switch with switching times on the order of 10 ns and short pulse widths of 20 ns is presented. Results of the switch being used as a high-voltage switch for a BNG have been shown as well as the successful separation of highly charged ions following a ToF separation. Due to its fast switching times, the switch is also used in other experiments, e.g., for fast switching of piezovalves or the electrode potentials on Penning traps at SHIPTRAP.[33]

SUPPLEMENTARY MATERIAL

The detailed electrical circuit of the switch is available in the supplementary material.

AUTHOR DECLARATIONS

Conflict of Interest

The authors have no conflicts to disclose.

Author Contributions

Christoph Schweiger: Conceptualization (equal); Data curation (equal); Formal analysis (equal); Investigation (equal); Methodology (equal); Writing – original draft (equal); Writing – review & editing (equal). **Menno Door:** Software (equal); Writing – review & editing (equal). **Pavel Filianin:** Supervision (equal); Writing - review & editing (equal). **Jost Herkenhoff:** Writing – review & editing (equal). **Kathrin Kromer:** Writing – review & editing (equal). **Daniel Lange:** Software (equal); Writing – review & editing (equal). **Domenik Marschall:** Conceptualization (equal); Investigation (equal); Methodology (equal). **Alexander Rischka:** Supervision (equal); Writing - review & editing (equal). **Thomas Wagner:** Conceptualization (equal); Investigation (equal); Methodology (equal); Resources (equal); Writing – review & editing (equal). **Sergey Eliseev:** Conceptualization (equal); Investigation; Methodology; Project administration; Supervision; Writing - review & editing. **Klaus Blaum:** Conceptualization (equal); Funding acquisition; Project administration; Resources; Supervision; Writing - review & editing

DATA AVAILABILITY

The data that support the findings of this study are available from the corresponding author upon reasonable request.

REFERENCES

[1] S. Sturm, I. Arapoglou, A. Egl, M. Höcker, S. Kraemer, T. Sailer, B. Tu, A. Weigel, R. Wolf, J. C. López-Urrutia, and K. Blaum, Eur. Phys. J. Spec. Top. **227**, 1425 (2019).

[2] P. Micke, T. Leopold, S. A. King, E. Benkler, L. J. Spieß, L. Schmöger, M. Schwarz, J. R. Crespo López-Urrutia, and P. O. Schmidt, Nature **578**, 60 (2020).

[3] J. Stark, C. Warnecke, S. Bogen, S. Chen, E. A. Dijck, S. Kühn, M. K. Rosner, A. Graf, J. Nauta, J.-H. Oelmann, L. Schmöger, M. Schwarz, D. Liebert, L. J. Spieß, S. A. King, T. Leopold, P. Micke, P. O. Schmidt, T. Pfeifer, and J. R. Crespo López-Urrutia, Rev. Sci. Instrum. **92**, 083203 (2021).

[4] P. Filianin, C. Lyu, M. Door, K. Blaum, W. J. Huang, M. Haverkort, P. Indelicato, C. H. Keitel, K. Kromer, D. Lange, Y. N. Novikov, A. Rischka, R. X. Schüssler, C. Schweiger, S. Sturm, S. Ulmer, Z. Harman, and S. Eliseev, Phys. Rev. Lett. **127**, 072502 (2021).

[5] M. A. Levine, R. E. Marrs, J. R. Henderson, D. A. Knapp, and M. B. Schneider, Phys. Scr. **T22**, 157 (1988).

[6] R. N. Wolf, D. Beck, K. Blaum, Ch. Böhm, Ch. Borgmann, M. Breitenfeldt, F. Herfurth, A. Herlert, M. Kowalska, S. Kreim, D. Lunney, S. Naimi, D. Neidherr, M. Rosenbusch, L. Schweikhard, J. Stanja, F. Wienholtz, and K. Zuber, Nucl. Instrum. Methods Phys. Res., Sect. A **686**, 82 (2012).

[7] M. Schmidt, H. Peng, G. Zschornack, and S. Sykora, Rev. Sci. Instrum. **80**, 063301 (2009).

[8] R. Rao, O. Kester, T. Sieber, D. Habs, and K. Rudolph, Nucl. Instrum. Methods Phys. Res., Sect. A **427**, 170 (1999).

[9] P. Micke, S. Kühn, L. Buchauer, J. R. Harries, T. M. Bücking, K. Blaum, A. Cieluch, A. Egl, D. Hollain, S. Kraemer, T. Pfeifer, P. O. Schmidt, R. X. Schüssler, C. Schweiger, T. Stöhlker, S. Sturm, R. N. Wolf, S. Bernitt, and J. R. Crespo López-Urrutia, Rev. Sci. Instrum. **89**, 063109 (2018).

[10] C. Schweiger, C. M. König, J. R. Crespo López-Urrutia, M. Door, H. Dorrer, C. E. Düllmann, S. Eliseev, P. Filianin, W. Huang, K. Kromer, P. Micke, M. Müller, D. Renisch, A. Rischka, R. X. Schüssler, and K. Blaum, Rev. Sci. Instrum. **90**, 123201 (2019).

[11] J. Repp, C. Böhm, J. R. Crespo López-Urrutia, A. Dörr, S. Eliseev, S. George, M. Goncharov, Y. N. Novikov, C. Roux, S. Sturm, S. Ulmer, and K. Blaum, Appl. Phys. B **107**, 983 (2012).

[12] N. E. Bradbury and R. A. Nielsen, Phys. Rev. **49**, 388 (1936).

[13] O. K. Yoon, I. A. Zuleta, M. D. Robbins, G. K. Barbula, and R. N. Zare, J. Am. Soc. Mass Spectrom. **18**, 1901 (2007).

[14] T. Brunner, A. R. Mueller, K. O'Sullivan, M. C. Simon, M. Kossick, S. Ettenauer, A. T. Gallant, E. Mané, D. Bishop, M. Good, G. Gratta, and J. Dilling, Int. J. Mass Spectrom. **309**, 97 (2012).

[15] Behlke Power Electronics GmbH, "Fast high voltage transistor switches," https://www.behlke.com/pdf/151-02_3x.pdf; accessed 4 February 2022.

[16] CGC Instruments, "Universeller digital gesteuerter dreifacher Analogschalter/Multiplexer NIM-AMX500-3 für Spannungen bis 500 V," http://www.cgc-instruments.com/data/Products/NIM/NIM-AMX500-3/Beschreibung-2.30_A.pdf; accessed 4 February 2022.

[17] Berkeley Nucleonics Corp., "BNC model 6040," https://www.berkeleynucleonics.com/sites/default/files/products/datasheets/model_6040_-ds-7-8-19_2.pdf; accessed 4 February 2022.

[18] R. J. Baker and M. D. Pocha, Rev. Sci. Instrum. **61**, 2211 (1990).

[19] R. E. Continetti, D. R. Cyr, and D. M. Neumark, Rev. Sci. Instrum. **63**, 1840 (1992).

[20] C. J. Dedman, E. H. Roberts, S. T. Gibson, and B. R. Lewis, Rev. Sci. Instrum. **72**, 2915 (2001).

[21] C. J. Dedman, E. H. Roberts, S. T. Gibson, and B. R. Lewis, Rev. Sci. Instrum. **72**, 3718 (2001).

[22] X.-w. Feng, X.-w. Long, and Z.-q. Tan, Rev. Sci. Instrum. **82**, 075102 (2011).

[23] M. Azizi, J. J. van Oorschot, and T. Huiskamp, IEEE Trans. Plasma Sci. **48**, 4262 (2020).

[24] T. P. Rutten, N. Wild, and P. J. Veitch, Rev. Sci. Instrum. **78**, 073108 (2007).

[25] Broadcom Inc., "HCPL-7723/0723 50-MBd 2-ns PWD high-speed CMOS optocoupler," https://docs.broadcom.com/doc/AV02-0643EN; accessed 4 February 2022.

[26] Wolfspeed Inc., "C2M0280120D silicon carbide power MOSFET," https://cms.wolfspeed.com/app/uploads/2020/12/C2M0280120D.pdf; accessed 4 February 2022.

[27] ST Microelectronics N.V., "STP45N40DM2AG Automotive-grade N-channel 400 V, 0.063 Ohm typ., 38 A MDmesh DM2 Power MOSFET in a TO-220 package," https://www.st.com/resource/en/datasheet/stp45n40dm2ag.pdf; accessed 4 February 2022.

[28] Texas Instruments Inc., "LMG341xR150 600-V, 150-mOhm, GaN FET with integrated driver and protection," https://www.ti.com/lit/gpn/lmg3410r150; accessed 4 February 2022.

[29] GaN Systems Inc., "GS-065-004-1-L 650 V E-mode GaN transistor Datasheet," https://gansystems.com/wp-content/uploads/2021/04/GS-065-004-1-L-DS-Rev-210322.pdf; accessed 4 February 2022.

[30] Semiconductor Components Industries, LLC, "NCP81074A, NCP81074B single channel 10 A high speed low-side MOSFET driver," https://www.onsemi.com/pdf/datasheet/ncp81074-d.pdf; accessed 4 February 2022.

[31] TESTEC Elektronik GmbH, "Modular oscilloscope probes 100:1 2500Vp," https://www.testec.de/assets/pdf/TT-HV/TT-HV-250_Datasheet_DE.pdf; accessed 4 February 2022.

[32] Rohde & Schwarz GmbH & Co. KG, "R&S RTB2000 oscilloscope," https://scdn.rohde-schwarz.com/ur/pws/dl_downloads/dl_common_library/dl_brochures_and_datasheets/pdf_1/RTB2000_dat-sw_en_3607-4270-22_v1500.pdf; accessed 4 February 2022.

[33] J. Ketelaer, J. Krämer, D. Beck, K. Blaum, M. Block, K. Eberhardt, G. Eitel, R. Ferrer, C. Geppert, S. George, F. Herfurth, J. Ketter, S. Nagy, D. Neidherr, R. Neugart, W. Nörtershäuser, J. Repp, C. Smorra, N. Trautmann, and C. Weber, Nucl. Instrum. Methods Phys. Res., Sect. A **594**, 162 (2008).

3.3 PUBLICATION 3: DIRECT HIGH-PRECISION MEASUREMENT OF THE ELECTRON CAPTURE Q-VALUE IN 163-HO FOR THE DETERMINATION OF THE EFFECTIVE ELECTRON NEUTRINO MASS

AUTHORS   **Ch. Schweiger**, M. Braß, V. Debierre, M. Door, H. Dorrer, Ch.E. Düllmann, C. Enss, P. Filianin, L. Gastaldo, Z. Harman, M.W. Haverkort, J. Herkenhoff, P. Indelicato, C.E. Keitel, K. Kromer, D. Lange, Yu.N. Novikov, D. Renisch, A. Rischka, R.X. Schüssler, S. Eliseev, K. Blaum.

AUTHOR'S CONTRIBUTIONS   **CS**, MD, PF, JH, KK and SE conducted the experiment and took the data. The ^{163}Ho samples were prepared by DR and HD. **CS**, MD and SE analyzed the data. MB, MWH, VD, ZH and PI performed the theoretical calculations. **CS** and SE wrote the manuscript except for the theoretical part. The theory part was written by VD, ZH, MB, MWH and PI. All authors took part in the critical review of the manuscript before and after submission.

ABSTRACT   The investigation of the absolute scale of the effective neutrino mass remains challenging due to the exclusively weak interaction of neutrinos with all known particles in the standard model of particle physics. Currently, the most precise and least model-dependent upper limit on the electron antineutrino mass is set by the KATRIN experiment from the analysis of the tritium β-decay. Another promising approach is the electron capture in ^{163}Ho, which is under investigation using microcalorimetry within the ECHo and HOLMES collaborations. An independently measured Q-value of this process is vital for the assessment of systematic uncertainties in the neutrino mass determination.

Here, we report a direct, independent determination of this Q-value by measuring the free-space cyclotron frequency ratio of highly charged ions of ^{163}Ho and ^{163}Dy in the Penning trap experiment PENTATRAP. Combining this ratio with atomic physics calculations of the electronic binding energies yields a Q-value of $2863.2(0.6)\,\text{eV}/c^2$ - a more than 50-fold improvement over the state-of-the-art. This will enable the determination of the electron neutrino mass on a sub-eV level from the analysis of the electron capture in ^{163}Ho.

Penning-trap measurement of the Q-value of the electron capture in ^{163}Ho for the determination of the electron neutrino mass

Christoph Schweiger[1][*], Martin Braß[2], Vincent Debierre[1], Menno Door[1], Holger Dorrer[3], Christoph E. Düllmann[3,4,5], Christian Enss[6], Pavel Filianin[1], Loredana Gastaldo[6], Zoltán Harman[1], Maurits W. Haverkort[2], Jost Herkenhoff[1], Paul Indelicato[7], Christoph H. Keitel[1], Kathrin Kromer[1], Daniel Lange[1,8], Yuri N. Novikov[9], Dennis Renisch[3,4], Alexander Rischka[1], Rima X. Schüssler[1], Sergey Eliseev[1] and Klaus Blaum[1]

[1]Max-Planck-Institut für Kernphysik, Saupfercheckweg 1, Heidelberg, 69117, Germany.
[2]Institute for Theoretical Physics, Heidelberg University, Philosophenweg 19, Heidelberg, 69120, Germany.
[3]Department Chemie - Kernchemie, Johannes Gutenberg-Universität Mainz, Fritz-Straßmann-Weg 2, Mainz, 55128, Germany.
[4]Helmholtz-Institut Mainz, Staudingerweg 18, Mainz, 55128, Germany.
[5]GSI Helmholtzzentrum für Schwerionenforschung GmbH, Planckstraße 1, Darmstadt, 64291, Germany.
[6]Kirchhoff-Institute for Physics, Heidelberg University, Im Neuenheimer Feld 227, Heidelberg, 69120, Germany.
[7]Laboratoire Kastler Brossel, CNRS, ENS-PSL Research University, Collège de France, Campus Pierre et Marie Curie, Sorbonne Université, 4 place Jussieu, Paris, 75005, France.
[8]Heidelberg University, Grabengasse 1, Heidelberg, 69117, Germany.
[9]NRC "Kurchatov Institute"-Petersburg Nuclear Physics Institute, Gatchina, 188300, Russia.

*Corresponding author(s). E-mail(s): christoph.schweiger@mpi-hd.mpg.de;

Present Address:
R.X. Schüssler: Van der Waals–Zeeman Institute, Institute of Physics, University of Amsterdam, Science Park 904, Amsterdam 1098XH, The Netherlands
Martin Braß: Institute of Solid State Physics, TU Wien, 1040 Vienna, Austria

Abstract

The investigation of the absolute scale of the effective neutrino mass remains challenging due to the exclusively weak interaction of neutrinos with all known particles in the standard model of particle physics. Currently, the most precise and least model-dependent upper limit on the electron antineutrino mass is set by the KATRIN experiment from the analysis of the tritium β-decay. Another promising approach is the electron capture in ^{163}Ho, which is under investigation using microcalorimetry within the ECHo and HOLMES collaborations. An independently measured Q-value of this process is vital for the assessment of systematic uncertainties in the neutrino mass determination. Here, we report a direct, independent determination of this Q-value by measuring the free-space cyclotron frequency ratio of highly charged ions of ^{163}Ho and ^{163}Dy in the Penning trap experiment PENTATRAP. Combining this ratio with atomic physics calculations of the electronic binding energies yields a Q-value of $\mathbf{2863.2(0.6)\,eV/c^2}$ - a more than 50-fold improvement over the state-of-the-art. This will enable the determination of the electron neutrino mass on a sub-eV level from the analysis of the electron capture in ^{163}Ho.

Keywords: Penning trap, neutrino physics, neutrino mass, high-precision mass spectrometry, Q-value, nuclear decay, electron capture

1 The absolute scale of the neutrino mass

The observation of the neutrino flavor oscillations proves that neutrinos are massive particles, establishing that the weak neutrino flavor eigenstates are a superposition of three neutrino-mass eigenstates in contradiction to the Standard Model of particle physics [1, 2]. In oscillation experiments merely the differences of the squared neutrino mass eigenvalues can be investigated, leaving the absolute scale of the neutrino mass an open question. Thus, the absolute scale of the neutrino mass remains one of the most sought-after quantities in nuclear and particle physics, cosmology and beyond Standard Model theories that could potentially explain the origin of the neutrino rest mass [3–6].

Neutrinos are produced in weak nuclear decays; a model-independent measurement of their rest mass can be performed in a kinematic study of the decay products, where the neutrino itself is not directly detected. Relying on energy and momentum conservation, this is currently the most model-independent approach for neutrino mass determinations. Kinematic investigations constrain the effective rest mass of

the electron neutrino or antineutrino $m_{\nu_e}^2 = \sum_{i=1}^3 |U_{ei}|^2 m_i^2$, where U_{fi} are the elements of the Pontecorvo–Maki–Nakagawa–Sakata (PMNS) matrix, which describes the superposition of mass eigenstates m_i ($i \in \{1, 2, 3\}$) in the flavor eigenstates ν_f ($f \in \{e, \mu, \tau\}$). The individual mass eigenstates are not resolved in these experiments since the squared mass differences are well below current instrumental resolutions, with the largest one being $\Delta m_{32}^2 = (2.453 \pm 0.033) \cdot 10^{-3}\,\mathrm{eV}^2/c^4$ [7].

The most stringent constraint on the neutrino mass scale comes from the analysis of the matter distribution in the universe which results in a limit on the sum of the neutrino masses of $< 120\,\mathrm{meV}/c^2$ [8] while the most stringent direct limit of $0.8\,\mathrm{eV}/c^2$ (90 % C.L.) from a kinematic study of the tritium β-decay is set by the KATRIN collaboration [9, 10].

Complementary to this approach, there are several experiments using calorimetric techniques to investigate the neutrino rest mass directly. Historically, the first calorimetric approaches were the MANU and MIBETA experiments investigating the ^{187}Re β-decay yielding upper limits of 19 and $15\,\mathrm{eV}^2/c^2$ (90% C.L.), respectively[11]. Two current experiments, namely ECHo [12, 13] and HOLMES [14, 15], investigate the electron-capture in ^{163}Ho $\rightarrow$ ^{163}Dy $+ \nu_e + E_{\mathrm{cal}}$, with E_{cal} being the energy detected in a calorimeter. The current upper limit of the electron neutrino rest mass is on a level of $< 150\,\mathrm{eV}/c^2$ [13] and the ECHo and HOLMES collaborations aim to achieve sensitivities well below $< 1\,\mathrm{eV}/c^2$ [12].

Within the ECHo collaboration, metallic magnetic calorimeters are used for the measurement of the energy of all emitted radiation except for the energy carried away by the neutrino. This is obtained by implanting ^{163}Ho ions directly into the absorber material of the detector. The calorimetrically measured decay spectrum is subsequently analyzed by fitting it to a theoretical spectral shape from which the Q-value as well as the effective electron neutrino mass m_{ν_e} can be determined. In order to quantitatively investigate systematic effects in the interpretation of the calorimetrically measured spectra, that might arise due to the ^{163}Ho ions being implanted into a metallic material, this Q-value is best compared to one obtained from an independent direct measurement. The required accuracy of $\sim 1\,\mathrm{eV}/c^2$ can currently only be reached using high-precision Penning-trap mass spectrometry (PTMS). In PTMS, the Q-value is addressed directly through a measurement of the mass difference of the mother and daughter nuclides, ^{163}Ho and ^{163}Dy, respectively [12, 16], by measuring the free cyclotron frequency ratio of the two species in a strong homogeneous magnetic field B. Within a magnetic field, an ion with charge-to-mass ratio q/m is forced onto a circular orbit where it revolves with the free-space cyclotron frequency $\nu_c = \frac{1}{2\pi} \frac{q}{m} B$. In a Penning trap, a superimposed weak quadrupolar electrostatic potential confines the ion along the magnetic field lines and modifies the ion's radial motion: The free-space cyclotron motion splits into the magnetron motion with the frequency ν_- and the modified cyclotron motion with frequency ν_+. In addition, the quadrupolar electrostatic potential induces a harmonic oscillatory motion with frequency ν_z along the magnetic field lines. From a measurement of all three motional eigenfrequencies, the free-space cyclotron frequency can be reconstructed using the invariance theorem $\nu_c^2 = \nu_+^2 + \nu_z^2 + \nu_-^2$ [17]. From subsequent measurements of the free-space cyclotron frequency the ratio $R_{q+} = \nu_c(^{163}\mathrm{Dy}^{q+})/\nu_c(^{163}\mathrm{Ho}^{q+})$

is determined, which finally allows the determination of the Q-value by including atomic physics calculations of the binding energy difference $\Delta E_{\mathrm{B}}^{q+}$ of the removed electrons:

$$Q = m_{\mathrm{Dy}}^{q+}\left(R_{q+} - 1\right) + \Delta E_{\mathrm{B}}^{q+}. \tag{1}$$

$\Delta E_{\mathrm{B}}^{q+}$ is given by the difference in the sum of the binding energies of the n missing electrons in the highly charged ions (HCIs) of both nuclides and m_{Dy}^{q+} is the "reference" mass of the HCI of dysprosium. $q = n \cdot e$ is the charge of the ions, with e being the elementary charge and n the number of removed electrons ("charge state"). In order to enhance the readability in formulas, sometimes q also denotes the number of missing electrons n.

2 The Penning-trap experiment PENTATRAP

Experimental setup

The measurement of the free-space cyclotron frequency ratio R of the two HCIs ^{163}Ho^{q+} and ^{163}Dy^{q+} was carried out with the high-precision Penning-trap mass spectrometer PENTATRAP located at the Max-Planck-Institute for Nuclear Physics in Heidelberg, Germany [18, 19]. An overview of the apparatus is given in Figure 1.

HCIs of the synthetic radioisotope ^{163}Ho, which was produced by neutron irradiation of stable ^{162}Er [21], and HCIs of the stable ^{163}Dy are produced in a compact room-temperature electron beam ion trap (EBIT) that is specifically designed and constructed for the production of HCIs from samples available only in limited quantities (TIP-EBIT) [20]. For the measurements reported here only $2 \cdot 10^{15}$ atoms of ^{163}Ho were used, with a typical sample containing about 10^{14} atoms of ^{163}Ho. HCIs of the two species are extracted with a kinetic energy of $4.4\,\mathrm{keV}/q$ from the EBIT and transported through an electrostatic beamline towards the Penning traps. Individual charge states $n = \{38, 39, 40\}$ are selected using a Bradbury-Nielsen Gate and a fast switching electronic circuit [22, 23] located about $1.5\,\mathrm{m}$ from the EBIT. Just before reaching the mass spectrometer, the HCIs are decelerated to a few eV/q by appropriately timed voltage pulses on two cylindrical drift tubes.

The mass spectrometer consists of a stack of five identical, cylindrical Penning traps located in the cold bore of a $7\,\mathrm{T}$, actively shielded superconducting magnet [18, 24]. The voltages applied to the Penning-trap electrodes are supplied from an ultra-stable voltage source [25]. The Penning traps as well as the detection system are located inside a vacuum chamber immersed in liquid helium at a temperature of about $4\,\mathrm{K}$. Two (trap 2 and trap 3, cf. Fig. 2 (a)) of the five Penning traps are equipped with a non-destructive image-current detection system [18, 26–28] and are used for the measurement of the ions' motional frequencies. Trap 1 and trap 4 serve as storage traps while trap 1 is also used as a capture trap when a new set of ions is loaded into the trap stack.

Environmental parameters affecting the magnetic field in the traps are stabilized e.g. the temperature in the laboratory to $0.1\,\mathrm{K/day}$ as well as the liquid helium level and pressure of helium gas inside the cold bore of the magnet. In these conditions the magnetic field exhibits a relative drift of a few 10^{-10} per hour [29]. Frequency
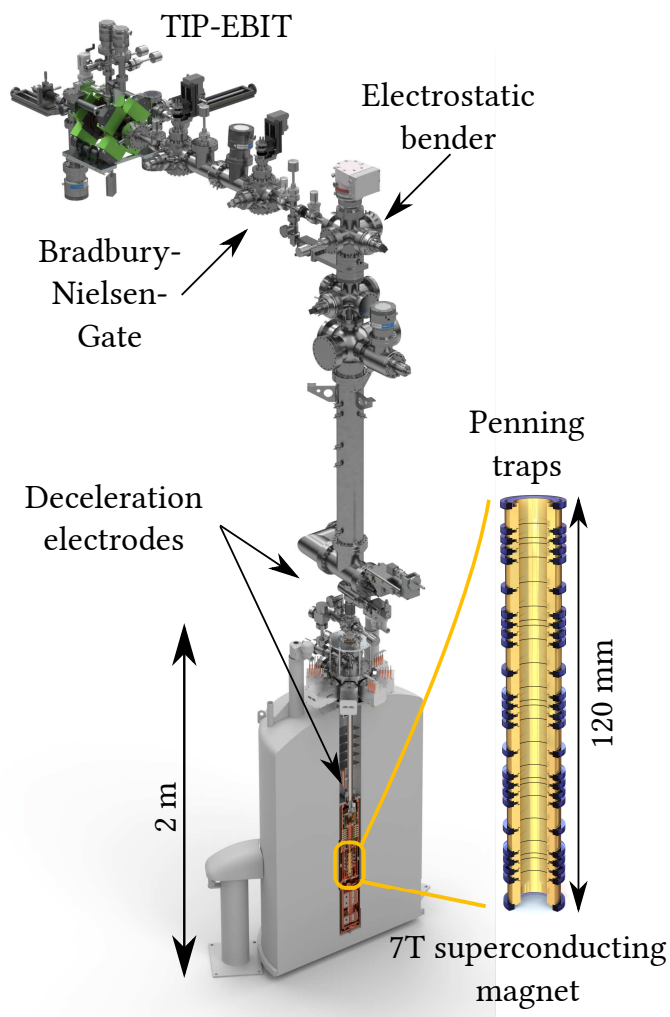
Fig. 1 Rendered overview of the PENTATRAP experimental setup. The upper horizontal part of the beamline is located on the ground floor while the superconducting magnet is located in a dedicated laboratory in the basement. The TIP-EBIT is an electron beam ion trap specifically designed for very small samples sizes [20]. Follwing the TIP-EBIT in the horizontal beamline, a Bradbury-Nielsen gate is used to separate a single charge state. HCIs produced in the TIP-EBIT are guided through the electrostatic beamline to the stack of five identical Penning traps in the superconducting magnet. For capturing the HCIs in the Penning traps deceleration electrodes with appropriately timed voltage pulses are used. A more detailed view of the Penning trap stack is shown on the right.

measurements are performed overnight and on weekends when external perturbations are minimal.

The measurement starts with loading a set of three ions, in the order ^{163}Dy, ^{163}Ho and ^{163}Dy into traps 2, 3, and 4, respectively (cf. Fig. 2 (a)). The motional frequencies of the HCIs in traps 2 and 3 are measured simultaneously, starting with the ions in position 1. Subsequently, the ions are shuttled to position 2, which effectively swaps the ion species in traps 2 and 3 (cf. Fig. 2 (a)) and the measurement is repeated. The resulting data structure is shown in Fig. 2 (b) where the free-space cyclotron frequency ν_c is plotted as a function of the measurement time. Alternating datapoints for ^{163}Dy and ^{163}Ho result from the swapping of the ion species in traps 2 and 3. More details on the ion preparation and the measurement sequence is given in the Methods Section 7.
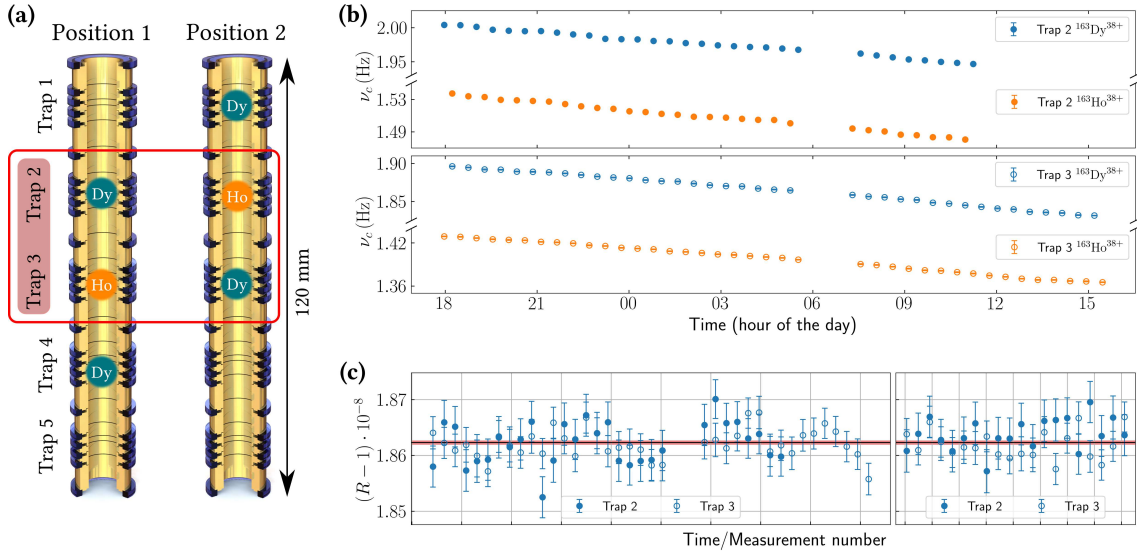
Fig. 2 Overview of the measurement procedure and resulting data structure. Error bars correspond to the 1σ statistical uncertainty which is propagated by Gaussian uncertainty propagation. (a) Rendering of the stack of five identical, cylindrical Penning traps of the PENTATRAP experiment. Traps 2 and 3, with labels marked in red, are used as measurement traps and are equipped with a detection system. Shuttling the ions from Position 1 into Position 2 effectively swaps the ion species in traps 2 and 3 resulting in the alternating data structure as shown in panel (b). The traps 1 and 4 are used as storage traps while trap 5 is not used in this measurement. (b) Exemplary dataset of the measured free cyclotron frequencies ν_c of ^{163}Ho (orange) and ^{163}Dy (blue) in the traps 2 (upper panel) and 3 (lower panel) for one measurement run in charge state $q = 38 \cdot e$. For trap 2 and 3 frequency offsets of 25081589 Hz and 25081620 Hz were subtracted. The linear drift of the free cyclotron frequency which can be attributed to the slow decay of the magnetic field of the superconducting magnet due to the flux creep effect [30, 31]. Please note that the vertical axis is broken for illustrative purposes while there are no left and right sub-panels. (c) Ratios R_i of the free cyclotron frequencies ν_c of ^{163}Dy and ^{163}Ho in traps 2 (filled circles) and 3 (empty circles) determined from the full dataset of two runs for the charge state $n = 38$. The data of each run is shown in a dedicated sub-panel where the ratios from (b) are shown in the left sub-panel. The horizontal black line indicates the weighted average of all measured ratios for this charge state with the light red band marking the 1σ uncertainty band.

Data analysis

In order to extract frequency ratios R from the free-space cyclotron frequencies ν_c, the magnetic field behavior has to be interpolated in-between the individual frequency measurement datapoints from one species to the time when the other species' frequencies were measured.

Fig. 2 (b) shows exemplary the free cyclotron frequencies from one measurement run performed on ions with the charge state $q = 38 \cdot e$. The linear slope of the data points can be attributed to the slow decay of the magnetic field of the superconducting magnet due to the flux creep effect [30, 31] and is on the order of a few 10^{-10} per hour relative to the absolute magnetic field of $\sim 7\,\mathrm{T}$.

In the data analysis, the frequency of ^{163}Dy is linearly interpolated between two datapoints to the time where ^{163}Ho was measured. From this interpolated datapoint the ratio R is determined as illustrated in Figure 3 (a). This procedure is followed for the full dataset. Residual non-linear behavior of the cyclotron frequency drift, originating from physical effects that alter the temperature and position of magnetic materials that surround the Penning traps and change the magnetic field within the
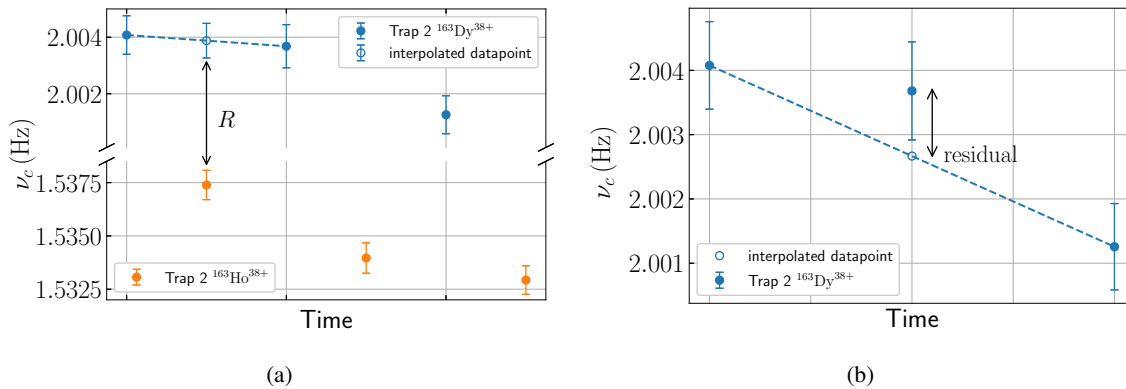
(a)   (b)

Fig. 3 Detailed plot of the first few datapoints of the cyclotron frequency ν_c from Figure 2 (b) in order to illustrate the data analysis procedure. From the frequency values an offset of 25081589 Hz is subtracted. For details on the analysis procedure see main text. Error bars correspond to the 1σ statistical uncertainty which is propagated by Gaussian uncertainty propagation. (a) Linear interpolation between two ^{163}Dy datapoints to the time at which ^{163}Ho was measured for the determination of the free-space cyclotron frequency ratio R. Please note that the vertical axis was broken for illustration purposes. (b) Exemplary estimation of the non-linearity by interpolation of the data onto itself. Here we linearly interpolate between the first and third datapoint and determine the difference between the measured datapoint in between and the interpolated one. The sum of these "residuals" divided by the number of residuals in the full dataset is taken into account as an additional uncertainty on the ratio.

traps is taken into account in the uncertainty of the interpolated R. For this, the frequency data points are interpolated back to themselves (see Figure 3 (b)), and the sum of the residuals divided by the number of residuals is included as an additional uncertainty in the ratio. The resulting ratios $R_i = \nu_{c,i}(^{163}\mathrm{Dy}^{38+})/\nu_{c,i}(^{163}\mathrm{Ho}^{38+})$ for the two measurement runs are shown in Fig. 2 (c) for both traps. The ratios for the individual traps are consistent, therefore the final ratio is calculated as the weighted average and shown as a red line including the 1σ uncertainty band. For the calculation of the uncertainty of the final ratio, the inner error σ^2_{int} and the outer error σ^2_{ext} are calculated and the larger of the two is used as the final uncertainty [32, 33]:

$$\sigma^2_{\mathrm{int}} = \frac{1}{\sum_i \frac{1}{\sigma_i^2}} \tag{2}$$

$$\sigma^2_{\mathrm{ext}} = \frac{\sum_i \frac{1}{\sigma_i^2}(R_i - \tilde{R})^2}{(N-1)\sum_i \frac{1}{\sigma_i^2}}. \tag{3}$$

Here, R_i and σ_i are individual cyclotron frequency ratios and their corresponding 1σ uncertainty, $\tilde{R}$ is the weighted average and N is the total number of ratios.

The total systematic uncertainty (e.g. field anharmonicities and inhomogeneity, image charge shift and relativistic shift) is strongly suppressed due to the fact that ^{163}Ho and ^{163}Dy in the same charge state form a unique mass doublet with a sufficiently small mass difference of about $2.8\,\mathrm{keV}$. With a difference in mass-to-charge ratio of only about 10^{-8} the same trapping potential is used for both ^{163}Ho and ^{163}Dy and the magnetron and axial frequencies are sufficiently equal. Thus, all systematic uncertainties in the free-space cyclotron frequency measurement cancel out

to a large extent in the determination of the frequency ratio R and are smaller than 10^{-12}. Extended Data Table 3 summarizes the considered systematic shifts. An additional systematic uncertainty can arise from the fact that HCIs might have long-lived low-energy atomic metastable states, as observed in previous measurements [34]. This is undesirable since it will shift the determined Q-value by the energy of the metastable state. In Section 4 we compare the Q-values resulting from the measurements of three different charge states which allows us to exclude potential shifts of the Q-value due to long-lived electronic metastable states that would influence each charge state differently. The final ratios of free cyclotron frequencies of the ions in the different charge states are summarized in Table 2.

3 Calculation of binding energy differences

Theoretical calculations provide the binding energies of the electrons removed from the neutral Ho and Dy atoms. The Dy and Ho atoms are in the $[\text{Xe}]4f^{10}6s^2\ ^5I_8$ and $[\text{Xe}]4f^{11}6s^2\ ^4I_{15/2}$ electronic states, respectively. For a better control of systematic effects, several HCI of Dy and Ho were considered in the experiment, namely, $\text{Dy}^{38+,39+,40+}$, with the ground states $[\text{Ar}]3d^{10,9,8}$, respectively, and $\text{Ho}^{38+,39+,40+}$ with $[\text{Ar}]3d^{10}4s$, $[\text{Ar}]3d^{10}$, and $[\text{Ar}]3d^9$, respectively.

Configuration interaction method

In a first set of calculations, the binding energies are calculated in Quanty [35–37] using the configuration interaction (CI) method. The starting point is a fully relativistic density functional theory (DFT) calculation with the full-potential local-orbital minimum-basis code FPLO [38–40]. The DFT calculation determines the ground-state density of the ion around which a CI expansion is made. The corresponding Kohn-Sham orbitals are used as single particle basis to construct the Slater determinants that span a configuration space. The Hamiltonian comprises Coulomb and static Breit interaction between the electrons as well as their relativistic kinetic energies and potential energies due to Coulomb attraction of the ion's nucleus. Diagonalization of this Hamiltonian on a given configuration space using the Lánczos algorithm determines the ground-state energy of an ion.

At first, only the space of the ground state configuration is considered. Subsequently the configuration space is iteratively expanded to include single, double and triple excitations of electrons into orbitals with higher principal quantum numbers. Details of these calculations are given in the Methods section. We arrive to the calculated binding energy differences given in Table 1.

Multiconfiguration Dirac-Hartree-Fock method

In the second set of calculations, we use the multiconfiguration Dirac-Hartree-Fock method (MCDHF) [41] and its combination with Brillouin-Wigner many-body perturbation theory [42, 43].

In the MCDHF method, the atomic state function is modeled as a superposition of configuration state functions (CSFs) with fixed angular momentum, magnetic and parity quantum numbers. The CSFs are built as Slater determinants of Dirac orbitals

in the jj coupling scheme. Using the parallel GRASP2018 codes [43], we expand the space of virtual orbitals used for the construction of CSFs by single and double electron exchanges in a systematic manner. The convergence of the energies with respect to the maximal principal quantum number of virtual orbitals is monitored, and the spread of values resulting from different correlation models is used as a measure of the leading contribution (90%) of the theoretical uncertainties. In case of the HCI, the set of CSFs is generated with exchanges including all occupied orbitals from $1s$ on, and with virtual orbitals up to typically $10h$. Virtual orbitals are optimized in a layer-by-layer fashion [43, 44]. Effects of the Breit interaction, recoil, and approximate quantum electrodynamic corrections are accounted for by the configuration interaction method using orbitals from the MCDHF procedure [43]. More details are given in the Methods. We obtain the theoretical values of the binding energy differences listed in Table 1.

In a third set of calculations, we use the Multiconfiguration Dirac-Fock General-Matrix-Elements (MCDFGME) code[45], to check the previous results. The calculation is performed in the *optimized level* mode, where all correlation orbitals are fully relaxed instead of the layer by layer method. Convergence is much more difficult in this case and limits the number of extra orbitals that can be added in the evaluation of correlation. In this calculation, the magnetic and retardation interaction at the Breit level are included in the Dirac-Fock equations on the same footing as the Coulomb interaction, meaning that the Breit interaction is included to all orders in the correlation energy [46]. The Uehling potential is also evaluated to all orders [47]. Finally, self-energy screening is calculated using both the Welton method [48] and the model operator method [49]. For the HCIs, energies obtained by exciting occupied orbitals from $3s$ or $3d$ to open shells ($4f$, $6p$, $5d$, $7s$, $7p$ and $5g$) were compared. For neutrals, values obtained by exciting the core from $3d$ and $4s$ were compared. Calculations included only single and double excitations, as triple excitations lead to unmanageably large numbers of magnetic and retardation integrals. All possible single excitations were included, even those obeying Brillouin's theorem [45]. The results are given in Table 1 and are in good agreement with the GRASP2018 evaluation. Both sets of values are in agreement with the uncorrelated values [50], confirming the good compensation of correlation between the two ions.

Final values for the binding energy difference

The final binding energy $\Delta E_{\mathrm{B}}^{q+}$ for each charge state q is calculated as the weighted average of the values from the CI and MCDHF calculations (cf. Table 1). The uncertainty is determined by comparing the inner and outer errors and using the larger one as final uncertainty on $\Delta E_{\mathrm{B}}^{q+}$. For the charge states $q = \{39, 40\} \cdot e$, the larger of the two uncertainties is averaged with the uncertainty assuming correlations between the CI and MCDHF methods, i.e. with the uncertainty of $0.8\,\mathrm{eV}$ of the MCDHF method. The resulting $\Delta E_{\mathrm{B}}^{q+}$ are consistent with the MCDFGME calculations described above as well as with the calculations recently published in [51].

q/e	$\Delta E_{\mathrm{B,CI}}$	$\Delta E_{\mathrm{B,MCDHF}}$	$\Delta E_{\mathrm{B,MCDFGME}}$	$\Delta E_{\mathrm{B}}^{q+}$
38	38.8 ± 1.0	36.5 ± 0.8	38.1 ± 1.5	37.4 ± 1.4
39	1148.2 ± 1.0	1146.7 ± 0.8	1148.1 ± 1.5	1147.3 ± 0.7
40	1116.6 ± 1.0	1115.1 ± 0.8	1116.4 ± 1.5	1115.7 ± 0.7

Table 1 Summary of the electronic binding energy differences for the three charge states (first column) in electron volts (eV) from the three theory calculations: Configuration interaction (CI) method (second column), the Multiconfiguration Dirac-Hartree-Fock (MCDHF) method (third column) and the Multiconfiguration Dirac-Fock General-Matrix-Elements (MCDFGME) method (fourth column). The given uncertainties correspond to the 1σ uncertainty. In the last column the final ΔE_{B} for the determination of the Q-value are given which were calculated as the weighted average of the CI and MCDHF methods. For details on the calculation of the uncertainties see main text.

4 Q-value determination

The Q-value of the electron capture in ^{163}Ho is determined from the measured ratio of the free cyclotron frequencies R (see Section 2) and the theoretically calculated binding energy differences $\Delta E_{\mathrm{B}}^{q+}$ (see Section 3 and Table 1) for each charge state $q = \{38, 39, 40\} \cdot e$ according to Equation 1. The (reference) mass m_{Dy}^{q+} of ^{163}Dy^{q+} is calculated starting from the mass of atomic ^{163}Dy, m_{Dy} [52], and subtracting the masses of the n missing electrons [53, 54] and their binding energies [55]. Table 2 lists the ratios R for the three measured charge states as well as the 1σ uncertainty δR which is computed using standard Gaussian uncertainty propagation.

Using Equation (1) and the binding energy differences, the final Q-values are calculated for the three charge states and are summarized in Table 2.

q/e	R	δR	$\Delta E_{\mathrm{B}}^{q+}$ (eV)	Q (eV/c^2)
38	1.000000018623	3.0E-12	37.4 ± 1.4	2863.4 ± 1.5
39	1.000000011307	4.1E-12	1147.3 ± 0.7	2863.2 ± 0.9
40	1.000000011516	3.5E-12	1115.7 ± 0.7	2863.2 ± 0.9

Table 2 Summary of the main results for the three charge states (column one): Weighted averages of the ratios (second column) and their uncertainty (third column), the weighted averages of the binding energy differences (fourth column, c.f. Table 1) and the calculated Q-values (fifth column) for the three measured charge states. Uncertainties correspond to the 1σ statistical uncertainty. For details on the calculation of the uncertainties see main text.

The resulting Q-values for the different charge states agree within their 1σ uncertainties. Resulting from the very good agreement, systematic deviations from either the free cyclotron ratio measurement or from the calculation of the binding energy difference can be excluded to a large extent. Furthermore, also the influence of unknown metastable electronic states can be largely ruled out since it is very unlikely that an electronic metastable state has exactly the same excitation energy in all three of the measured charge states.

The final Q-value is calculated as the weighted average of the Q-values obtained for the three charge states resulting in:

$$Q = 2863.2(0.6) \, \mathrm{eV}/c^2. \tag{4}$$

This value is in 1σ agreement with the previously measured value at SHIPTRAP of $2833(34)\text{eV}/c^2$ [56] but 50 times more precise. In Figure 4 the most recent measurements of the Q-value of ^{163}Ho from cryogenic microcalorimetry, PTMS and the Atomic Mass Evaluation (AME) 2020 are shown. The value from the AME 2020 is an average from three different microcalorimetric measurements. Our value is slightly higher than the current AME adjustment and agrees within 1.2σ.
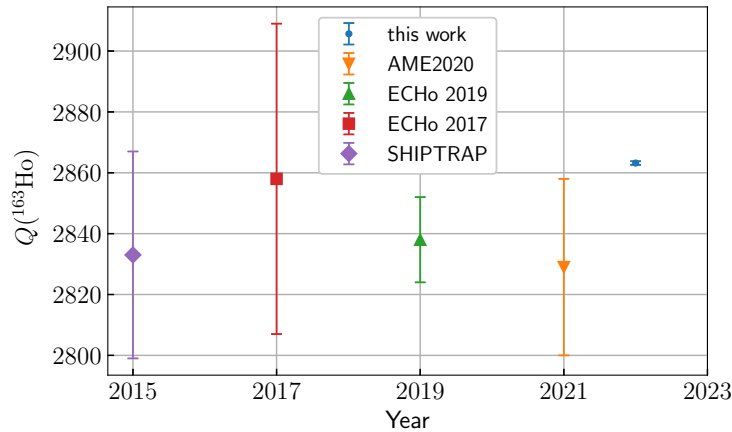

Fig. 4 Comparison of the most recent measurements of the ^{163}Ho EC Q-value from PTMS (SHIP-TRAP [56] and "this work"), microcalorimetry (ECHo 2017 [57] and ECHo 2019 [13]) and the most recent AME adjustment 2020 [52].

The ^{163}Ho Q_{EC}-value was obtained by combining a high-precision measurement of the free-space cyclotron frequency of HCIs of the mother and daughter nuclide in a Penning trap and precise atomic physics calculations of the electronic binding energies of the missing electrons. Experiments investigating the electron neutrino mass by microcalorimetric measurements of the decay spectrum of ^{163}Ho such as those of the ECHo and HOLMES collaborations are now provided with an independently measured Q-value with an unprecedented precision of $0.6\,\text{eV}$, which allows the assessment of systematic uncertainties in the neutrino mass determination using cryogenic microcalorimetry on a level of $< 1\,\text{eV}$.

5 Acknowledgements

6 Author contributions statement

Conceived and designed the experiments

Ch. Schweiger, M. Door, Ch. E. Düllmann, C. Enss, P. Filianin, L. Gastaldo, Yu. N. Novikov, A. Rischka, R.X. Schüssler, S. Eliseev, K. Blaum.

Performed the experiments

Ch. Schweiger, M. Door, P. Filianin, J. Herkenhoff, K. Kromer, S. Eliseev.

Analyzed the data

Ch. Schweiger, S. Eliseev.

Performed and evaluated the theoretical calculations

M. Braß, V. Debierre, Z. Harman, M.W. Haverkort, P. Indelicato

Supervision, interpretation and discussion of the theoretical calculations

M. Braß, V. Debierre, Z. Harman, M.W. Haverkort, C.H. Keitel, P. Indelicato

Contributed materials/analysis tools

Ch. Schweiger, M. Door, H. Dorrer, Ch. E. Düllmann, K. Kromer, D. Lange, D. Renisch, S. Eliseev, K. Blaum.

Wrote the paper

Ch. Schweiger, M. Braß, V. Debierre, Z. Harman, M.W. Haverkort, P. Indelicato, S. Eliseev.

All authors took part in the critical review of the manuscript.

References

[1] Fukuda, Y., Hayakawa, T., Ichihara, E., Inoue, K., Ishihara, K., Ishino, H., Itow, Y., Kajita, T., Kameda, J., Kasuga, S., Kobayashi, K., Kobayashi, Y., Koshio, Y., Miura, M., Nakahata, M., Nakayama, S., Okada, A., Okumura, K., Sakurai, N., Shiozawa, M., Suzuki, Y., Takeuchi, Y., Totsuka, Y., Yamada, S., Earl, M., Habig, A., Kearns, E., Messier, M.D., Scholberg, K., Stone, J.L., Sulak, L.R., Walter, C.W., Goldhaber, M., Barszczxak, T., Casper, D., Gajewski, W., Halverson, P.G., Hsu, J., Kropp, W.R., Price, L.R., Reines, F., Smy, M., Sobel, H.W., Vagins, M.R., Ganezer, K.S., Keig, W.E., Ellsworth, R.W., Tasaka, S., Flanagan, J.W., Kibayashi, A., Learned, J.G., Matsuno, S., Stenger, V.J., Takemori, D., Ishii, T., Kanzaki, J., Kobayashi, T., Mine, S., Nakamura, K., Nishikawa, K., Oyama, Y., Sakai, A., Sakuda, M., Sasaki, O., Echigo, S., Kohama, M., Suzuki, A.T., Haines, T.J., Blaufuss, E., Kim, B.K., Sanford, R., Svoboda, R., Chen, M.L., Conner, Z., Goodman, J.A., Sullivan, G.W., Hill, J., Jung, C.K., Martens, K., Mauger, C., McGrew, C., Sharkey, E., Viren, B., Yanagisawa, C., Doki, W., Miyano, K., Okazawa, H., Saji, C., Takahata, M., Nagashima, Y., Takita, M., Yamaguchi, T., Yoshida, M., Kim, S.B., Etoh, M., Fujita, K., Hasegawa, A., Hasegawa, T., Hatakeyama, S., Iwamoto, T., Koga, M., Maruyama, T., Ogawa, H., Shirai, J., Suzuki, A., Tsushima, F., Koshiba, M., Nemoto, M., Nishijima, K., Futagami, T., Hayato, Y., Kanaya, Y., Kaneyuki, K., Watanabe, Y., Kielczewska, D., Doyle, R.A., George, J.S., Stachyra, A.L., Wai, L.L., Wilkes, R.J., Young, K.K.: Evidence for oscillation of atmospheric neutrinos. Phys. Rev. Lett. **81**, 1562–1567 (1998). https://doi.org/10.1103/PhysRevLett.81.1562

[2] Ahmad, Q.R., Allen, R.C., Andersen, T.C., D.Anglin, J., Barton, J.C., Beier, E.W., Bercovitch, M., Bigu, J., Biller, S.D., Black, R.A., Blevis, I., Boardman, R.J., Boger, J., Bonvin, E., Boulay, M.G., Bowler, M.G., Bowles, T.J., Brice, S.J., Browne, M.C., Bullard, T.V., Bühler, G., Cameron, J., Chan, Y.D., Chen, H.H., Chen, M., Chen, X., Cleveland, B.T., Clifford, E.T.H., Cowan, J.H.M., Cowen, D.F., Cox, G.A., Dai, X., Dalnoki-Veress, F., Davidson, W.F., Doe, P.J., Doucas, G., Dragowsky, M.R., Duba, C.A., Duncan, F.A., Dunford, M., Dunmore, J.A., Earle, E.D., Elliott, S.R., Evans, H.C., Ewan, G.T., Farine, J., Fergani, H., Ferraris, A.P., Ford, R.J., Formaggio, J.A., Fowler, M.M., Frame, K., Frank, E.D., Frati, W., Gagnon, N., Germani, J.V., Gil, S., Graham, K., Grant, D.R., Hahn, R.L., Hallin, A.L., Hallman, E.D., Hamer, A.S., Hamian, A.A., Handler, W.B., Haq, R.U., Hargrove, C.K., Harvey, P.J., Hazama, R., Heeger, K.M., Heintzelman, W.J., Heise, J., Helmer, R.L., Hepburn, J.D., Heron, H., Hewett, J., Hime, A., Howe, M., Hykawy, J.G., Isaac, M.C.P., Jagam, P., Jelley, N.A., Jillings, C., Jonkmans, G., Kazkaz, K., Keener, P.T., Klein, J.R., Knox, A.B., Komar, R.J., Kouzes, R., Kutter, T., Kyba, C.C.M., Law, J., Lawson, I.T., Lay, M., Lee, H.W., Lesko, K.T., Leslie, J.R., Levine, I., Locke, W., Luoma, S., Lyon, J., Majerus, S., Mak, H.B., Maneira, J., Manor, J., Marino, A.D., McCauley, N., McDonald, A.B., McDonald, D.S., McFarlane, K., McGregor, G., Meijer Drees, R., Mifflin, C., Miller, G.G., Milton, G., Moffat, B.A., Moorhead, M., Nally, C.W., Neubauer, M.S., Newcomer, F.M.,

Ng, H.S., Noble, A.J., Norman, E.B., Novikov, V.M., O'Neill, M., Okada, C.E., Ollerhead, R.W., Omori, M., Orrell, J.L., Oser, S.M., Poon, A.W.P., Radcliffe, T.J., Roberge, A., Robertson, B.C., Robertson, R.G.H., Rosendahl, S.S.E., Rowley, J.K., Rusu, V.L., Saettler, E., Schaffer, K.K., Schwendener, M.H., Schülke, A., Seifert, H., Shatkay, M., Simpson, J.J., Sims, C.J., Sinclair, D., Skensved, P., Smith, A.R., Smith, M.W.E., Spreitzer, T., Starinsky, N., Steiger, T.D., Stokstad, R.G., Stonehill, L.C., Storey, R.S., Sur, B., Tafirout, R., Tagg, N., Tanner, N.W., Taplin, R.K., Thorman, M., Thornewell, P.M., Trent, P.T., Tserkovnyak, Y.I., Van Berg, R., Van de Water, R.G., Virtue, C.J., Waltham, C.E., Wang, J.-X., Wark, D.L., West, N., Wilhelmy, J.B., Wilkerson, J.F., Wilson, J.R., Wittich, P., Wouters, J.M., Yeh, M.: Direct evidence for neutrino flavor transformation from neutral-current interactions in the sudbury neutrino observatory. Phys. Rev. Lett. **89**, 011301 (2002). https://doi.org/10.1103/PhysRevLett.89.011301

[3] King, S.F.: Neutrino mass models. Reports on Progress in Physics **67**(2), 107–157 (2003). https://doi.org/10.1088/0034-4885/67/2/r01

[4] Drexlin, G., Hannen, V., Mertens, S., Weinheimer, C.: Current direct neutrino mass experiments. Advances in High Energy Physics **2013**, 293986 (2013). https://doi.org/10.1155/2013/293986

[5] Formaggio, J.A., de Gouvêa, A.L.C., Robertson, R.G.H.: Direct measurements of neutrino mass. Physics Reports **914**, 1–54 (2021). https://doi.org/10.1016/j.physrep.2021.02.002

[6] de Gouvêa, A.: Neutrino mass models. Annual Review of Nuclear and Particle Science **66**(1), 197–217 (2016) https://doi.org/10.1146/annurev-nucl-102115-044600. https://doi.org/10.1146/annurev-nucl-102115-044600

[7] Workman, R.L., Others: Review of Particle Physics. PTEP **2022**, 083–01 (2022). https://doi.org/10.1093/ptep/ptac097

[8] Planck Collaboration, Aghanim, N., Akrami, Y., Ashdown, M., Aumont, J., Baccigalupi, C., Ballardini, M., Banday, A. J., Barreiro, R. B., Bartolo, N., Basak, S., Battye, R., Benabed, K., Bernard, J.-P., Bersanelli, M., Bielewicz, P., Bock, J. J., Bond, J. R., Borrill, J., Bouchet, F. R., Boulanger, F., Bucher, M., Burigana, C., Butler, R. C., Calabrese, E., Cardoso, J.-F., Carron, J., Challinor, A., Chiang, H. C., Chluba, J., Colombo, L. P. L., Combet, C., Contreras, D., Crill, B. P., Cuttaia, F., de Bernardis, P., de Zotti, G., Delabrouille, J., Delouis, J.-M., Di Valentino, E., Diego, J. M., Doré, O., Douspis, M., Ducout, A., Dupac, X., Dusini, S., Efstathiou, G., Elsner, F., Enßlin, T. A., Eriksen, H. K., Fantaye, Y., Farhang, M., Fergusson, J., Fernandez-Cobos, R., Finelli, F., Forastieri, F., Frailis, M., Fraisse, A. A., Franceschi, E., Frolov, A., Galeotta, S., Galli, S., Ganga, K., Génova-Santos, R. T., Gerbino, M., Ghosh, T., González-Nuevo, J., Górski, K. M., Gratton, S., Gruppuso, A., Gudmundsson, J. E., Hamann, J., Handley, W., Hansen, F. K., Herranz, D., Hildebrandt, S.

R., Hivon, E., Huang, Z., Jaffe, A. H., Jones, W. C., Karakci, A., Keihänen, E., Keskitalo, R., Kiiveri, K., Kim, J., Kisner, T. S., Knox, L., Krachmalnicoff, N., Kunz, M., Kurki-Suonio, H., Lagache, G., Lamarre, J.-M., Lasenby, A., Lattanzi, M., Lawrence, C. R., Le Jeune, M., Lemos, P., Lesgourgues, J., Levrier, F., Lewis, A., Liguori, M., Lilje, P. B., Lilley, M., Lindholm, V., López-Caniego, M., Lubin, P. M., Ma, Y.-Z., Macías-Pérez, J. F., Maggio, G., Maino, D., Mandolesi, N., Mangilli, A., Marcos-Caballero, A., Maris, M., Martin, P. G., Martinelli, M., Martínez-González, E., Matarrese, S., Mauri, N., McEwen, J. D., Meinhold, P. R., Melchiorri, A., Mennella, A., Migliaccio, M., Millea, M., Mitra, S., Miville-Deschênes, M.-A., Molinari, D., Montier, L., Morgante, G., Moss, A., Natoli, P., Nørgaard-Nielsen, H. U., Pagano, L., Paoletti, D., Partridge, B., Patanchon, G., Peiris, H. V., Perrotta, F., Pettorino, V., Piacentini, F., Polastri, L., Polenta, G., Puget, J.-L., Rachen, J. P., Reinecke, M., Remazeilles, M., Renzi, A., Rocha, G., Rosset, C., Roudier, G., Rubiño-Martín, J. A., Ruiz-Granados, B., Salvati, L., Sandri, M., Savelainen, M., Scott, D., Shellard, E. P. S., Sirignano, C., Sirri, G., Spencer, L. D., Sunyaev, R., Suur-Uski, A.-S., Tauber, J. A., Tavagnacco, D., Tenti, M., Toffolatti, L., Tomasi, M., Trombetti, T., Valenziano, L., Valiviita, J., Van Tent, B., Vibert, L., Vielva, P., Villa, F., Vittorio, N., Wandelt, B. D., Wehus, I. K., White, M., White, S. D. M., Zacchei, A., Zonca, A.: Planck 2018 results - vi. cosmological parameters. A&A **641**, 6 (2020). https://doi.org/10.1051/0004-6361/201833910

[9] Aker, M., Altenmüller, K., Amsbaugh, J.F., Arenz, M., Babutzka, M., Bast, J., Bauer, S., Bechtler, H., Beck, M., Beglarian, A., Behrens, J., Bender, B., Berendes, R., Berlev, A., Besserer, U., Bettin, C., Bieringer, B., Blaum, K., Block, F., Bobien, S., Böttcher, M., Bohn, J., Bokeloh, K., Bolz, H., Bornschein, B., Bornschein, L., Bouquet, H., Boyd, N.M., Brunst, T., Burritt, T.H., Caldwell, T.S., Chaoui, Z., Chilingaryan, S., Choi, W., Corona, T.J., Cox, G.A., Debowski, K., Deffert, M., Descher, M., Barrero, D.D., Doe, P.J., Dragoun, O., Drexlin, G., Dunmore, J.A., Dyba, S., Edzards, F., Eichelhardt, F., Eitel, K., Ellinger, E., Engel, R., Enomoto, S., Erhard, M., Eversheim, D., Fedkevych, M., Felden, A., Fischer, S., Formaggio, J.A., Fränkle, F.M., Franklin, G.B., Frenzel, H., Friedel, F., Fulst, A., Gauda, K., Gehring, R., Gil, W., Glück, F., Görhardt, S., Grimm, J., Grössle, R., Groh, S., Grohmann, S., Gumbsheimer, R., Hackenjos, M., Häßler, D., Hannen, V., Harms, F., Harper, G.C., Hartmann, J., Haußmann, N., Heizmann, F., Helbing, K., Held, M., Hickford, S., Hilk, D., Hillen, B., Hiller, R., Hillesheimer, D., Hinz, D., Höhn, T., Hötzel, M., Holzmann, S., Horn, S., Houdy, T., Howe, M.A., Huber, A., James, T., Jansen, A., Kaiser, M., Karl, C., Kazachenko, O., Kellerer, J., Kippenbrock, L., Kleesiek, M., Kleifges, M., Kleinfeller, J., Klein, M., Köhler, C., Köllenberger, L., Kopmann, A., Korzeczek, M., Kosmider, A., Kovalík, A., Krasch, B., Krause, H., Kraus, M., Kuckert, L., Kumb, A., Kunka, N., Lasserre, T., Cascio, L.L., Lebeda, O., Leber, M.L., Lehnert, B., Leiber, B., Letnev, J., Lewis, R.J., Le, T.L., Lichter, S., Lokhov, A., Poyato, J.M.L., Machatschek, M., Malcherek, E., Mark, M., Marsteller, A., Martin, E.L., Mehret, K., Meloni, M., Melzer, C., Menshikov, A., Mertens, S., (née Bodine), L.I.M., Monreal, B., Mostafa, J., Müller, K., Myers, A.W.,

Naumann, U., Neumann, H., Niemes, S., Oelpmann, P., Off, A., Ortjohann, H.-W., Osipowicz, A., Ostrick, B., Parno, D.S., Peterson, D.A., Plischke, P., Poon, A.W.P., Prall, M., Priester, F., Ranitzsch, P.C.-O., Reich, J., Renschler, P., Rest, O., Rinderspacher, R., Robertson, R.G.H., Rodejohann, W., Rodenbeck, C., Röllig, M., Röttele, C., Rohr, P., Rupp, S., Ryšavý, M., Sack, R., Saenz, A., Sagawe, M., Schäfer, P., (née Pollithy), A.S., Schimpf, L., Schlösser, K., Schlösser, M., Schlüter, L., Schneidewind, S., Schön, H., Schönung, K., Schrank, M., Schulz, B., Schwarz, J., Šefčík, M., Seitz-Moskaliuk, H., Seller, W., Sibille, V., Siegmann, D., Slezák, M., Spanier, F., Steidl, M., Sturm, M., Sun, M., Tcherniakhovski, D., Telle, H.H., Thorne, L.A., Thümmler, T., Titov, N., Tkachev, I., Trost, N., Urban, K., Valerius, K., VanDevender, B.A., Wechel, T.D.V., Vénos, D., Verbeek, A., Vianden, R., Hernández, A.P.V., Vogt, K., Wall, B.L., Wandkowsky, N., Weber, M., Weingardt, H., Weinheimer, C., Weiss, C., Welte, S., Wendel, J., Wierman, K.J., Wilkerson, J.F., Wolf, J., Wüstling, S., Xu, W., Yen, Y.-R., Zacher, M., Zadoroghny, S., Zboril, M., Zeller, G.: The design, construction, and commissioning of the KATRIN experiment. Journal of Instrumentation **16**(08), 08015 (2021). https://doi.org/10.1088/1748-0221/16/08/t08015

[10] Aker, M., Beglarian, A., Behrens, J., Berlev, A., Besserer, U., Bieringer, B., Block, F., Bobien, S., Böttcher, M., Bornschein, B., Bornschein, L., Brunst, T., Caldwell, T.S., Carney, R.M.D., La Cascio, L., Chilingaryan, S., Choi, W., Debowski, K., Deffert, M., Descher, M., Díaz Barrero, D., Doe, P.J., Dragoun, O., Drexlin, G., Eitel, K., Ellinger, E., Engel, R., Enomoto, S., Felden, A., Formaggio, J.A., Fränkle, F.M., Franklin, G.B., Friedel, F., Fulst, A., Gauda, K., Gil, W., Glück, F., Grössle, R., Gumbsheimer, R., Gupta, V., Höhn, T., Hannen, V., Haußmann, N., Helbing, K., Hickford, S., Hiller, R., Hillesheimer, D., Hinz, D., Houdy, T., Huber, A., Jansen, A., Karl, C., Kellerer, F., Kellerer, J., Kleifges, M., Klein, M., Köhler, C., Köllenberger, L., Kopmann, A., Korzeczek, M., Kovalík, A., Krasch, B., Krause, H., Kunka, N., Lasserre, T., Le, T.L., Lebeda, O., Lehnert, B., Lokhov, A., Machatschek, M., Malcherek, E., Mark, M., Marsteller, A., Martin, E.L., Melzer, C., Menshikov, A., Mertens, S., Mostafa, J., Müller, K., Neumann, H., Niemes, S., Oelpmann, P., Parno, D.S., Poon, A.W.P., Poyato, J.M.L., Priester, F., Ramachandran, S., Robertson, R.G.H., Rodejohann, W., Röllig, M., Röttele, C., Rodenbeck, C., Ryšavý, M., Sack, R., Saenz, A., Schäfer, P., Schaller née Pollithy, A., Schimpf, L., Schlösser, K., Schlösser, M., Schlüter, L., Schneidewind, S., Schrank, M., Schulz, B., Schwemmer, A., Šefčík, M., Sibille, V., Siegmann, D., Slezák, M., Spanier, F., Steidl, M., Sturm, M., Sun, M., Tcherniakhovski, D., Telle, H.H., Thorne, L.A., Thümmler, T., Titov, N., Tkachev, I., Urban, K., Valerius, K., Vénos, D., Vizcaya Hernández, A.P., Weinheimer, C., Welte, S., Wendel, J., Wilkerson, J.F., Wolf, J., Wüstling, S., Wydra, J., Xu, W., Yen, Y.-R., Zadoroghny, S., Zeller, G., Collaboration, T.K.: Direct neutrino-mass measurement with sub-electronvolt sensitivity. Nature Physics **18**(2), 160–166 (2022). https://doi.org/10.1038/s41567-021-01463-1

[11] Nucciotti, A.: The use of low temperature detectors for direct measurements of the mass of the electron neutrino. Advances in High Energy Physics **2016**, 9153024 (2016). https://doi.org/10.1155/2016/9153024

[12] Gastaldo, L., Blaum, K., Chrysalidis, K., Day Goodacre, T., Domula, A., Door, M., Dorrer, H., Düllmann, C.E., Eberhardt, K., Eliseev, S., Enss, C., Faessler, A., Filianin, P., Fleischmann, A., Fonnesu, D., Gamer, L., Haas, R., Hassel, C., Hengstler, D., Jochum, J., Johnston, K., Kebschull, U., Kempf, S., Kieck, T., Köster, U., Lahiri, S., Maiti, M., Mantegazzini, F., Marsh, B., Neroutsos, P., Novikov, Y.N., Ranitzsch, P.C.O., Rothe, S., Rischka, A., Saenz, A., Sander, O., Schneider, F., Scholl, S., Schüssler, R.X., Schweiger, C., Simkovic, F., Stora, T., Szücs, Z., Türler, A., Veinhard, M., Weber, M., Wegner, M., Wendt, K., Zuber, K.: The electron capture in 163ho experiment – echo. The European Physical Journal Special Topics **226**(8), 1623–1694 (2017). https://doi.org/10.1140/epjst/e2017-70071-y

[13] Velte, C., Ahrens, F., Barth, A., Blaum, K., Braß, M., Door, M., Dorrer, H., Düllmann, C.E., Eliseev, S., Enss, C., Filianin, P., Fleischmann, A., Gastaldo, L., Goeggelmann, A., Goodacre, T.D., Haverkort, M.W., Hengstler, D., Jochum, J., Johnston, K., Keller, M., Kempf, S., Kieck, T., König, C.M., Köster, U., Kromer, K., Mantegazzini, F., Marsh, B., Novikov, Y.N., Piquemal, F., Riccio, C., Richter, D., Rischka, A., Rothe, S., Schüssler, R.X., Schweiger, C., Stora, T., Wegner, M., Wendt, K., Zampaolo, M., Zuber, K.: High-resolution and low-background ^{163}Ho spectrum: interpretation of the resonance tails. The European Physical Journal C **79**(12), 1026 (2019). https://doi.org/10.1140/epjc/s10052-019-7513-x

[14] Faverzani, M., Alpert, B., Backer, D., Bennet, D., Biasotti, M., Brofferio, C., Ceriale, V., Ceruti, G., Corsini, D., Day, P.K., De Gerone, M., Dressler, R., Ferri, E., Fowler, J., Fumagalli, E., Gard, J., Gatti, F., Giachero, A., Hays-Wehle, J., Heinitz, S., Hilton, G., Köster, U., Lusignoli, M., Maino, M., Mates, J., Nisi, S., Nizzolo, R., Nucciotti, A., Orlando, A., Parodi, L., Pessina, G., Pizzigoni, G., Puiu, A., Ragazzi, S., Reintsema, C., Ribeiro-Gomez, M., Schmidt, D., Schuman, D., Siccardi, F., Sisti, M., Swetz, D., Terranova, F., Ullom, J., Vale, L.: The holmes experiment. Journal of Low Temperature Physics **184**(3), 922–929 (2016). https://doi.org/10.1007/s10909-016-1540-x

[15] Nucciotti, A., Alpert, B., Balata, M., Becker, D., Bennett, D., Bevilacqua, A., Biasotti, M., Ceriale, V., Ceruti, G., Corsini, D., De Gerone, M., Dressler, R., Faverzani, M., Ferri, E., Fowler, J., Gallucci, G., Gard, J., Gatti, F., Giachero, A., Hays-Wehle, J., Heinitz, S., Hilton, G., Köster, U., Lusignoli, M., Mates, J., Nisi, S., Orlando, A., Parodi, L., Pessina, G., Puiu, A., Ragazzi, S., Reintsema, C., Ribeiro-Gomez, M., Schmidt, D., Schuman, D., Siccardi, F., Swetz, D., Ullom, J., Vale, L.: Status of the holmes experiment to directly measure the neutrino mass. Journal of Low Temperature Physics **193**(5), 1137–1145 (2018). https://doi.org/10.1007/s10909-018-2025-x

[16] Eliseev, S., Novikov, Y.N., Blaum, K.: Penning-trap mass spectrometry and neutrino physics. Annalen der Physik **525**(8-9), 707–719 (2013) https://onlinelibrary.wiley.com/doi/pdf/10.1002/andp.201300056. https://doi.org/10.1002/andp.201300056

[17] Brown, L.S., Gabrielse, G.: Geonium theory: Physics of a single electron or ion in a penning trap. Rev. Mod. Phys. **58**, 233–311 (1986). https://doi.org/10.1103/RevModPhys.58.233

[18] Repp, J., Böhm, C., Crespo López-Urrutia, J.R., Dörr, A., Eliseev, S., George, S., Goncharov, M., Novikov, Y.N., Roux, C., Sturm, S., Ulmer, S., Blaum, K.: Pentatrap: a novel cryogenic multi-penning-trap experiment for high-precision mass measurements on highly charged ions. Applied Physics B **107**(4), 983–996 (2012). https://doi.org/10.1007/s00340-011-4823-6

[19] Filianin, P., Lyu, C., Door, M., Blaum, K., Huang, W.J., Haverkort, M., Indelicato, P., Keitel, C.H., Kromer, K., Lange, D., Novikov, Y.N., Rischka, A., Schüssler, R.X., Schweiger, C., Sturm, S., Ulmer, S., Harman, Z., Eliseev, S.: Direct q-value determination of the β^- decay of ^{187}Re. Phys. Rev. Lett. **127**, 072502 (2021). https://doi.org/10.1103/PhysRevLett.127.072502

[20] Schweiger, C., König, C.M., Crespo López-Urrutia, J.R., Door, M., Dorrer, H., Düllmann, C.E., Eliseev, S., Filianin, P., Huang, W., Kromer, K., Micke, P., Müller, M., Renisch, D., Rischka, A., Schüssler, R.X., Blaum, K.: Production of highly charged ions of rare species by laser-induced desorption inside an electron beam ion trap. Review of Scientific Instruments **90**(12), 123201 (2019) https://doi.org/10.1063/1.5128331. https://doi.org/10.1063/1.5128331

[21] Dorrer, H., Chrysalidis, K., Goodacre, T.D., Düllmann, C.E., Eberhardt, K., Enss, C., Gastaldo, L., Haas, R., Harding, J., Hassel, C., Johnston, K., Kieck, T., Köster, U., Marsh, B., Mokry, C., Rothe, S., Runke, J., Schneider, F., Stora, T., Türler, A., Wendt, K.: Production, isolation and characterization of radiochemically pure 163ho samples for the echo-project. Radiochimica Acta **106**(7), 535–547 (2018). https://doi.org/10.1515/ract-2017-2877

[22] Bradbury, N.E., Nielsen, R.A.: Absolute values of the electron mobility in hydrogen. Phys. Rev. **49**, 388–393 (1936). https://doi.org/10.1103/PhysRev.49.388

[23] Schweiger, C., Door, M., Filianin, P., Herkenhoff, J., Kromer, K., Lange, D., Marschall, D., Rischka, A., Wagner, T., Eliseev, S., Blaum, K.: Fast silicon carbide MOSFET based high-voltage push–pull switch for charge state separation of highly charged ions with a Bradbury–Nielsen gate. Review of Scientific Instruments **93**(9), 094702 (2022) https://pubs.aip.org/aip/rsi/article-pdf/doi/10.1063/5.0083515/16722559/094702_1_online.pdf. https://doi.org/10.1063/5.0083515

[24] Roux, C., Böhm, C., Dörr, A., Eliseev, S., George, S., Goncharov, M., Novikov, Y.N., Repp, J., Sturm, S., Ulmer, S., Blaum, K.: The trap design of pentatrap. Applied Physics B **107**(4), 997–1005 (2012). https://doi.org/10.1007/s00340-011-4825-4

[25] Böhm, C., Sturm, S., Rischka, A., Dörr, A., Eliseev, S., Goncharov, M., Höcker, M., Ketter, J., Köhler, F., Marschall, D., Martin, J., Obieglo, D., Repp, J., Roux, C., Schüssler, R.X., Steigleder, M., Streubel, S., Wagner, T., Westermann, J., Wieder, V., Zirpel, R., Melcher, J., Blaum, K.: An ultra-stable voltage source for precision penning-trap experiments. Nuclear Instruments and Methods in Physics Research Section A: Accelerators, Spectrometers, Detectors and Associated Equipment **828**, 125–131 (2016). https://doi.org/10.1016/j.nima.2016.05.044

[26] Wineland, D.J., Dehmelt, H.G.: Principles of the stored ion calorimeter. Journal of Applied Physics **46**(2), 919–930 (1975) https://doi.org/10.1063/1.321602. https://doi.org/10.1063/1.321602

[27] Feng, X., Charlton, M., Holzscheiter, M., Lewis, R.A., Yamazaki, Y.: Tank circuit model applied to particles in a penning trap. Journal of Applied Physics **79**(1), 8–13 (1996) https://doi.org/10.1063/1.360947. https://doi.org/10.1063/1.360947

[28] Nagahama, H., Schneider, G., Mooser, A., Smorra, C., Sellner, S., Harrington, J., Higuchi, T., Borchert, M., Tanaka, T., Besirli, M., Blaum, K., Matsuda, Y., Ospelkaus, C., Quint, W., Walz, J., Yamazaki, Y., Ulmer, S.: Highly sensitive superconducting circuits at $\sim$700 khz with tunable quality factors for image-current detection of single trapped antiprotons. Review of Scientific Instruments **87**(11), 113305 (2016) https://doi.org/10.1063/1.4967493. https://doi.org/10.1063/1.4967493

[29] Kromer, K., Lyu, C., Door, M., Filianin, P., Harman, Z., Herkenhoff, J., Huang, W., Keitel, C.H., Lange, D., Novikov, Y.N., Schweiger, C., Eliseev, S., Blaum, K.: High-precision mass measurement of doubly magic ^{208}Pb. The European Physical Journal A **58**(10), 202 (2022). https://doi.org/10.1140/epja/s10050-022-00860-1

[30] Anderson, P.W.: Theory of flux creep in hard superconductors. Phys. Rev. Lett. **9**, 309–311 (1962). https://doi.org/10.1103/PhysRevLett.9.309

[31] Anderson, P.W., Kim, Y.B.: Hard superconductivity: Theory of the motion of abrikosov flux lines. Rev. Mod. Phys. **36**, 39–43 (1964). https://doi.org/10.1103/RevModPhys.36.39

[32] Nagy, S., Blaum, K., Schuch, R.: Highly-charged ions and high-resolution mass spectrometry in a Penning trap, pp. 1–36. Springer, Berlin, Heidelberg (2008). https://doi.org/10.1007/978-3-540-77817-2_5. https://doi.org/10.1007/

978-3-540-77817-2_5

[33] Birge, R.T.: The calculation of errors by the method of least squares. Phys. Rev. **40**, 207–227 (1932). https://doi.org/10.1103/PhysRev.40.207

[34] Schüssler, R.X., Bekker, H., Braß, M., Cakir, H., Crespo López-Urrutia, J.R., Door, M., Filianin, P., Harman, Z., Haverkort, M.W., Huang, W.J., Indelicato, P., Keitel, C.H., König, C.M., Kromer, K., Müller, M., Novikov, Y.N., Rischka, A., Schweiger, C., Sturm, S., Ulmer, S., Eliseev, S., Blaum, K.: Detection of metastable electronic states by penning trap mass spectrometry. Nature **581**(7806), 42–46 (2020). https://doi.org/10.1038/s41586-020-2221-0

[35] Haverkort, M.W., Zwierzycki, M., Andersen, O.K.: Multiplet ligand-field theory using wannier orbitals. Phys. Rev. B **85**, 165113 (2012). https://doi.org/10.1103/PhysRevB.85.165113

[36] Quanty. [Online; accessed 23-March-2022]. http://www.quanty.org

[37] Braβ, M., Haverkort, M.W.: *Abinitio* calculation of the electron capture spectrum of ^{163}Ho: Auger–Meitner decay into continuum states. New J. Phys. **22**(9), 093018 (2020) arXiv:2002.05989 [nucl-th]. https://doi.org/10.1088/1367-2630/abac72

[38] Koepernik, K., Eschrig, H.: Full-potential nonorthogonal local-orbital minimum-basis band-structure scheme. Phys. Rev. B **59**, 1743–1757 (1999). https://doi.org/10.1103/PhysRevB.59.1743

[39] Opahle, I., Koepernik, K., Eschrig, H.: Full-potential band-structure calculation of iron pyrite. Phys. Rev. B **60**, 14035–14041 (1999). https://doi.org/10.1103/PhysRevB.60.14035

[40] Eschrig, H., Richter, M., Opahle, I.: Chapter 12 - relativistic solid state calculations. In: Schwerdtfeger, P. (ed.) Relativistic Electronic Structure Theory. Theoretical and Computational Chemistry, vol. 14, pp. 723–776. Elsevier, ??? (2004). https://doi.org/10.1016/S1380-7323(04)80039-6. https://www.sciencedirect.com/science/article/pii/S1380732304800396

[41] Grant, I.P.: Relativistic calculation of atomic structures. Adv. Phys. **19**, 747 (1970)

[42] Kotochigova, S., Kirby, K.P., Tupitsyn, I.I.: Ab initio fully relativistic calculations of x-ray spectra of highly charged ions. Phys. Rev. A **76**, 052513 (2007). https://doi.org/10.1103/PhysRevA.76.052513

[43] Fischer, C.F., Gaigalas, G., Jönsson, P., Bieroń, J.: Grasp2018 – a fortran 95 version of the general relativistic atomic structure package. Comput. Phys. Commun. **237**, 184–187 (2019). https://doi.org/10.1016/j.cpc.2018.10.032

[44] Fischer, C.F., Godefroid, M., Brage, T., Jönsson, P., Gaigalas, G.: Advanced multiconfiguration methods for complex atoms: I. energies and wave functions. J. Phys. B **49**(18), 182004 (2016). https://doi.org/10.1088/0953-4075/49/18/182004

[45] Indelicato, P., Lindroth, E., Desclaux, J.P.: Nonrelativistic Limit of Dirac-Fock Codes: The Role of Brillouin Configurations **94**(1), 013002 (2005)

[46] Indelicato, P.: Projection operators in Multiconfiguration Dirac-Fock calculations. Application to the ground state of heliumlike ions. **51**(2), 1132 (1995)

[47] Indelicato, P.: Nonperturbative Evaluation of Some QED Contributions to the Muonic Hydrogen N=2 Lamb Shift and Hyperfine Structure **87**(2), 022501 (2013)

[48] Indelicato, P., Gorceix, O., Desclaux, J.P.: MCDF studies of two electron ions II: Radiative corrections and comparison with experiment. **20**(4), 651 (1987)

[49] Shabaev, V.M., Tupitsyn, I.I., Yerokhin, V.A.: Model operator approach to the Lamb shift calculations in relativistic many-electron atoms **88**(1), 012513 (2013)

[50] Rodrigues, G.C., Indelicato, P., Santos, J.P., Patté, P., Parente, F.: Systematic Calculation of Total Atomic Energies of Ground State Configurations **86**(2), 117 (2004)

[51] Savelyev, I.M., Kaygorodov, M.Y., Kozhedub, Y.S., Tupitsyn, I.I., Shabaev, V.M.: Calculations of the binding-energy differences for highly-charged ho and dy ions. JETP Letters **118**(2), 87–91 (2023). https://doi.org/10.1134/S0021364023601975

[52] Wang, M., Huang, W.J., Kondev, F.G., Audi, G., Naimi, S.: The AME 2020 atomic mass evaluation (II). tables, graphs and references∗. Chinese Physics C **45**(3), 030003 (2021). https://doi.org/10.1088/1674-1137/abddaf

[53] Tiesinga, E., Mohr, P.J., Newell, D.B., Taylor, B.N.: Codata recommended values of the fundamental physical constants: 2018. Rev. Mod. Phys. **93**, 025010 (2021). https://doi.org/10.1103/RevModPhys.93.025010

[54] Sturm, S., Köhler, F., Zatorski, J., Wagner, A., Harman, Z., Werth, G., Quint, W., Keitel, C.H., Blaum, K.: High-precision measurement of the atomic mass of the electron. Nature **506**(7489), 467–470 (2014). https://doi.org/10.1038/nature13026

[55] Kramida, A., Yu. Ralchenko, Reader, J., and NIST ASD Team NIST Atomic Spectra Database (ver. 5.9), [Online]. Available: https://physics.nist.gov/asd [2022, February 18]. National

Institute of Standards and Technology, Gaithersburg, MD. (2021)

[56] Eliseev, S., Blaum, K., Block, M., Chenmarev, S., Dorrer, H., Düllmann, C.E., Enss, C., Filianin, P.E., Gastaldo, L., Goncharov, M., Köster, U., Lautenschläger, F., Novikov, Y.N., Rischka, A., Schüssler, R.X., Schweikhard, L., Türler, A.: Direct measurement of the mass difference of ^{163}Ho and ^{163}Dy solves the q-value puzzle for the neutrino mass determination. Phys. Rev. Lett. **115**, 062501 (2015). https://doi.org/10.1103/PhysRevLett.115.062501

[57] Ranitzsch, P.C.-O., Hassel, C., Wegner, M., Hengstler, D., Kempf, S., Fleischmann, A., Enss, C., Gastaldo, L., Herlert, A., Johnston, K.: Characterization of the ^{163}Ho electron capture spectrum: A step towards the electron neutrino mass determination. Phys. Rev. Lett. **119**, 122501 (2017). https://doi.org/10.1103/PhysRevLett.119.122501

[58] Cornell, E.A., Weisskoff, R.M., Boyce, K.R., Pritchard, D.E.: Mode coupling in a penning trap: π pulses and a classical avoided crossing. Phys. Rev. A **41**, 312–315 (1990). https://doi.org/10.1103/PhysRevA.41.312

[59] Heiße, F., Rau, S., Köhler-Langes, F., Quint, W., Werth, G., Sturm, S., Blaum, K.: High-precision mass spectrometer for light ions. Phys. Rev. A **100**, 022518 (2019). https://doi.org/10.1103/PhysRevA.100.022518

[60] Cornell, E.A., Weisskoff, R.M., Boyce, K.R., Flanagan, R.W., Lafyatis, G.P., Pritchard, D.E.: Single-ion cyclotron resonance measurement of $m(co^+)/m(n_2^+)$. Phys. Rev. Lett. **63**, 1674–1677 (1989). https://doi.org/10.1103/PhysRevLett.63.1674

[61] Rischka, A., Cakir, H., Door, M., Filianin, P., Harman, Z., Huang, W.J., Indelicato, P., Keitel, C.H., König, C.M., Kromer, K., Müller, M., Novikov, Y.N., Schüssler, R.X., Schweiger, C., Eliseev, S., Blaum, K.: Mass-difference measurements on heavy nuclides with an eV/c^2 accuracy in the pentatrap spectrometer. Phys. Rev. Lett. **124**, 113001 (2020). https://doi.org/10.1103/PhysRevLett.124.113001

[62] Ketter, J., Eronen, T., Höcker, M., Schuh, M., Streubel, S., Blaum, K.: Classical calculation of relativistic frequency-shifts in an ideal penning trap. International Journal of Mass Spectrometry **361**, 34–40 (2014). https://doi.org/10.1016/j.ijms.2014.01.028

[63] Ketter, J., Eronen, T., Höcker, M., Streubel, S., Blaum, K.: First-order perturbative calculation of the frequency-shifts caused by static cylindrically-symmetric electric and magnetic imperfections of a penning trap. International Journal of Mass Spectrometry **358**, 1–16 (2014). https://doi.org/10.1016/j.ijms.2013.10.005

[64] Schuh, M., Heiße, F., Eronen, T., Ketter, J., Köhler-Langes, F., Rau, S., Segal,

T., Quint, W., Sturm, S., Blaum, K.: Image charge shift in high-precision penning traps. Phys. Rev. A **100**, 023411 (2019). https://doi.org/10.1103/PhysRevA.100.023411

7 Methods

Measurement preparation and sequence

The measurement preparation starts with loading a set of three ions, in the order ^{163}Dy, ^{163}Ho and ^{163}Dy into traps 2, 3, and 4, respectively (cf. Fig. 2 (a)). Each HCI is first loaded into trap 2 where its motional amplitudes are reduced by resistive cooling [17, 58]. Great care is taken to ensure that only a single HCI is captured in a trap and cooled. For this also the "magnetron cleaning" technique is applied [59]. After being prepared in this way, the ion is moved to one of the following traps and stored until the set of ions for a measurement is complete.

In both measurement traps (traps 2 and 3), the motional frequencies of the HCIs are measured using the single-dip, double-dip and Pulse-and-Phase (PnP) techniques [58, 60]. The magnetron frequency is small compared to the other two motional frequencies and depends only very weakly on the ion's mass and is therefore measured only once a day using the double-dip technique prior to the main measurement sequence. Thus, the main measurement sequence reduces to a measurement of the modified cyclotron frequency (PnP technique) and the axial frequency (double-dip technique) which are performed simultaneously in traps 2 and 3. Compared to a single-trap measurement, this effectively doubles the statistics and furthermore allows different analysis methods to be employed as well as systematic checks by comparing the results obtained in both traps.

In the PnP cycle, the starting phase of the cyclotron motion is set by exciting it using a dipolar pulse with the frequency determined with the double-dip method during the preparation. The modified cyclotron motion then evolves freely during the phase evolution time T_{evol} (about $40\,\text{s}$) while the axial frequency is determined using a dip measurement [19, 29, 61]. Following the phase evolution time, the phase information that accumulated in the modified cyclotron motion is coupled to the axial motion using a π-pulse on the sideband frequency and the final phase is measured with the image current detection system [60]. This is done in traps 2 and 3, starting with the ions in position 1. Subsequently, the ions are shuttled to position 2, which effectively swaps the ion species in traps 2 and 3 and the measurement is repeated (cf. Fig. 2 (a)). This sequence is repeated 24 times in one main measurement loop and can be continued in principle infinitely long. Typically, the measurement is stopped due to either external magnetic field perturbations or charge exchange of the HCIs. Lifetimes of the HCIs until a charge exchange process happens are up to 36 hours. Reloading ions is beneficial since it allows one to compare different sets of ions and therefore also systematic checks for contaminant ions that might be present in the Penning traps during the measurement or for possible metastable electronically excited states in the HCIs [34].

Convergence studies with the Configuration Interaction and Multiconfiguration Dirac-Dock methods

In the configuration interaction calculations with the Quanty code, we iteratively expanded the configuration space with single, double and triple excitations into single-electron states with higher principal quantum numbers. Explicitly for the ions this implies iterative inclusion of excitations into orbitals with $n = 4, 5, 6, 7, 8$ and for the neutral atom $n = 5, 6$.

The evolution of ground-state energy with expanding configuration space is monitored and shows to good approximation a $1/n$ behaviour which allows extrapolation of the ground-state energy to estimate its uncertainty due to a truncated configuration space. Considering further uncertainties due to numerical accuracy, choice of single particle basis sets and triple excitations, we arrive at a total uncertainty of 1 eV for the estimation of the differences in binding energies of Ho^{q+} and Dy^{q+}.

As consistency check, for every step where the configuration space is increased the binding energy difference between Ho^{q+} and Dy^{q+} is calculated. It shows an approximate $1/n^2$ behavior, which again allows for extrapolation. Within our uncertainties we obtain the same results as in Table 1 in the article.

In case of the Multiconfiguration Dirac-Fock calculations with the GRASP2018 package, as described in the article, we have found that for neutral atoms, the inclusion of all spectroscopic orbitals into the active space would lead to several tens of millions of CSFs and is currently not tractable. For these systems, we include exchanges from the $3s$ orbital up to typically $8h$. To bridge the different models used for the neutrals and the HCIs, we also study the intermediate Pd-like HCIs Dy^{20+} and Ho^{21+}, with excitations from the $2s$ orbital to typically $10h$. We observe that correlation terms largely cancel in energy differences such as $[E(\text{Ho}) - E(\text{Ho}^{21+})] - [E(\text{Dy}) - E(\text{Dy}^{20+})]$ and $[E(\text{Ho}^{21+}) - E(\text{Ho}^{40+})] - [E(\text{Dy}^{20+}) - E(\text{Dy}^{40+})]$ due to structural similarities of nearby charge states. These differences converge more quickly when extending the set of virtual orbitals than the individual energies $E(\text{Ho})$ and $E(\text{Dy})$ of the neutrals. We note that such an inclusion of an intermediate system is useful because of the high charge states $38+$, $39+$ and $40+$ in the experiment, and allows reducing uncertainties.

8 Extended Data

Systematic shift	Magnitude
Relativistic shift	$\delta R < 10^{-12}$ [62]
Field anharmonicities/imperfections	$\delta R < 10^{-13}$ [24, 63]
Image charge shift	$\delta R < 10^{-13}$ [24, 64]
Dip lineshape	$\delta R < 10^{-13}$
$C_1 B_1$	Effect cancels in the ratio.
$C_1 C_3$	Effect cancels in the ratio.

Table 3 Overview of the considered systematic shifts in the determination of the frequency ratio. The relativistic shift was estimated assuming conservatively that both radii agree within 1%.

DISCUSSION AND OUTLOOK

The publications presented in Sections 3.1 and 3.2 summarize the developments on the HCI source of the PENTATRAP mass spectrometer aiming at the main motivation of a measurement of the Q-value of ^{163}Ho. The successful measurement of this Q-value is reported in the third publication in Section 3.3. In this chapter I will discuss the main results of this work also in the context of present and future measurements.

DEVELOPMENT OF AN HCI SOURCE FOR PENTATRAP   The reported developments on the HCI source expand the envelope of isotopes available for high-precision mass measurements at the PENTATRAP experiment and facilitate or allow the use of isotopes that are available only in small amounts. While the main motivation for this development was initially the Q-value of ^{163}Ho the technique is in general beneficial in the following cases:

- Isotopes that are in general available only in limited quantities, e.g. because they have to be produced artificially in radioactive ion beam facilities (e.g. ISOLDE at CERN) or by neutron irradiation (as is the case in ^{163}Ho) and where the separation process of the rare isotope is complex.

- Isotopes that have a long enough lifetime for a transport to the PENTATRAP mass spectrometer and a subsequent measurement but where the lifetime is still short such that larger samples would be difficult to handle due to the high activity and possibly elevated legal restrictions on the handling (e.g. for a Q-value measurement of ^{7}Be).

- Isotopes where small amounts of isotopically enriched material (in the μg-regime as e.g. ^{163}Dy used in this work) are commercially available. This facilitates a measurement e.g. when several stable isotopes exist but the abundance of the required one is only in the percent or sub-percent range (e.g. calcium or ytterbium isotopic chains of stable isotopes recently measured at PENTATRAP). These samples can now be prepared using the PLA target preparation outlined in Section 2.1.

The great advantage of the described technique is, that the isotope of interest does not have to be introduced into the background vacuum in gaseous form as it was previously the case [54, 105]. In future measurements, this technique is planned to be used for the measurement of the mass difference of ^{35}Cl and ^{36}Cl for a direct test of the

theory of special relativity [69] and it was recently used in a measurement of the mass of ^{238}U [81]. Due to the simplicity of the target preparation and system operation the injection system is also used as the state-of-the-art technique for bulk material samples such as for ^{208}Pb [80].

Initially, an EBIT was constructed using the "wire probe" injection technique [48] which was not able to produce any detectable amount of HCIs of the stable holmium isotope ^{165}Ho. Following these initial experiments, the in-trap laser desorption technique was developed where a single, few nanoseconds long laser pulse of about 1 mJ pulse energy is used to desorb atoms from a sample holder very close (tens of micrometers distance) to the electron beam and the trapping region inside the EBIT. The desorbed atoms are released directly into the electron beam in the EBIT, resulting in a high efficiency compared to the typically used injection techniques for EBITs where a gas or volatile organic compounds [18] are introduced into the background vacuum of the EBIT. Within the scope of this thesis it was demonstrated that HCIs can be produced reliably and efficiently from samples as small as 10^{12} atoms of ^{165}Ho (for the development of this technique the stable isotope of holmium was used), which corresponds to only ~ 300 pg [111].

In EBITs a distribution of charge states is produced as the process of electron impact ionization is countered by different recombination processes. For high precision mass measurements in PENTATRAP only a single HCI in the correct charge state q is required per measurement run. In previous measurements a sector magnet was used for the selection of the required charge state [54] which turned out to be not sufficiently efficient in combination with the existing beam transport system. For this purpose a completely new beamline including ion optical elements and a charge state separation based on the ToF of the HCIs was developed. While reaching sufficient resolution for the separation of the correct charge state, the new beam transport system and especially the charge state separation by ToF using a BNG is more efficient than the previous system. The successful separation of individual charge states from the EBIT was demonstrated and allowed the loading of individual HCIs in the correct charge state into the Penning traps of the PENTATRAP mass spectrometer [112].

While this system works very well for mono-isotopic species (^{165}Ho and the chemically separated ^{163}Ho) and isotopically enriched samples (^{163}Dy), the resolving power of about 100 is not sufficient to separate charge states and isotopes as those can be very close in ToF and the distance of about 1.5 m from the EBIT to the BNG is not long enough for a separation. This can in principle be overcome using a high resolution sector magnet for the separation or a small Multi-Reflection Time-of-Flight (MR-ToF) mass spectrometer - however, both would reduce the efficiency again. In addition, when the isotope of interest has a

small abundance and is injected into the EBIT together with the more abundant isotopes, a similarly small fraction of the isotope of interest is extracted from the EBIT as only a maximum number of HCIs can be trapped. The use of small amounts of enriched samples in these cases is therefore unavoidable and the relatively small mass resolving power of the ToF separation is not a limitation as it acts mainly as a pre-filter. Experimentally, reloading a new HCI from the EBIT into the PT is a rather fast process and the identification of the HCI with the detection system in the PT is by orders of magnitude more accurate than any mass pre-filtering system. The pre-selection of the charge state of interest is therefore sufficient as long as the background of unwanted isotopes is not dominating.

MEASUREMENT OF THE ^{163}Ho Q-VALUE   The Q-value measurement reported in Section 3.3 constitutes one of the most precise mass measurements today where a fractional uncertainty in the determined cyclotron frequency ratio of $3 \cdot 10^{-12}$ was reached. Including the calculations of the electronic binding energy differences an ultra-precise Q-value of $2863.2(0.6)$ eV was achieved.

For this very precise Q-value determination a tremendous effort on both the experimental and theoretical sides was required to carefully assess and avoid any systematic shifts.

Experimentally, the very small Q-value of ^{163}Ho translates to the fact that the mother and daughter nuclides are very close in mass, i.e. they form a so called "mass-doublet" with a difference in charge-to-mass ratio on the order of 10^{-8}. For the cyclotron frequency ratio measurement this means that within the Penning trap the same trapping potential can be used for both species and the systematic shifts are either negligible or cancel out when the cyclotron frequency ratio is determined from the measured cyclotron frequencies.

With the stack of five Penning traps of the Penning-trap mass spectrometer PENTATRAP simultaneous measurements of the cyclotron frequency ratio in two Penning traps were conducted. In the analysis, the ratios from both traps were compared and systematic shifts due to contaminant ions or possible exited metastable electronic states in the HCI can be detected and the data discarded.

In the calculation of the Q-value from the cyclotron frequency ratio R_{q+} and the binding energy difference $\Delta E_{\mathrm{B}}^{q+}$

$$Q = m_{\mathrm{Dy}}^{q+} \left(R_{q+} - 1 \right) + \Delta E_{\mathrm{B}}^{q+}, \tag{4.1}$$

one can see that neither the experimental measurement of the cyclotron frequency ratio nor the theoretical calculations can be verified on their own. In order to exclude systematic shifts in experiment or theory, the charge states $q = 38+, 39+, 40+$ were investigated and the binding energy differences calculated. Due to the different charge states, the cyclotron frequency ratio for each charge state is different and can not

be compared among the different charge states. A comparison is only possible when the binding energy difference calculations are included. The resulting Q-values can be compared where a perfect agreement, well within the one sigma uncertainty band of the obtained Q-values, was achieved. In principle it would be very unlikely that a systematic shift in the experiment would be compensated by a similar systematic shift from the binding energy difference calculations. This argument is strengthened when the increase of the binding energy difference from the charge state $q = 38+$ to the charge state $q = 39+$ is considered:

$$\Delta E_{\mathrm{B}}^{38+} = 37.4 \pm 1.4 \, \mathrm{eV}$$
$$\Delta E_{\mathrm{B}}^{39+} = 1147.3 \pm 0.7 \, \mathrm{eV}.$$

This is a large increase relative to the Q-value of $2863.2 \pm 0.6 \, \mathrm{eV}/c^2$ and underlines the extremely good agreement of the Q-values for the different charge states and supports the exclusion of systematic shifts. Furthermore, systematic shifts due to metastable electronically excited states can be excluded which would affect each charge state differently. The final uncertainty of $0.6 \, \mathrm{eV}/c^2$ originates in equal parts from the cyclotron frequency ratio measurement and the averaged theoretical calculations from two groups.

This measurement is more than a factor 50 more precise and in good agreement with the so far best direct measurement of this Q-value [46], see Figure 4.1. For the first phase of the ECHo experiment with a sensitivity on the neutrino mass on the order of $\sim 10 \, \mathrm{eV}/c^2$ the previous measurement was sufficiently precise and allowed to solve the discrepancies from several other measurements of this Q-value where different techniques were used and confirmed the Q-values obtained from microcalorimetry. The following phases of the ECHo experiment use a larger activity of ^{163}Ho in order to acquire more events and thereby increase the sensitivity to the neutrino mass. With the Q-value determined within this work the ECHo experiment is able to investigate possible systematic uncertainties related to the decay of ^{163}Ho within the solid gold absorber material of the microcalorimeters on a sub-eV level. A comparison of the determined Q-value with the most recent calorimetric measurements and the AME adjustment 2020 is given in Figure 4.1. A perfect agreement is reached with the ECHo measurement from 2017 [102] while the Q-value in this work is slightly higher than the AME adjustment 2020 [122] and the ECHo 2017 measurement and in agreement within 1.2σ and 1.8σ, respectively.

Currently, the KATRIN experiment is the leading experiment investigating the effective electron anti-neutrino mass. Depending on the results of KATRIN in the coming years and the progress of the ECHo and HOLMES experiments, a refined measurement approaching a level of $0.1 \, \mathrm{eV}$ might be required allowing both calorimetry based experiments to approach this sensitivity level and possibly complement the measurement of the KATRIN experiment. In this case, a refined mea-
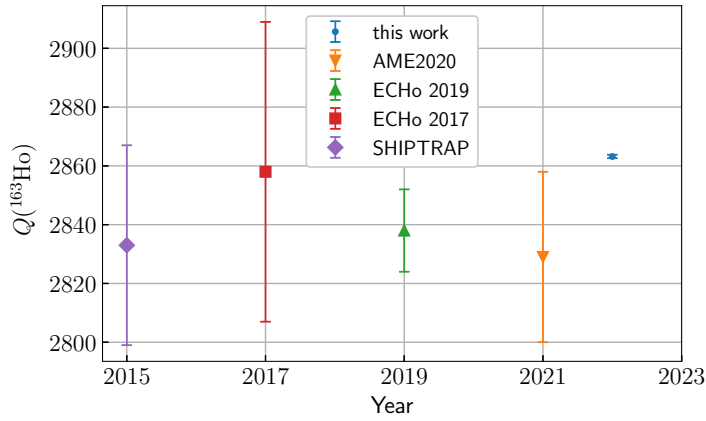
Figure 4.1: The most recent measurements of the ^{163}Ho Q-value are shown together with the determination from this work. The shown data is based on the previous direct measurement using PTMS (SHIPTRAP [46]), microcalorimetric measurements from ECHo2017 [102] and ECHo2019 [121] as well as the value from the AME adjustment 2020 [122]. Figure taken from [113].

surement of this Q-value is possible at PENTATRAP by acquisition of more statistics approaching a fractional uncertainty on the frequency ratio of 10^{-12}. In addition, the axial frequency measurement can be improved as it is the dominating uncertainty in the determination of the cyclotron frequency in the reported measurement. Similarly, the theoretical calculations of the binding energy difference would have to be improved to the same level as well.

SUMMARY

This cumulative thesis summarizes the work that was done in the years between 2018 and 2021 at the Pentatrap experiment in constructing and building an EBIT and a whole beamline section capable of operating with minuscule sample sizes in the range of tens of picograms of ^{163}Ho this corresponds to about 10^{14} atoms. Ultimately, these developments allowed the measurement of the ^{163}Ho Q-value in the summer of 2021 with the Penning-trap mass spectrometer Pentatrap for the ECHo collaboration which is the final and main result of this thesis.

With the three publications presented in Chapter 3 the following milestones were made for the Pentatrap experiment within this thesis:

1. A source of HCIs was developed and constructed that allows the reliable and efficient injection of samples from bulk material to very small samples of only 10^{12} atoms into an EBIT. This is achieved by introducing the samples very close to the electron beam and trapping region inside the EBIT, at a distance of tens of micrometers from the electron beam. Synchronized to the trapping cycle in the EBIT, a single laser pulse of about 1 mJ of energy is used to desorb atoms from the sample directly into the electron beam region where the atoms are ionized to high charge states. This technique has applications for a variety of isotopes to be studied beyond the work presented in this thesis. Due to the simplicity of the technique it can be used for almost all types of samples with the exception of gaseous species which are still introduced into the residual gas as in the mass measurement of neon [67]. Since its introduction at the Pentatrap experiment the injection technique was used in a substantial number of high-precision mass measurement campaigns on ^{208}Pb [79, 80], ^{238}Pb [81] and the not yet published measurements on several isotopes of calcium and ytterbium. During the testing phase, the EBIT has shown a very good performance in the production of HCIs for a table-top room-temperature device where charge states up to hydrogen-like ^{40}Ca^{19+}, which requires an ionization energy 5.1 keV, were observed.

2. Several different target preparation techniques were tested in the course of this theses which are documented in Section 2.1, most notably the PLA targets where the sample is enclosed in an organic plastic compound made from lactic acid. The developed targets allow a very fast turn-around time: When the target is

changed in the afternoon which takes about 30 minutes it can be used after one night of evacuation time. This is mainly the result of the construction of the target system which can be retracted into a separate vacuum chamber and closed off from the EBIT. This allows to leave the EBIT in ultrahigh vacuum conditions while only a small volume needs to be evacuated following a target change.

3. Following the EBIT in the beamline towards the PENTATRAP mass spectrometer, a BNG and a fast switching electronic circuit were developed and integrated that allow the separation of an individual charge states from the charge state distribution that is produced within the EBIT. Upon ejection all charge states are accelerated by the same electric field but have, depending on their charge state, different velocities and will arrive at different times at the BNG. Using the fast switching electronic circuit, the potentials applied on the BNG wires can be switched fast enough such that the HCIs arriving fast or later than the required charge state can be deflected. For voltages up to 300 V rise and fall times on the order of 10 ns were achieved which allowed the separation of individual charge states of HCIs of ^{163}Dy that were extracted from the EBIT with an energy of 4 keV and which are separated at the position of the BNG by a ToF of 70 ns. Also this system is now in use at the PENTATRAP mass spectrometer since its integration and was used in the aforementioned measurements.

4. In the context of the injection system for the EBIT and the BNG with the associated electronics, a completely new beamline including ion optical elements, mainly Einzel lenses with deflectors and cylindrical benders, was developed and installed in order to ensure an efficient and reliable transport of the HCIs from the EBIT to the Penning traps.

5. Following the mentioned developments the measurement of the ^{163}Ho Q-value of 2863.2(0.6) eV$/c^2$ with an unprecedented uncertainty of only 0.6 eV was achieved which is the main result of this thesis. This result will enable the ECHo and HOLMES experiments to investigate possible systematic effects in their determination of the electron neutrino mass on a sub-eV level.

In summary, the technical developments within this thesis have shown their tremendous capability with the used samples of 10^{14} atoms of ^{163}Ho in the measurement of the electron capture Q-value resulting in one of the most precise mass measurements today and extended the applications of the PENTATRAP experiment significantly. The obtained Q-value of ^{163}Ho will enable the ECHo and HOLMES experiments to investigate the electron neutrino mass on a sub-eV level allowing them to assess possible systematic uncertainties that originate

from the implantation of the ^{163}Ho into the solid gold absorber of the calorimeter.

BIBLIOGRAPHY

[1] C. Abel et al. "Measurement of the Permanent Electric Dipole Moment of the Neutron." In: *Phys. Rev. Lett.* 124 (8 2020), p. 081803. DOI: 10.1103/PhysRevLett.124.081803. URL: https://link.aps.org/doi/10.1103/PhysRevLett.124.081803.

[2] M. Agostini et al. "Final Results of GERDA on the Search for Neutrinoless Double-β Decay." In: *Phys. Rev. Lett.* 125 (25 2020), p. 252502. DOI: 10.1103/PhysRevLett.125.252502. URL: https://link.aps.org/doi/10.1103/PhysRevLett.125.252502.

[3] M. Agostini et al. "Final Results of GERDA on the Two-Neutrino Double-β Decay Half-Life of ^{76}Ge." In: *Phys. Rev. Lett.* 131 (14 2023), p. 142501. DOI: 10.1103/PhysRevLett.131.142501. URL: https://link.aps.org/doi/10.1103/PhysRevLett.131.142501.

[4] D. P. Aguillard et al. "Measurement of the Positive Muon Anomalous Magnetic Moment to 0.20 ppm." In: *Phys. Rev. Lett.* 131 (16 2023), p. 161802. DOI: 10.1103/PhysRevLett.131.161802. URL: https://link.aps.org/doi/10.1103/PhysRevLett.131.161802.

[5] Q. R. Ahmad et al. "Direct Evidence for Neutrino Flavor Transformation from Neutral-Current Interactions in the Sudbury Neutrino Observatory." In: *Phys. Rev. Lett.* 89 (1 2002), p. 011301. DOI: 10.1103/PhysRevLett.89.011301. URL: https://link.aps.org/doi/10.1103/PhysRevLett.89.011301.

[6] M. Aker et al. "Direct neutrino-mass measurement with sub-electronvolt sensitivity." In: *Nature Physics* 18.2 (2022), pp. 160–166. ISSN: 1745-2481. DOI: 10.1038/s41567-021-01463-1. URL: https://doi.org/10.1038/s41567-021-01463-1.

[7] M. Aker et al. "KATRIN: status and prospects for the neutrino mass and beyond." In: *J. Phys. G* 49.10 (2022), p. 100501. DOI: 10.1088/1361-6471/ac834e. URL: https://dx.doi.org/10.1088/1361-6471/ac834e.

[8] P. W. Anderson. "Theory of Flux Creep in Hard Superconductors." In: *Phys. Rev. Lett.* 9 (7 1962), pp. 309–311. DOI: 10.1103/PhysRevLett.9.309. URL: https://link.aps.org/doi/10.1103/PhysRevLett.9.309.

[9] P. W. Anderson and Y. B. Kim. "Hard Superconductivity: Theory of the Motion of Abrikosov Flux Lines." In: *Rev. Mod. Phys.* 36 (1 1964), pp. 39–43. DOI: 10.1103/RevModPhys.36.39. URL: https://link.aps.org/doi/10.1103/RevModPhys.36.39.

[10] V. Andreev et al. "Improved limit on the electric dipole moment of the electron." In: *Nature* 562.7727 (2018), pp. 355–360. ISSN: 1476-4687. DOI: 10.1038/s41586-018-0599-8. URL: https://doi.org/10.1038/s41586-018-0599-8.

[11] D. M. Asner et al. "Single-Electron Detection and Spectroscopy via Relativistic Cyclotron Radiation." In: *Phys. Rev. Lett.* 114 (16 2015), p. 162501. DOI: 10.1103/PhysRevLett.114.162501. URL: https://link.aps.org/doi/10.1103/PhysRevLett.114.162501.

[12] F. W. Aston. "The Constitution of the Elements." In: *Nature* 104.2616 (1919), pp. 393–393. ISSN: 1476-4687. DOI: 10.1038/104393b0. URL: https://doi.org/10.1038/104393b0.

[13] F. W. Aston. "Atoms and their Packing Fractions." In: *Nature* 120.3035 (1927), pp. 956–959. ISSN: 1476-4687. DOI: 10.1038/120956a0. URL: https://doi.org/10.1038/120956a0.

[14] D. Atanasov et al. "Precision Mass Measurements of $^{129-131}$Cd and Their Impact on Stellar Nucleosynthesis via the Rapid Neutron Capture Process." In: *Phys. Rev. Lett.* 115 (23 2015), p. 232501. DOI: 10.1103/PhysRevLett.115.232501. URL: https://link.aps.org/doi/10.1103/PhysRevLett.115.232501.

[15] I. Bergström, C. Carlberg, T. Fritioff, G. Douysset, J. Schönfelder, and R. Schuch. "SMILETRAP—A Penning trap facility for precision mass measurements using highly charged ions." In: *Nucl. Instrum. Methods Phys. Res. A* 487.3 (2002), pp. 618–651. ISSN: 0168-9002. DOI: https://doi.org/10.1016/S0168-9002(01)02178-7. URL: https://www.sciencedirect.com/science/article/pii/S0168900201021787.

[16] Raymond T. Birge. "The Calculation of Errors by the Method of Least Squares." In: *Phys. Rev.* 40 (2 1932), pp. 207–227. DOI: 10.1103/PhysRev.40.207. URL: https://link.aps.org/doi/10.1103/PhysRev.40.207.

[17] Klaus Blaum. "High-accuracy mass spectrometry with stored ions." In: *Phys. Rep.* 425.1 (2006), pp. 1–78. ISSN: 0370-1573. DOI: https://doi.org/10.1016/j.physrep.2005.10.011. URL: https://www.sciencedirect.com/science/article/pii/S0370157305004643.

[18] S. L. Bogomolov, A. E. Bondarchenko, A. A. Efremov, K. I. Kuzmenkov, A. N. Lebedev, K. V. Lebedev, V. Ya. Lebedev, V. N. Loginov, V. E. Mironov, and N. Yu. Yazvitsky. "Production of intense metal ion beams from ECR ion sources using the MIVOC method." In: *Phys. Part. Nucl. Lett.* 12.7 (2015), pp. 824–830. ISSN: 1531-8567. DOI: 10.1134/S1547477115070043. URL: https://doi.org/10.1134/S1547477115070043.

[19]   Christine Böhm. "High-precision mass measurements of neutron-deficient Tl isotopes at ISOLTRAP and the development of an ultra-stable voltage source for the PENTATRAP experiment." eng. PhD thesis. Heidelberg: Ruprechts-Karls-Universität, 2015. DOI: 10.17617/2.2083636.

[20]   M. J. Borchert et al. "A 16-parts-per-trillion measurement of the antiproton-to-proton charge–mass ratio." In: *Nature* 601.7891 (2022), pp. 53–57. ISSN: 1476-4687. DOI: 10.1038/s41586-021-04203-w. URL: https://doi.org/10.1038/s41586-021-04203-w.

[21]   M. Borghesi et al. "An updated overview of the HOLMES status." In: *Nucl. Instrum. Methods Phys. Res. A* 1051 (2023), p. 168205. ISSN: 0168-9002. DOI: https://doi.org/10.1016/j.nima.2023.168205. URL: https://www.sciencedirect.com/science/article/pii/S016890022300195X.

[22]   Norris E. Bradbury and Russell A. Nielsen. "Absolute Values of the Electron Mobility in Hydrogen." In: *Phys. Rev.* 49 (5 1936), pp. 388–393. DOI: 10.1103/PhysRev.49.388. URL: https://link.aps.org/doi/10.1103/PhysRev.49.388.

[23]   Lowell S. Brown and Gerald Gabrielse. "Precision spectroscopy of a charged particle in an imperfect Penning trap." In: *Phys. Rev. A* 25 (4 1982), pp. 2423–2425. DOI: 10.1103/PhysRevA.25.2423. URL: https://link.aps.org/doi/10.1103/PhysRevA.25.2423.

[24]   Lowell S. Brown and Gerald Gabrielse. "Geonium theory: Physics of a single electron or ion in a Penning trap." In: *Rev. Mod. Phys.* 58 (1 1986), pp. 233–311. DOI: 10.1103/RevModPhys.58.233. URL: https://link.aps.org/doi/10.1103/RevModPhys.58.233.

[25]   T. Brunner et al. "A large Bradbury Nielsen ion gate with flexible wire spacing based on photo-etched stainless steel grids and its characterization applying symmetric and asymmetric potentials." In: *Int. J. Mass Spectrom.* 309 (2012), pp. 97–103. ISSN: 1387-3806. DOI: https://doi.org/10.1016/j.ijms.2011.09.004. URL: https://www.sciencedirect.com/science/article/pii/S1387380611003770.

[26]   W. Byron et al. "First Observation of Cyclotron Radiation from MeV-Scale $e^{\pm}$ following Nuclear β Decay." In: *Phys. Rev. Lett.* 131 (8 2023), p. 082502. DOI: 10.1103/PhysRevLett.131.082502. URL: https://link.aps.org/doi/10.1103/PhysRevLett.131.082502.

[27]   Ch. Böhm et al. "An ultra-stable voltage source for precision Penning-trap experiments." In: *Nucl. Instrum. Methods Phys. Res. A* 828 (2016), pp. 125–131. ISSN: 0168-9002. DOI:

https://doi.org/10.1016/j.nima.2016.05.044. URL: https://www.sciencedirect.com/science/article/pii/S0168900216304259.

[28] William B. Cairncross, Daniel N. Gresh, Matt Grau, Kevin C. Cossel, Tanya S. Roussy, Yiqi Ni, Yan Zhou, Jun Ye, and Eric A. Cornell. "Precision Measurement of the Electron's Electric Dipole Moment Using Trapped Molecular Ions." In: *Phys. Rev. Lett.* 119 (15 2017), p. 153001. DOI: 10.1103/PhysRevLett.119.153001. URL: https://link.aps.org/doi/10.1103/PhysRevLett.119.153001.

[29] Laurent Canetti, Marco Drewes, and Mikhail Shaposhnikov. "Matter and antimatter in the universe." In: *New J. Phys.* 14.9 (2012), p. 095012. DOI: 10.1088/1367-2630/14/9/095012. URL: https://dx.doi.org/10.1088/1367-2630/14/9/095012.

[30] LEGEND Collaboration et al. *LEGEND-1000 Preconceptual Design Report.* 2021. arXiv: 2107.11462 [physics.ins-det].

[31] Project 8 Collaboration et al. *The Project 8 Neutrino Mass Experiment.* 2022. arXiv: 2203.07349 [nucl-ex]. URL: https://doi.org/10.48550/arXiv.2203.07349.

[32] Project 8 Collaboration et al. *Tritium Beta Spectrum and Neutrino Mass Limit from Cyclotron Radiation Emission Spectroscopy.* 2023. arXiv: 2212.05048 [nucl-ex]. URL: https://doi.org/10.48550/arXiv.2212.05048.

[33] IceCube Collaboration*† et al. "Observation of high-energy neutrinos from the Galactic plane." In: *Science* 380.6652 (2023), pp. 1338–1343. DOI: 10.1126/science.adc9818. eprint: https://www.science.org/doi/pdf/10.1126/science.adc9818. URL: https://www.science.org/doi/abs/10.1126/science.adc9818.

[34] Eric A. Cornell, Robert M. Weisskoff, Kevin R. Boyce, Robert W. Flanagan, Gregory P. Lafyatis, and David E. Pritchard. "Single-ion cyclotron resonance measurement of $M(CO^+)/M(N_2^+)$." In: *Phys. Rev. Lett.* 63 (16 1989), pp. 1674–1677. DOI: 10.1103/PhysRevLett.63.1674. URL: https://link.aps.org/doi/10.1103/PhysRevLett.63.1674.

[35] Eric A. Cornell, Robert M. Weisskoff, Kevin R. Boyce, and David E. Pritchard. "Mode coupling in a Penning trap: π pulses and a classical avoided crossing." In: *Phys. Rev. A* 41 (1 1990), pp. 312–315. DOI: 10.1103/PhysRevA.41.312. URL: https://link.aps.org/doi/10.1103/PhysRevA.41.312.

[36] Costa, J.-L. "Spectres de masse de quelques éléments légers." In: *Ann. Phys.* 10.4 (1925), pp. 425–456. DOI: 10.1051/anphys/192510040425. URL: https://doi.org/10.1051/anphys/192510040425.

[37] C. L. Cowan, F. Reines, F. B. Harrison, H. W. Kruse, and A. D. McGuire. "Detection of the Free Neutrino: a Confirmation." In: *Science* 124.3212 (1956), pp. 103–104. DOI: `10.1126/science. 124.3212.103`. eprint: `https://www.science.org/doi/pdf/ 10.1126/science.124.3212.103`. URL: `https://www.science. org/doi/abs/10.1126/science.124.3212.103`.

[38] F.W. Aston M.A. D.Sc. "XLIV. The constitution of atmospheric neon." In: *The London, Edinburgh, and Dublin Philosophical Magazine and Journal of Science* 39.232 (1920), pp. 449–455. DOI: `10.1080/14786440408636058`. eprint: `https://doi.org/10. 1080/14786440408636058`. URL: `https://doi.org/10.1080/ 14786440408636058`.

[39] F. DiFilippo, V. Natarajan, M. Bradley, F. Palmer, and D. E. Pritchard. "Accurate atomic mass measurements from Penning trap mass comparisons of individual ions." In: *Physica Scripta* 1995.T59 (1995), p. 144. DOI: `10.1088/0031-8949/1995/T59/018`. URL: `https://dx.doi.org/10.1088/0031-8949/1995/T59/018`.

[40] J. Dilling, P. Bricault, M. Smith, and H.-J. Kluge. "The proposed TITAN facility at ISAC for very precise mass measurements on highly charged short-lived isotopes." In: *Nucl. Instrum. Methods Phys. Res. B* 204 (2003). 14th International Conference on Electromagnetic Isotope Separators and Techniques Related to their Applications, pp. 492–496. ISSN: 0168-583X. DOI: `https://doi.org/10.1016/S0168-583X(02)02118-3`. URL: `https://www.sciencedirect.com/science/article/pii/ S0168583X02021183`.

[41] Jens Dilling, Klaus Blaum, Maxime Brodeur, and Sergey Eliseev. "Penning-Trap Mass Measurements in Atomic and Nuclear Physics." In: *Annu. Rev. Nucl. Part. Sci.* 68.1 (2018), pp. 45–74. DOI: `10.1146/annurev-nucl-102711-094939`. eprint: `https: //doi.org/10.1146/annurev-nucl-102711-094939`. URL: `https://doi.org/10.1146/annurev-nucl-102711-094939`.

[42] Michael Dine and Alexander Kusenko. "Origin of the matter-antimatter asymmetry." In: *Rev. Mod. Phys.* 76 (1 2003), pp. 1–30. DOI: `10.1103/RevModPhys.76.1`. URL: `https://link.aps.org/ doi/10.1103/RevModPhys.76.1`.

[43] R.S. Van Dyck, D.L. Farnham, and P.B. Schwinberg. "A Compensated Penning Trap Mass Spectrometer and the 3." In: *J. Mod. Opt.* 39.2 (1992), pp. 243–255. DOI: `10.1080/09500349214550251`. eprint: `https://doi.org/10.1080/09500349214550251`. URL: `https://doi.org/10.1080/09500349214550251`.

[44] A. Einstein. "Zur Elektrodynamik bewegter Körper." In: *Annalen der Physik* 322.10 (1905), pp. 891–921. DOI: `https://doi. org/10.1002/andp.19053221004`. eprint: `https://onlinelibrary.`

wiley.com/doi/pdf/10.1002/andp.19053221004. URL: https://onlinelibrary.wiley.com/doi/abs/10.1002/andp.19053221004.

[45]   S. Eliseev, K. Blaum, M. Block, C. Droese, M. Goncharov, E. Minaya Ramirez, D. A. Nesterenko, Yu. N. Novikov, and L. Schweikhard. "Phase-Imaging Ion-Cyclotron-Resonance Measurements for Short-Lived Nuclides." In: *Phys. Rev. Lett.* 110 (8 2013), p. 082501. DOI: 10.1103/PhysRevLett.110.082501. URL: https://link.aps.org/doi/10.1103/PhysRevLett.110.082501.

[46]   S. Eliseev et al. "Direct Measurement of the Mass Difference of ^{163}Ho and ^{163}Dy Solves the Q-Value Puzzle for the Neutrino Mass Determination." In: *Phys. Rev. Lett.* 115 (6 2015), p. 062501. DOI: 10.1103/PhysRevLett.115.062501. URL: https://link.aps.org/doi/10.1103/PhysRevLett.115.062501.

[47]   Sergey Eliseev, Yuri N. Novikov, and Klaus Blaum. "Penning-trap mass spectrometry and neutrino physics." In: *Annalen der Physik* 525.8-9 (2013), pp. 707–719. DOI: https://doi.org/10.1002/andp.201300056. eprint: https://onlinelibrary.wiley.com/doi/pdf/10.1002/andp.201300056. URL: https://onlinelibrary.wiley.com/doi/abs/10.1002/andp.201300056.

[48]   S.R. Elliott and R.E. Marrs. "A wire probe as an ion source for an electron beam ion trap." In: *Nucl. Instrum. Methods Phys. Res. B* 100.4 (1995), pp. 529–535. ISSN: 0168-583X. DOI: https://doi.org/10.1016/0168-583X(95)00327-4. URL: https://www.sciencedirect.com/science/article/pii/0168583X95003274.

[49]   F. Englert and R. Brout. "Broken Symmetry and the Mass of Gauge Vector Mesons." In: *Phys. Rev. Lett.* 13 (9 1964), pp. 321–323. DOI: 10.1103/PhysRevLett.13.321. URL: https://link.aps.org/doi/10.1103/PhysRevLett.13.321.

[50]   T. Eronen et al. "JYFLTRAP: a Penning trap for precision mass spectroscopy and isobaric purification." In: *Eur. Phys. J. A* 48.4 (2012), p. 46. ISSN: 1434-601X. DOI: 10.1140/epja/i2012-12046-1. URL: https://doi.org/10.1140/epja/i2012-12046-1.

[51]   X. Fan, T. G. Myers, B. A. D. Sukra, and G. Gabrielse. "Measurement of the Electron Magnetic Moment." In: *Phys. Rev. Lett.* 130 (7 2023), p. 071801. DOI: 10.1103/PhysRevLett.130.071801. URL: https://link.aps.org/doi/10.1103/PhysRevLett.130.071801.

[52]   Toni Feder. "Precision measurements bring the search for new physics to the table." In: *Physics Today* 76.12 (Dec. 2023), pp. 19–21. ISSN: 0031-9228. DOI: 10.1063/PT.3.5357. eprint: https://pubs.aip.org/physicstoday/article-pdf/76/12/19/

18227530/19_1_pt.3.5357.pdf. URL: https://doi.org/10.
1063/PT.3.5357.

[53] X. Feng, M. Charlton, M. Holzscheiter, R. A. Lewis, and Y. Yamazaki. "Tank circuit model applied to particles in a Penning trap." In: *J. Appl. Phys.* 79.1 (Jan. 1996), pp. 8–13. ISSN: 0021-8979. DOI: 10.1063/1.360947. eprint: https://pubs.aip.org/aip/jap/article-pdf/79/1/8/8047414/8_1_online.pdf. URL: https://doi.org/10.1063/1.360947.

[54] P. Filianin et al. "Direct Q-Value Determination of the β^- Decay of ^{187}Re." In: *Phys. Rev. Lett.* 127 (7 2021), p. 072502. DOI: 10.1103/PhysRevLett.127.072502. URL: https://link.aps.org/doi/10.1103/PhysRevLett.127.072502.

[55] Pavel Filianin. "Measurements of low decay energies of beta-processes using Penning traps." PhD thesis. Heidelberg: Ruprecht-Karls-Universität, 2019.

[56] A. Fleischmann, C. Enss, and G.M. Seidel. "Metallic Magnetic Calorimeters." In: *Cryogenic Particle Detection*. Ed. by Christian Enss. Berlin, Heidelberg: Springer Berlin Heidelberg, 2005, pp. 151–216. ISBN: 978-3-540-31478-3. DOI: 10.1007/10933596_4. URL: https://doi.org/10.1007/10933596_4.

[57] L. Fleischmann et al. "Physics and applications of metallic magnetic calorimeters for particle detection." In: *J. Phys. Conf. Ser.* 150.1 (2009), p. 012013. DOI: 10.1088/1742-6596/150/1/012013. URL: https://dx.doi.org/10.1088/1742-6596/150/1/012013.

[58] Y. Fukuda et al. "Evidence for Oscillation of Atmospheric Neutrinos." In: *Phys. Rev. Lett.* 81 (8 1998), pp. 1562–1567. DOI: 10.1103/PhysRevLett.81.1562. URL: https://link.aps.org/doi/10.1103/PhysRevLett.81.1562.

[59] G. Gabrielse, L. Haarsma, and S.L. Rolston. "Open-endcap Penning traps for high precision experiments." In: *Int. J. Mass Spectrom.* 88.2 (1989), pp. 319–332. ISSN: 0168-1176. DOI: https://doi.org/10.1016/0168-1176(89)85027-X. URL: https://www.sciencedirect.com/science/article/pii/016811768985027X.

[60] L. Gastaldo et al. "The Electron Capture ^{163}Ho Experiment ECHo." In: *J. Low Temp. Phys.* 176.5 (2014), pp. 876–884. ISSN: 1573-7357. DOI: 10.1007/s10909-014-1187-4. URL: https://doi.org/10.1007/s10909-014-1187-4.

[61] L. Gastaldo et al. "The electron capture in 163Ho experiment – ECHo." In: *Eur. Phys. J. Spec. Top.* 226.8 (2017), pp. 1623–1694. ISSN: 1951-6401. DOI: 10.1140/epjst/e2017-70071-y. URL: https://doi.org/10.1140/epjst/e2017-70071-y.

[62]   Sheldon L. Glashow. "The renormalizability of vector meson interactions." In: *Nuclear Physics* 10 (1959), pp. 107–117. ISSN: 0029-5582. DOI: https://doi.org/10.1016/0029-5582(59)90196-8. URL: https://www.sciencedirect.com/science/article/pii/0029558259901968.

[63]   André de Gouvêa. "Neutrino Mass Models." In: *Annu. Rev. Nucl. Part. Sci.* 66.1 (2016), pp. 197–217. DOI: 10.1146/annurev-nucl-102115-044600. eprint: https://doi.org/10.1146/annurev-nucl-102115-044600. URL: https://doi.org/10.1146/annurev-nucl-102115-044600.

[64]   G. Gräff, H. Kalinowsky, and J. Traut. "A direct determination of the proton electron mass ratio." In: *Zeitschrift für Physik A Atoms and Nuclei* 297.1 (1980), pp. 35–39. ISSN: 0939-7922. DOI: 10.1007/BF01414243. URL: https://doi.org/10.1007/BF01414243.

[65]   R. Haas, S. Lohse, Ch.E. Düllmann, K. Eberhardt, C. Mokry, and J. Runke. "Development and characterization of a Drop-on-Demand inkjet printing system for nuclear target fabrication." In: *Nucl. Instrum. Methods Phys. Res. A* 874 (2017), pp. 43–49. ISSN: 0168-9002. DOI: https://doi.org/10.1016/j.nima.2017.08.027. URL: https://www.sciencedirect.com/science/article/pii/S0168900217308987.

[66]   F. Heiße, S. Rau, F. Köhler-Langes, W. Quint, G. Werth, S. Sturm, and K. Blaum. "High-precision mass spectrometer for light ions." In: *Phys. Rev. A* 100 (2 2019), p. 022518. DOI: 10.1103/PhysRevA.100.022518. URL: https://link.aps.org/doi/10.1103/PhysRevA.100.022518.

[67]   F. Heiße et al. "High-Precision Determination of g Factors and Masses of $^{20}\mathrm{Ne}^{9+}$ and $^{22}\mathrm{Ne}^{9+}$." In: *Phys. Rev. Lett.* 131 (25 2023), p. 253002. DOI: 10.1103/PhysRevLett.131.253002. URL: https://link.aps.org/doi/10.1103/PhysRevLett.131.253002.

[68]   Peter W. Higgs. "Broken Symmetries and the Masses of Gauge Bosons." In: *Phys. Rev. Lett.* 13 (16 1964), pp. 508–509. DOI: 10.1103/PhysRevLett.13.508. URL: https://link.aps.org/doi/10.1103/PhysRevLett.13.508.

[69]   Michael Jentschel and Klaus Blaum. "Balancing energy and mass with neutrons." In: *Nature Physics* 14.5 (2018), pp. 524–524. ISSN: 1745-2481. DOI: 10.1038/s41567-018-0132-x. URL: https://doi.org/10.1038/s41567-018-0132-x.

[70]   M. Jung et al. "First observation of bound-state β^- decay." In: *Phys. Rev. Lett.* 69 (15 1992), pp. 2164–2167. DOI: 10.1103/PhysRevLett.69.2164. URL: https://link.aps.org/doi/10.1103/PhysRevLett.69.2164.

[71] J. Karthein et al. "Q_{EC}-value determination for ^{21}Na $\rightarrow^{21}$ Ne and ^{23}Mg $\rightarrow^{23}$ Na mirror-nuclei decays using high-precision mass spectrometry with ISOLTRAP at the CERN ISOLDE facility." In: *Phys. Rev. C* 100 (1 2019), p. 015502. DOI: `10.1103/PhysRevC.100.015502`. URL: `https://link.aps.org/doi/10.1103/PhysRevC.100.015502`.

[72] D. K. Keblbeck, R. Bhandari, N. D. Gamage, M. Horana Gamage, K. G. Leach, X. Mougeot, and M. Redshaw. "Updated evaluation of potential ultralow Q-value β-decay candidates." In: *Phys. Rev. C* 107 (1 2023), p. 015504. DOI: `10.1103/PhysRevC.107.015504`. URL: `https://link.aps.org/doi/10.1103/PhysRevC.107.015504`.

[73] Jochen Ketter, Tommi Eronen, Martin Höcker, Marc Schuh, Sebastian Streubel, and Klaus Blaum. "Classical calculation of relativistic frequency-shifts in an ideal Penning trap." In: *Int. J. Mass Spectrom.* 361 (2014), pp. 34–40. ISSN: 1387-3806. DOI: `https://doi.org/10.1016/j.ijms.2014.01.028`. URL: `https://www.sciencedirect.com/science/article/pii/S1387380614000426`.

[74] S. F. King. "Neutrino mass models." In: *Rep. Prog. Phys.* 67.2 (2003), p. 107. DOI: `10.1088/0034-4885/67/2/R01`. URL: `https://dx.doi.org/10.1088/0034-4885/67/2/R01`.

[75] H. Koivisto, J. Arje, and M. Nurmia. "Metal ions from the volatile compounds method for the production of metal ion beams." In: *Rev. Sci. Instrum.* 69.2 (Feb. 1998), pp. 785–787. ISSN: 0034-6748. DOI: `10.1063/1.1148539`. eprint: `https://pubs.aip.org/aip/rsi/article-pdf/69/2/785/11350361/785\_1\_online.pdf`. URL: `https://doi.org/10.1063/1.1148539`.

[76] A. Kramida, Yu. Ralchenko, J. Reader, and and NIST ASD Team. NIST Atomic Spectra Database (ver. 5.9), [Online]. Available: `https://physics.nist.gov/asd` [2022, February 18]. National Institute of Standards and Technology, Gaithersburg, MD. 2021.

[77] H. Kreckel, H. Bruhns, K. A. Miller, E. Wåhlin, A. Davis, S. Höckh, and D. W. Savin. "A simple double-focusing electrostatic ion beam deflector." In: *Rev. Sci. Instrum.* 81.6 (June 2010), p. 063304. ISSN: 0034-6748. DOI: `10.1063/1.3433485`. eprint: `https://pubs.aip.org/aip/rsi/article-pdf/doi/10.1063/1.3433485/16120231/063304\_1\_online.pdf`. URL: `https://doi.org/10.1063/1.3433485`.

[78] Kathrin Kromer. "Environmentally-induced systematic effects at the high-precision mass spectrometer PENTATRAP." MA thesis. Heidelberg: Ruprecht-Karls-Universität, 2019.

[79]   Kathrin Kromer et al. "High-precision mass measurement of doubly magic ^{208}Pb." In: *Eur. Phys. J. A* 58.10 (2022), p. 202. ISSN: 1434-601X. DOI: 10.1140/epja/s10050-022-00860-1. URL: https://doi.org/10.1140/epja/s10050-022-00860-1.

[80]   Kathrin Kromer et al. "Observation of a Low-Lying Metastable Electronic State in Highly Charged Lead by Penning-Trap Mass Spectrometry." In: *Phys. Rev. Lett.* 131 (22 2023), p. 223002. DOI: 10.1103/PhysRevLett.131.223002. URL: https://link.aps.org/doi/10.1103/PhysRevLett.131.223002.

[81]   Kathrin Kromer et al. "Atomic mass determination of Uranium-238." In: *Phys. Rev. C* 109 (2 2024), p. L021301. DOI: 10.1103/PhysRevC.109.L021301. URL: https://link.aps.org/doi/10.1103/PhysRevC.109.L021301.

[82]   Julien Lesgourgues, Gianpiero Mangano, Gennaro Miele, and Sergio Pastor. *Neutrino Cosmology*. Cambridge University Press, 2013. ISBN: 9781139012874. DOI: https://doi.org/10.1017/CBO9781139012874.

[83]   Julien Lesgourgues and Sergio Pastor. "Neutrino Mass from Cosmology." In: *Adv. High Energy Phys.* 2012 (2012), p. 608515. ISSN: 1687-7357. DOI: 10.1155/2012/608515. URL: https://doi.org/10.1155/2012/608515.

[84]   V.M. Lobashev and P.E. Spivak. "A method for measuring the electron antineutrino rest mass." In: *Nucl. Instrum. Methods Phys. Res. A* 240.2 (1985), pp. 305–310. ISSN: 0168-9002. DOI: https://doi.org/10.1016/0168-9002(85)90640-0. URL: https://www.sciencedirect.com/science/article/pii/0168900285906400.

[85]   D. Lunney and (on behalf of the ISOLTRAP Collaboration). "Extending and refining the nuclear mass surface with ISOLTRAP." In: *J. Phys. G* 44.6 (2017), p. 064008. DOI: 10.1088/1361-6471/aa6752. URL: https://dx.doi.org/10.1088/1361-6471/aa6752.

[86]   P. Micke et al. "The Heidelberg compact electron beam ion traps." In: *Rev. Sci. Instrum.* 89.6 (2018), p. 063109. DOI: 10.1063/1.5026961. eprint: https://doi.org/10.1063/1.5026961. URL: https://doi.org/10.1063/1.5026961.

[87]   Benjamin Monreal and Joseph A. Formaggio. "Relativistic cyclotron radiation detection of tritium decay electrons as a new technique for measuring the neutrino mass." In: *Phys. Rev. D* 80 (5 2009), p. 051301. DOI: 10.1103/PhysRevD.80.051301. URL: https://link.aps.org/doi/10.1103/PhysRevD.80.051301.

[88] Léo Morel, Zhibin Yao, Pierre Cladé, and Saïda Guellati-Khélifa. "Determination of the fine-structure constant with an accuracy of 81 parts per trillion." In: *Nature* 588.7836 (2020), pp. 61–65. ISSN: 1476-4687. DOI: `10.1038/s41586-020-2964-7`. URL: `https://doi.org/10.1038/s41586-020-2964-7`.

[89] M. Mukherjee et al. "ISOLTRAP: An on-line Penning trap for mass spectrometry on short-lived nuclides." In: *Eur. Phys. J. A* 35.1 (2008), pp. 1–29. ISSN: 1434-601X. DOI: `10.1140/epja/i2007-10528-9`. URL: `https://doi.org/10.1140/epja/i2007-10528-9`.

[90] Edmund G. Myers. "The most precise atomic mass measurements in Penning traps." In: *Int. J. Mass Spectrom.* 349-350 (2013). 100 years of Mass Spectrometry, pp. 107–122. ISSN: 1387-3806. DOI: `https://doi.org/10.1016/j.ijms.2013.03.018`. URL: `https://www.sciencedirect.com/science/article/pii/S1387380613001097`.

[91] H. Nagahama et al. "Highly sensitive superconducting circuits at 700 kHz with tunable quality factors for image-current detection of single trapped antiprotons." In: *Rev. Sci. Instrum.* 87.11 (2016), p. 113305. DOI: `10.1063/1.4967493`. eprint: `https://doi.org/10.1063/1.4967493`. URL: `https://doi.org/10.1063/1.4967493`.

[92] Sz. Nagy, K. Blaum, and R. Schuch. "Highly-charged ions and high-resolution mass spectrometry in a Penning trap." In: *Trapped Charged Particles and Fundamental Interactions*. Berlin, Heidelberg: Springer Berlin Heidelberg, 2008, pp. 1–36. ISBN: 978-3-540-77817-2. DOI: `10.1007/978-3-540-77817-2_5`. URL: `https://doi.org/10.1007/978-3-540-77817-2_5`.

[93] L. Nies et al. "Further Evidence for Shape Coexistence in $^{79}\text{Zn}^m$ near Doubly Magic ^{78}Ni." In: *Phys. Rev. Lett.* 131 (22 2023), p. 222503. DOI: `10.1103/PhysRevLett.131.222503`. URL: `https://link.aps.org/doi/10.1103/PhysRevLett.131.222503`.

[94] A. Nucciotti. "The Use of Low Temperature Detectors for Direct Measurements of the Mass of the Electron Neutrino." In: *Adv. High Energy Phys.* 2016 (2016), p. 9153024. ISSN: 1687-7357. DOI: `10.1155/2016/9153024`. URL: `https://doi.org/10.1155/2016/9153024`.

[95] Richard H. Parker, Chenghui Yu, Weicheng Zhong, Brian Estey, and Holger Müller. "Measurement of the fine-structure constant as a test of the Standard Model." In: *Science* 360.6385 (2018), pp. 191–195. DOI: `10.1126/science.aap7706`. eprint: `https://www.science.org/doi/pdf/10.1126/science.aap7706`. URL: `https://www.science.org/doi/abs/10.1126/science.aap7706`.

[96] S. T. Petcov. "The Nature of Massive Neutrinos." In: *Adv. High Energy Phys.* 2013 (2013), p. 852987. ISSN: 1687-7357. DOI: 10.1155/2013/852987. URL: https://doi.org/10.1155/2013/852987.

[97] A. Picard et al. "A solenoid retarding spectrometer with high resolution and transmission for keV electrons." In: *Nucl. Instrum. Methods Phys. Res. B* 63.3 (1992), pp. 345–358. ISSN: 0168-583X. DOI: https://doi.org/10.1016/0168-583X(92)95119-C. URL: https://www.sciencedirect.com/science/article/pii/0168583X9295119C.

[98] D. B. Pinegar, S. L. Zafonte, and R. S. Van Dyck. "The UW-PTMS." In: *Hyperfine Interact.* 174.1 (2007), pp. 47–53. ISSN: 1572-9540. DOI: 10.1007/s10751-007-9563-y. URL: https://doi.org/10.1007/s10751-007-9563-y.

[99] Planck Collaboration et al. "Planck 2013 results. XVI. Cosmological parameters." In: *A&A* 571 (2014), A16. DOI: 10.1051/0004-6361/201321591. URL: https://doi.org/10.1051/0004-6361/201321591.

[100] Planck Collaboration et al. "Planck 2018 results - VI. Cosmological parameters." In: *A&A* 641 (2020), A6. DOI: 10.1051/0004-6361/201833910. URL: https://doi.org/10.1051/0004-6361/201833910.

[101] Simon Rainville, James K. Thompson, and David E. Pritchard. "An Ion Balance for Ultra-High-Precision Atomic Mass Measurements." In: *Science* 303.5656 (2004), pp. 334–338. DOI: 10.1126/science.1092320. eprint: https://www.science.org/doi/pdf/10.1126/science.1092320. URL: https://www.science.org/doi/abs/10.1126/science.1092320.

[102] P. C.-O. Ranitzsch, C. Hassel, M. Wegner, D. Hengstler, S. Kempf, A. Fleischmann, C. Enss, L. Gastaldo, A. Herlert, and K. Johnston. "Characterization of the ^{163}Ho Electron Capture Spectrum: A Step Towards the Electron Neutrino Mass Determination." In: *Phys. Rev. Lett.* 119 (12 2017), p. 122501. DOI: 10.1103/PhysRevLett.119.122501. URL: https://link.aps.org/doi/10.1103/PhysRevLett.119.122501.

[103] Sascha Rau, Fabian Heiße, Florian Köhler-Langes, Sangeetha Sasidharan, Raphael Haas, Dennis Renisch, Christoph E. Düllmann, Wolfgang Quint, Sven Sturm, and Klaus Blaum. "Penning trap mass measurements of the deuteron and the HD+ molecular ion." In: *Nature* 585.7823 (2020), pp. 43–47. ISSN: 1476-4687. DOI: 10.1038/s41586-020-2628-7. URL: https://doi.org/10.1038/s41586-020-2628-7.

[104] J. Repp et al. "PENTATRAP: a novel cryogenic multi-Penning-trap experiment for high-precision mass measurements on highly charged ions." In: *Appl. Phys. B* 107.4 (2012), pp. 983–996. ISSN: 1432-0649. DOI: 10.1007/s00340-011-4823-6. URL: https://doi.org/10.1007/s00340-011-4823-6.

[105] A. Rischka et al. "Mass-Difference Measurements on Heavy Nuclides with an eV/c^2 Accuracy in the PENTATRAP Spectrometer." In: *Phys. Rev. Lett.* 124 (11 2020), p. 113001. DOI: 10.1103/PhysRevLett.124.113001. URL: https://link.aps.org/doi/10.1103/PhysRevLett.124.113001.

[106] Alexander Rischka. "Aufbau des Stabilisierungssystems des Heliumdrucks und Heliumlevels und Konstruktion eines kryogenen Faraday-Bechers für PENTATRAP." deu. MA thesis. Heidelberg: Karl-Ruprecht-Universität, 2014.

[107] Tanya S. Roussy et al. "An improved bound on the electron's electric dipole moment." In: *Science* 381.6653 (2023), pp. 46–50. DOI: 10.1126/science.adg4084. eprint: https://www.science.org/doi/pdf/10.1126/science.adg4084. URL: https://www.science.org/doi/abs/10.1126/science.adg4084.

[108] C. Roux et al. "The trap design of PENTATRAP." In: *Appl. Phys. B* 107.4 (2012), pp. 997–1005. ISSN: 1432-0649. DOI: 10.1007/s00340-011-4825-4. URL: https://doi.org/10.1007/s00340-011-4825-4.

[109] Abdus Salam and J. C. Ward. "Weak and electromagnetic interactions." In: *Il Nuovo Cimento (1955-1965)* 11.4 (1959), pp. 568–577. ISSN: 1827-6121. DOI: 10.1007/BF02726525. URL: https://doi.org/10.1007/BF02726525.

[110] Ch. Schweiger. "Construction and commissioning of a room-temperature electron beam ion trap and development of a wire probe injection system." MA thesis. Heidelberg: Ruprecht-Karls-Universität, 2017. URL: https://hdl.handle.net/11858/00-001M-0000-002D-76F6-C.

[111] Christoph Schweiger et al. "Production of highly charged ions of rare species by laser-induced desorption inside an electron beam ion trap." In: *Rev. Sci. Instrum.* 90.12 (2019), p. 123201. DOI: 10.1063/1.5128331. eprint: https://doi.org/10.1063/1.5128331. URL: https://doi.org/10.1063/1.5128331.

[112] Christoph Schweiger et al. "Fast silicon carbide MOSFET based high-voltage push–pull switch for charge state separation of highly charged ions with a Bradbury–Nielsen gate." In: *Rev. Sci. Instrum.* 93.9 (2022), p. 094702. DOI: 10.1063/5.0083515. eprint: https://doi.org/10.1063/5.0083515. URL: https://doi.org/10.1063/5.0083515.

[113] Christoph Schweiger et al. *Penning-trap measurement of the Q-value of the electron capture in* ^{163}Ho *for the determination of the electron neutrino mass.* 2024. arXiv: 2402.06464 [nucl-ex].

[114] R. X. Schüssler et al. "Recent Developments at the High-Precision Mass Spectrometer PENTATRAP." In: *Proceedings of the 12th International Conference on Low Energy Antiproton Physics (LEAP2016).* DOI: 10.7566/JPSCP.18.011020. eprint: https://journals.jps.jp/doi/pdf/10.7566/JPSCP.18.011020. URL: https://journals.jps.jp/doi/abs/10.7566/JPSCP.18.011020.

[115] R. X. Schüssler et al. "Detection of metastable electronic states by Penning trap mass spectrometry." In: *Nature* 581.7806 (2020), pp. 42–46. ISSN: 1476-4687. DOI: 10.1038/s41586-020-2221-0. URL: https://doi.org/10.1038/s41586-020-2221-0.

[116] S. Sturm, F. Köhler, J. Zatorski, A. Wagner, Z. Harman, G. Werth, W. Quint, C. H. Keitel, and K. Blaum. "High-precision measurement of the atomic mass of the electron." In: *Nature* 506.7489 (2014), pp. 467–470. ISSN: 1476-4687. DOI: 10.1038/nature13026. URL: https://doi.org/10.1038/nature13026.

[117] S. Sturm, G. Werth, and K. Blaum. "Electron g-factor determinations in Penning traps." In: *Annalen der Physik* 525.8-9 (2013), pp. 620–635. DOI: https://doi.org/10.1002/andp.201300052. eprint: https://onlinelibrary.wiley.com/doi/pdf/10.1002/andp.201300052. URL: https://onlinelibrary.wiley.com/doi/abs/10.1002/andp.201300052.

[118] S. Sturm et al. "The ALPHATRAP experiment." In: *Eur. Phys. J. Spec. Top.* 227.13 (2019), pp. 1425–1491. ISSN: 1951-6401. DOI: 10.1140/epjst/e2018-800225-2. URL: https://doi.org/10.1140/epjst/e2018-800225-2.

[119] Joseph John Thomson. "Bakerian Lecture: Rays of positive electricity." In: *Proc. R. Soc. Lond. A* 89.607 (1913), pp. 1–20. DOI: 10.1098/rspa.1913.0057. eprint: https://royalsocietypublishing.org/doi/pdf/10.1098/rspa.1913.0057. URL: https://royalsocietypublishing.org/doi/abs/10.1098/rspa.1913.0057.

[120] Eite Tiesinga, Peter J. Mohr, David B. Newell, and Barry N. Taylor. "CODATA recommended values of the fundamental physical constants: 2018." In: *Rev. Mod. Phys.* 93 (2 2021), p. 025010. DOI: 10.1103/RevModPhys.93.025010. URL: https://link.aps.org/doi/10.1103/RevModPhys.93.025010.

[121] Velte, C. et al. "High-resolution and low-background ^{163}Ho spectrum: interpretation of the resonance tails." In: *Eur. Phys. J. C* 79.12 (2019), p. 1026. DOI: 10.1140/epjc/s10052-019-7513-x. URL: https://doi.org/10.1140/epjc/s10052-019-7513-x.

[122] Meng Wang, W.J. Huang, F.G. Kondev, G. Audi, and S. Naimi. "The AME 2020 atomic mass evaluation (II). Tables, graphs and references*." In: *Chin. Phys. C* 45.3 (2021), p. 030003. DOI: 10.1088/1674-1137/abddaf. URL: https://dx.doi.org/10.1088/1674-1137/abddaf.

[123] Steven Weinberg. "A Model of Leptons." In: *Phys. Rev. Lett.* 19 (21 1967), pp. 1264–1266. DOI: 10.1103/PhysRevLett.19.1264. URL: https://link.aps.org/doi/10.1103/PhysRevLett.19.1264.

[124] D. J. Wineland and H. G. Dehmelt. "Principles of the stored ion calorimeter." In: *J. Appl. Phys.* 46.2 (Sept. 1975), pp. 919–930. ISSN: 0021-8979. DOI: 10.1063/1.321602. eprint: https://pubs.aip.org/aip/jap/article-pdf/46/2/919/7403708/919_1_online.pdf. URL: https://doi.org/10.1063/1.321602.

[125] R. N. Wolf et al. "Plumbing Neutron Stars to New Depths with the Binding Energy of the Exotic Nuclide ^{82}Zn." In: *Phys. Rev. Lett.* 110 (4 2013), p. 041101. DOI: 10.1103/PhysRevLett.110.041101. URL: https://link.aps.org/doi/10.1103/PhysRevLett.110.041101.

[126] R.N. Wolf et al. "On-line separation of short-lived nuclei by a multi-reflection time-of-flight device." In: *Nucl. Instrum. Methods Phys. Res. A* 686 (2012), pp. 82–90. ISSN: 0168-9002. DOI: https://doi.org/10.1016/j.nima.2012.05.067. URL: https://www.sciencedirect.com/science/article/pii/S016890021200575X.

[127] R. L. Workman and Others. "Review of Particle Physics." In: *Prog. Theor. Exp. Phys.* 2022 (2022), p. 083C01. DOI: 10.1093/ptep/ptac097.

ACKNOWLEDGMENTS

Mein größter Dank gilt meiner Familie für die bedingungslose Liebe und Unterstützung die ich immer in meinem Leben von Euch erfahren durfte. Ganz besonders danke ich meinen Eltern, Karin und Ludwig und meiner Schwester Edith.

Liebe Janine, du bist der wundervollste Mensch den ich kenne. Danke für dein unendliches Verständnis und dafür, dass du mir gerade in letzter Zeit so oft den Rücken frei gehalten hast und mich jederzeit unterstützt hast. Ich bin so unendlich dankbar dich zu kennen und freue mich so sehr, dass wir Aurelius gemeinsam beim Entdecken der Welt begleiten dürfen.